Titre: Title:	Regional study of geochemical alteration associated with the Normetal deposit, Abitibi Greenstone Belt, Quebec
Auteur: Author:	Nicholas Teasdale
Date:	1993
Type:	Mémoire ou thèse / Dissertation or Thesis
Référence: Citation:	Teasdale, N. (1993). Regional study of geochemical alteration associated with the Normetal deposit, Abitibi Greenstone Belt, Quebec [Master's thesis, Polytechnique Montréal]. PolyPublie. https://publications.polymtl.ca/57022/

UNIVERSITÉ DE MONTRÉAL

Regional Study of Geochemical Alteration Associated with the Normetal Deposit, Abitibi Greenstone Belt, Quebec.

par

Nicholas TEASDALE

DÉPARTEMENT DE GÉNIE MINERAL

ÉCOLE POLYTECHNIQUE

MÉMOIRE PRÉSENTÉ EN VUE DE L'OBTENTION
DU GRADE DE MAÎTRE ÈS SCIENCES APPLIQUÉES (M.Sc.A.)
(GÉOLOGIE MINIÈRE)

Janvier 1993

ISBN 0-315-86476-1

UNIVERSITÉ DE MONTRÉAL

ÉCOLE POLYTECHNIQUE

Ce mémoire intitulé:

Regional Study of Geochemical Alteration Associated with the Normetal Deposit,

Abitibi Greenstone belt, Quebec.

présenté par: Nicholas TEASDALE

en vue de l'obtention du grade de: MAÎTRE ÈS SCIENCES APPLIQUÉES

a été dûment accepté par le jury d'examen constitué de:

M. POULIOT, Gaston, Ph.d., Président

M. Brown, Alex C., Ph.d., membre et directeur de recherche

M. DARLING, Richard, Ph.d., membre

SOMMAIRE

Le gisement de Normétal, situé à 110 km au nord de Rouyn-Noranda, a produit plus de 11 millions de tonnes de minerai de sulfures massifs à 2.15% Cu, 5.12% Zn, 0.549 g/t Au et 45.25 g/t Ag. Contrairement au camp minier de Rouyn-Noranda où plusieurs gisements de sulfurs massifs on été découverts, un seul gisement ainsi qu'une petite lentille satellite (40,000 tonnes) furent trouvés depuis la découverte du gisement en 1925 dans le camp de Normétal. En se basant sur une meilleure compréhension de la stratigraphie des roches volcaniques, cette étude cherche à mieux définir les patrons d'altération régionale, possiblement associés à une circulation de fluides hydrothermaux ainsi que d'interpréter les directions de circulation de ces fluides à l'échelle régionale.

Le gisement est interpreté comme étant de type sulfures massifs volcanogène (VSM) proximal avec plusieurs caractéristiques d'altération communes aux dépôts du sous type Mattabi. Parmi ces caractérisitiques on retrouve une altération régionale généralement concordante contrairement aux cheminées d'altération classiques discordantes de type Noranda. Cette altération est caractérisée par l'assemblage minéralogique ankérite-séricite-chloritoïde. De plus, la volcanologie physique suggère une association avec des pyroclastiques felsiques et des sédiments dérivés d'origine épiclastiques. Stratigraphiquement, le dépôt se situe dans une zone de transition entre des

rhyolites et des andésites au-dessus d'un horizon sédimentaire dont la continuité latérale est tracée sur plus d'une douzaine de kilomètres.

Les données de géochimie régionale de l'Horizon de la Mine et des rhyolites situées sous l'horizon sédimentaire (RBS) gisant stratigraphiquement sous le dépôt suggèrent que l'échantillonage d'un horizon sous un autre horizon potentiellement minéralisé (paléo-fond marin, pour les dépôts de type VSM) est une approche efficace pour évaluer les patrons de circulation des fluides. Les calculs de changement de masse et des analyses quantitatives par microsonde de la minéralogie d'altération dans les rhyolites RBS suggèrent une évolution chimique progressive des fluides qui est latérallement traçable sur des distances atteignant 3 à 4 km du dépôt. Des variations de MnO dans les échantillons géochimiques et dans les analyses de minéraux d'altération démontrent clairement leur utilité comme indicateurs de minéralisation. De plus, l'absence de tendances d'altération géochimique latéralement équivalentes dans l'Horizon de la Mine est attribuée à la décharge localisée d'exhalations hydrothermales au niveau du fond marin. Notre étude démontre aussi que les données isotopiques d'oxygène peuvent aider à distinguer entre des zones d'altération produites par des eaux marines froides et des zones d'altération produites par la circulation de fluides hydrothermaux.

ABSTRACT

The Normetal deposit, located 110 km north of Rouyn-Noranda, mined continuously from 1937 to 1975, yielded over 11 million tonnes of massive sulphide ore grading 2.15% Cu, 5.12% Zn, 0.549 g/t Au and 45.25 g/t Ag. In sharp contrast to the Noranda camp, only one deposit and one much smaller satellite lens (40,000 tons) were found in the Normetal camp since discovery in 1925. Based on a better comprehension of volcanic stratigraphy, this study's principal goal is to better define regional alteration trends possibly associated with hydrothermal alteration, which is believed to have been responsible for ore deposition, and attempt to interpret fluid-flow paths on a regional scale in order to help find other similar deposits within the Normetal camp.

Based on our study, the deposit is interpreted as a proximal volcanogenic massive sulphide (VMS) deposit with numerous alteration characteristics common to the Mattabi-type subgroup of VMS deposits. These characteristics include broad regional semi-conformable and highly-conformable alteration as opposed to classic cross-cutting footwall alteration pipes of the Noranda-type. The alteration is characterized by an ankerite-sericite-chloritoid mineralogical assemblage. Physical volcanology also suggests an association with felsic pyroclastics and their derived epiclastic sediments. The deposit is hosted in a transition zone between rhyolites and andesites and overlies a laterally extensive (>12 km) sedimentary horizon which may have acted as an aquitard, effectively

controlling and focusing the upward convection of hydrothermal fluids driven by a deep syn-volcanic intrusion (possibly the Normetal pluton).

Based on regional geochemical data, including whole rock analyses, microprobe analyses and oxygen isotopes from both the Mine Horizon and from rhyolites below the sediment (RBS) horizon lying stratigraphically below the deposit, it is suggested that sampling of a specific horizon (e.g., the RBS) below a potentially mineralized horizon (paleo-seafloor for VMS deposits) may be an effective way of evaluating regional fluid-flow patterns. Mass-change data and quantitative microprobe analysis of alteration minerals (chlorite, chloritoid and ankerite) in the RBS show a progressive chemical evolution of fluids traceable laterally over distances reaching 3 to 4 km from the VMS deposit. MnO variations in whole rocks and in alteration minerals which concentrate MnO clearly suggest their usefulness as indicators of mineralization. Furthermore, an absence of equally extensive regional geochemical alteration trends within the Mine Horizon, is attributed to the focussed discharge of hydrothermal exhalations at the seafloor. Oxygen isotope data from both the Mine Horizon and from the RBS were were found to be usefull in distinguishing between areas of cold seawater alteration and areas of circulation of evolved fluids capable of forming VMS deposits.

RÉSUMÉ

Le gisement de Normétal, d'âge archéen, est situé à 110 km au nord de Rouyn-Noranda (fig. 1) dans la partie centrale de la ceinture verte de l'Abitibi. Géologiquement, il se trouve à l'intérieur du complexe volcanique de Joutel-Normétal (Goodwin et Ridler, 1970) ou plus précisément, dans le groupe de Gale (Latulippe, 1976).

Les roches volcaniques de la région ont une orientation nord-ouest sud-est avec des pendages abrupts vers le nord (Moore 1990, Tessier, 1991a). Les polarités stratigraphiques sont généralement interprétées comme étant vers le sud-ouest, donc indiquant un empilement volcanique inversé. Au nord, les roches volcaniques se buttent contre un large intrusif granodioritique nommé, de façon informelle, le pluton de Normétal. Une intrusion de taille beaucoup moins importante (l'intrusion du Lac du Dome), d'une épaisseur d'environ 450 mètres, se retrouve à l'est de Normétal.

Le gisement de Normétal a produit plus de 11 millions de tonnes de minerai de sulfures massifs à 2.15% Cu, 5.12% Zn, 0.549 g/t Au et 45.25 g/t Ag. Stratigraphiquement, l'horizon de la mine se retrouve dans une zone de composition transitionelle (voir fig. 2) entre des rhyolites et des andésites au-dessus d'un horizon sédimentaire. Cet horizon repère sédimentaire, ayant une continuité régionale ateignant

plus d'une douzaine de kilomètres a permis aux géologues de Cominco de mieux définir la stratigraphie de l'empilement volcanique à l'échelle régionale (fig. 3).

L'Horizon de la Mine est caractérisé par une altération qui est concordante à la stratigraphie et est marqué d'un assemblage minéralogique de séricite - ankérite - chloritoïde. Cette altération est traçable sur une distance d'une dizaine de kilomètres (voir fig. 4). Une zone riche en chlorite et magnétite se trouvant dans l'éponte inférieure immédiate du gisement (Moore, 1990; Brown 1948) est interprétée comme représentant une zone d'altération nourricière du gisement.

En se basant sur ces caractéristiques d'altération ainsi que sur une association à des faciès pyroclastiques felsiques, le gisement est interpreté comme étant de type sulfures massifs volcanogène (VSM) du sous-type Mattabi (Morton, 1990; Morton and Franklin, 1987).

Contrairement au camp minier de Rouyn-Noranda où plusieur gisements on été découverts, un seul gisement ainsi qu'une petite lentille satellite (40,000 tonnes) furent trouvés dans le camp de Normétal depuis la découverte du gisement en 1925. En se basant sur une meilleure compréhension de la stratigraphie des roches volcaniques, cette étude cherche à mieux définir et quantifier les patrons d'altération régionale dans la zone d'altération concordante et dans la partie supérieure des rhyolites directement au-dessous

des sédiments repères. Ce deuxième horizon a été choisi pour vérifier une hypothèse qui suggère que les sédiments aient pu agir comme aquitard et donc ayant potentiellement canalisé des fluides hydrothermaux vers le gisement de Normétal sous lequel les sédiments sembleraient être absents (voir fig. 2). Le but de cette étude est donc d'arriver à interpréter les patrons de circulation de ces fluides à l'échelle régionale pour mieux comprendre les processus associés au gisement de Normétal ainsi que pour en définir les métallotectes positifs utiles à la découverte de nouveaux gisements.

Une autre zone d'altération, celle-ci recoupant la stratigraphie à l'ouest de Normétal (voir fig. 4), est importante à noter. Elle est marquée par deux isogrades dont le premier est défini par l'apparition de chloritoïde. Un deuxième isograde, situé à l'intérieur à la base du premier, est défini par l'apparition additionelle de tourmaline.

Les méthodes d'études de ce travail incluent (1) des analyses de roches pour élements majeurs et élements en traces par fluorescence X, (2) des analyses pétrographiques (128 lammes minces) et aussi des analyses quantitatives (65 des 128 lammes minces par microsonde) de la composition des minéraux d'altération (les ankérites, les chloritoïdes, les chlorites et les séricites), et (3) des analyses isotopiques d'oxygène (48 analyses).

Toutes les données des analyses géochimiques des échantillons de roches utilisées dans ce travail sont présentées à 100% anhydre dans les annexes 2, 3 et 4. Celles-ci ont été recalculées selon la méthode de Maclean (1990) pour en déterminer les pertes et gains de masse. Ces variations de masse sont représentées graphiquement sur les figures 12 et 14 ainsi que schématiquement sur la figure 26.

Les résultats de ces analyses démontrent des patrons d'altérations fort différents pour les deux horizons. Dans les rhyolites situées en-dessous des sédiments (fig. 12), on remarque une nette augmentation en gain de SiO_2 (jusqu'à +20%) et de K_2O (jusqu'à +8%) vers le gisement de Normétal. Parallèlement des pertes importantes en Na_2O (jusqu'à -6%) et en CaO (jusqu'à -4%) sont marquées vers le gisement de Normétal dans ces rhyolites. Pour l'Horizon de la Mine, des augmentations en Fe_2O_3 (jusqu'à +20%) et en MnO (jusqu'à +0.35%) sembleraient être les meilleurs indicateurs de minéralisation. Des augmentations semblables en Fe_2O_3 et en MnO se reproduisent 6 kilomètres à l'est de Normétal et représentent donc une cible d'intérêt pour l'exploration. Contrairement aux rhyolites situées sous les sédiments, l'horizon de la mine démontre des pertes en Na_2O et des gains en K_2O seulement à l'est de Normétal, au dessus de l'intrusif du Lac du Dome, sans démontrer des gains en SiO_2, en Fe_2O_3 ou en MnO.

De ces données d'analyses de roches, cinq conclusions importantes sont à retenir. 1.) Les meilleurs indicateurs de minéralisation dans l'Horizon de la Mine en terme de

changement de masse sont les gains en Fe_2O_3 et en MnO. 2.) Les meilleurs indicateurs de minéralisation pour les rhyolites sous-jacentes aux sédiments, en terme de changement de masse sont les gains en SiO_2, en K_2O et les pertes en Na_2O et en CaO. 3.) Des gains en Fe_2O_3 et en MnO à 6 km à l'est de Normétal représentent une cible intéressante pour l'exploration. 4.) L'altération dans les rhyolites sous-jacentes aux sédiments démontre les plus importants changements de masse (pertes et gains) en-dessous du gisement de Normétal. Ceci suggère que les fluides hydrothermaux responsables pour la minéralisation dans ces rhyolites furent aussi canalisés en-dessous du gisement. 5.) Des pertes importantes en Na_2O et des gains en K_2O, au-dessus de l'intrusion du Lac du Dome, suggèrent une circulation localisée d'une importante quantité d'eau au-dessus de cette intrusion (à faible profondeur).

Des analyses quantitatives à la microsonde de 135 chloritoïdes, 119 ankéries, 81 chlorites et 44 séricites ont été éfectuées pour cette étude. Ces analyses ont permis d'évaluer le potentiel de ces minéraux comme indicateurs d'altération ou de minéralisation. À partir de ces analyses, la chlorite, la chloritoïde et l'ankérite semblent démontrer de fortes corrélations entre leurs contenus en MnO et la proximité d'altération ou de minéralisation. Ces indicateurs sont mis en évidence encore plus en construisant des rapports entre le MnO et le FeO ou le MgO contre les coordonnées est-ouest topographiques des échantillons par rapport au gisement de Normétal à 0 km (voir fig. 17,18 et19). Comme pour les données de pertes et gains de masse, dans l'horizon de la

mine des concentrations élevées en MnO dans les ankérites suggèrent une cible d'exploration intéressante située à quelques 6 km à l'est de Normétal.

Les analyses isotopiques d'oxygène ont été éfectuées pour repérer les zones ayant été exposées à des volumes anormaux d'eau ou à des fluides à températures élevées. En se basant sur les valeurs isotopiques moyennes des deux horizons échantillonés (fig. 21), les données suggèrent que les roches de l'Horizon de la Mine ont probablement été altérées par des fluides à basse température ($\delta^{18} \approx$ de 10 à 12‰) par rapport au rhyolites sous-jacentes ($\delta^{18} \approx$ de 12 à 16‰). Des graphiques représentant les mêmes données selon leurs horizons (fig. 22 et 23) nous permettent d'identifier les zones ayant été exposées à des circulations localisés d'eau (valeurs en δ^{18} basse par rapport à la moyenne). De telles zones coïncident avec la zone d'altération discordante à l'ouest de Normétal, avec l'Horizon de la Mine au dessus de l'intrusion du Lac du Dome et avec un trou de forage dans des rhyolites sous-jacentes aux sédiments près du gisement de Normétal.

En conclusion les données géochimiques régionales suggèrent que l'échantillonage d'un horizon sous un autre horizon potentiellement minéralisé (paléo-fond marin, pour les dépôts de type VSM) est une approche efficace pour repérer les zones de forte circulation (fig. 25). Les calculs de changement de masse et des analyses quantitatives par microsonde de minéralogie d'altération dans les rhyolites sous-jacentes aux sédiments suggèrent une évolution chimique latérallement progressive des fluides qui est traçable sur

des distances atteignant 3 à 4 km du dépôt. Des variations de MnO, dans les échantillons géochimiques et dans les analyses de minéraux d'altération, démontrent clairement leur utilité comme indicateurs de minéralisation. De plus, l'absence de telles tendances géochimiques régionales équivalentes dans l'Horizon de la Mine est attribuée à la décharge localisée d'exhalations hydrothermales au niveau du fond marin. Les données isotopiques d'oxygène de l'Horizon de la Mine et des rhyolites sous-jacentes aux sédiments aident à faire la distinction entre les zones d'altération produites par des eaux marines froides et les zones de circulation de fluides hydrothermaux ayant la capacité de former des dépôts de type VSM.

ACKNOWLEDGEMENTS

The author wishes to express his gratitude to Alex C. Brown, the thesis advisor, for his help in reading and rereading the contents of this thesis in order to transform it into it's present state, as well as for recruiting me into graduate studies.

Dave Moore and André Tessier of Cominco Ltd. are thanked for the project itself, for all the necessary funding to perform the numerous analyses involved in this study and for indirectly putting me together with my wife (not necessarily in that order).

Gaston Pouliot and Richard Darling served as members of the thesis committee and added many pertinent comments and suggestions which also helped to improve the final copy of this text.

Lawrence Hoy is acknowledged for performing all of my isotope analyses as well as for guiding me to numerous references which have helped me to view fluids as the essence of ore-forming processes. Gaston Gélinas prepared all of my thin and polished sections which Paul Samson helped me to analyse with the microprobe.

Finally I want to thank my wife Valérie for her help and for putting up with me through all the long hours I spent with my computer instead of with her.

TABLE OF CONTENTS

LIST OF FIGURES

List of Figures (Continued)

LIST OF APPENDICES

INTRODUCTION

The Normetal volcanogenic massive sulphide (VMS) deposit located 110 km north of Rouyn-Noranda (Fig. 1), is hosted in the upper part of a typically andesitic to dacitic transition zone between a thick sequence of rhyolites and overlying intermediate to mafic volcanic rocks (see Fig. 2). A distinctive marker horizon consisting of laminated mudstones and siltstones at the top of the main rhyolite sequence has helped geologists at Cominco Ltd. to establish a good stratigraphic control within the Normetal camp. Directly underlying the deposit is a continuous chlorite- and magnetite-rich zone interpreted to represent possible footwall alteration. A concordant sericite - ankerite - chloritoid mineral assemblage is also highly characteristic of the deposit along the Mine Horizon and extends laterally for greater than 10 kilometres. The purpose of this study is to identify, describe and quantify chemical and mineralogical variations in this concordant alteration zone and in the rhyolite directly underlying "impermeable" sediments that may have controlled upward fluid flow.

In terms of regional exploration, the study was designed so that resultant data, after evaluation on the Normetal deposit, could be used to investigate other similar horizons that may host massive sulphide deposits within the Normetal region. A further goal (over and beyond the possibility of finding new ore deposits) was to use these data to describe the metallogenic setting of the Normetal deposit. Previous lithogeochemical

work, including a geostatistical analyses by Marcotte (in Valiquette et al, 1978) and a regional study by Mellinger (in Valiquette et al, 1978 and 1980) used a stratigraphy-transecting approach to sampling as opposed to the stratigraphy-parallel approach of this study.

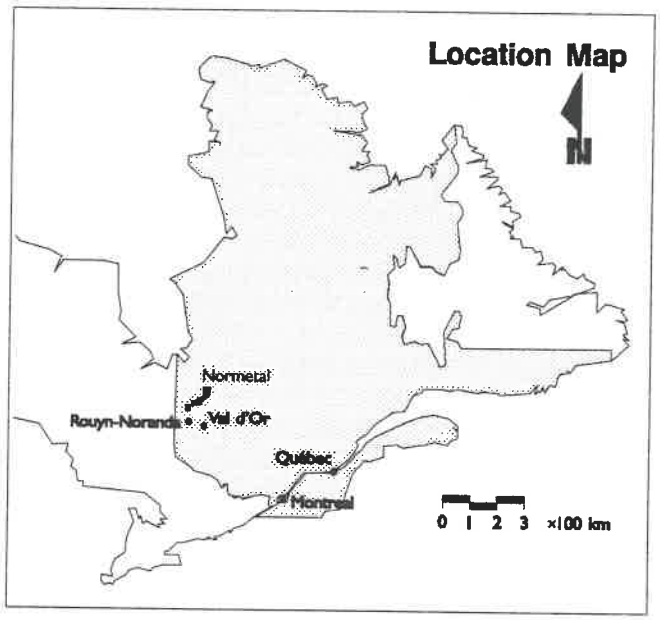

Figure 1: Location of the Normetal mining camp within the province of Québec.

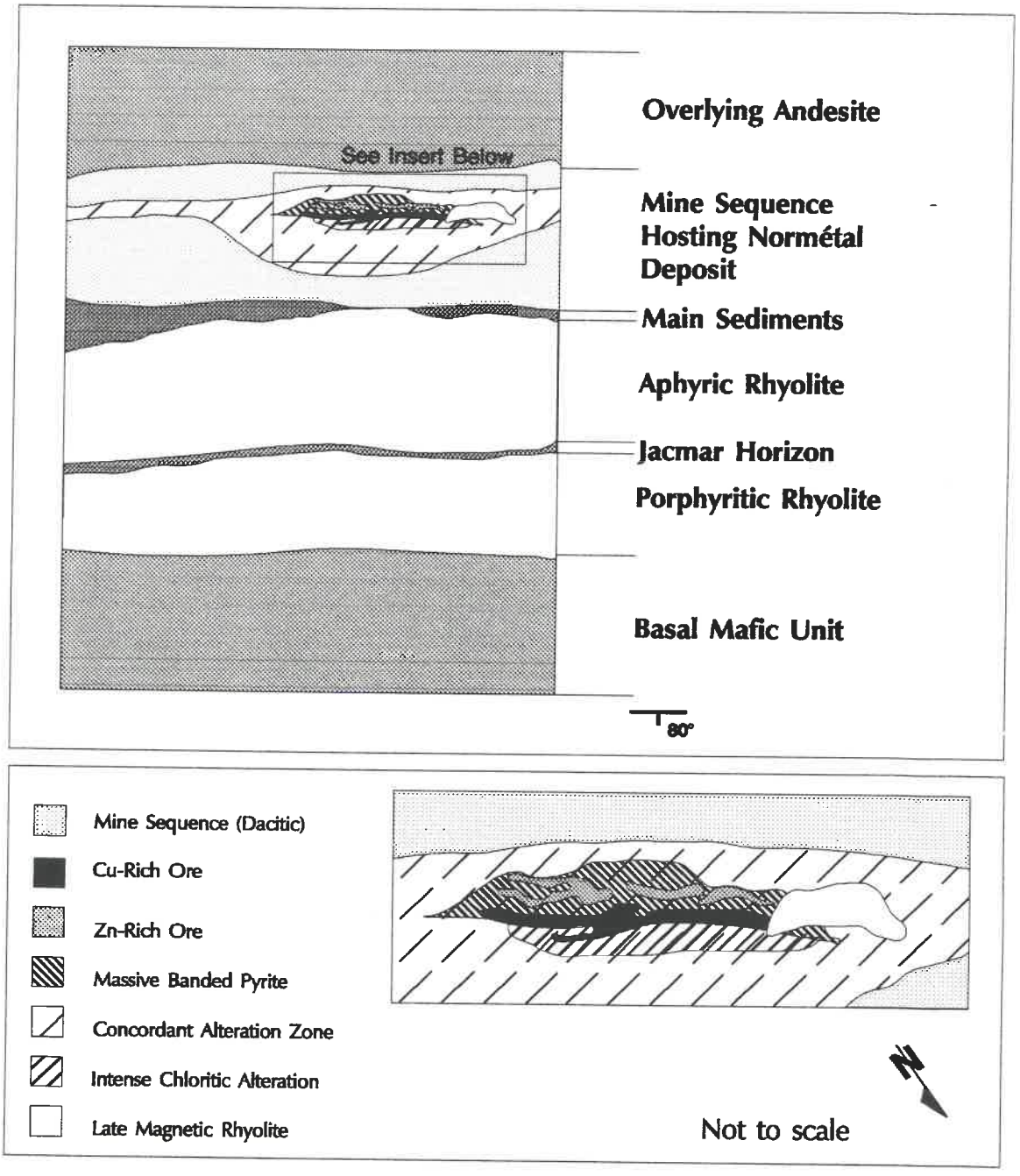

Figure 2: Schematic surface plan of the stratigraphy hosting the Normetal deposit.

CHAPTER 1

GENERAL METHODOLOGY OF THE STUDY

1.1 Introduction

The methodology of this project included (1) microprobe analyses of particular mineralogical species (particularly the alteration minerals ankerite, chlorite, chloritoid and sericite), (2) a study of oxygen isotopic variations, and (3) a review of abundant whole-rock analyses.

In conducting microprobe analyses of particular mineralogical species, we hoped to recognize chemical variations that correlate directly or inversely with the proximity of the orebody, as has been done with chlorite analyses (iron to magnesium ratios) on other deposits. Oxygen isotope analyses were performed to help identify and possibly quantify areas of important hydrothermal circulation. In order to more easily correlate data with proximity to the Normetal deposit and to better understand factors causing variations in the data, two distinct horizons were sampled extensively laterally away from the past-producing Normetal mine for both microprobe and $\delta^{18}O$ analyses. Most samples were obtained from recent diamond drill holes (Appendix 1). This sampling covers two distinct horizons which can then be treated as distinct parallel one-dimensional arrays (see Figure 3). It was also hoped that by isolating these horizons individually, variations due to

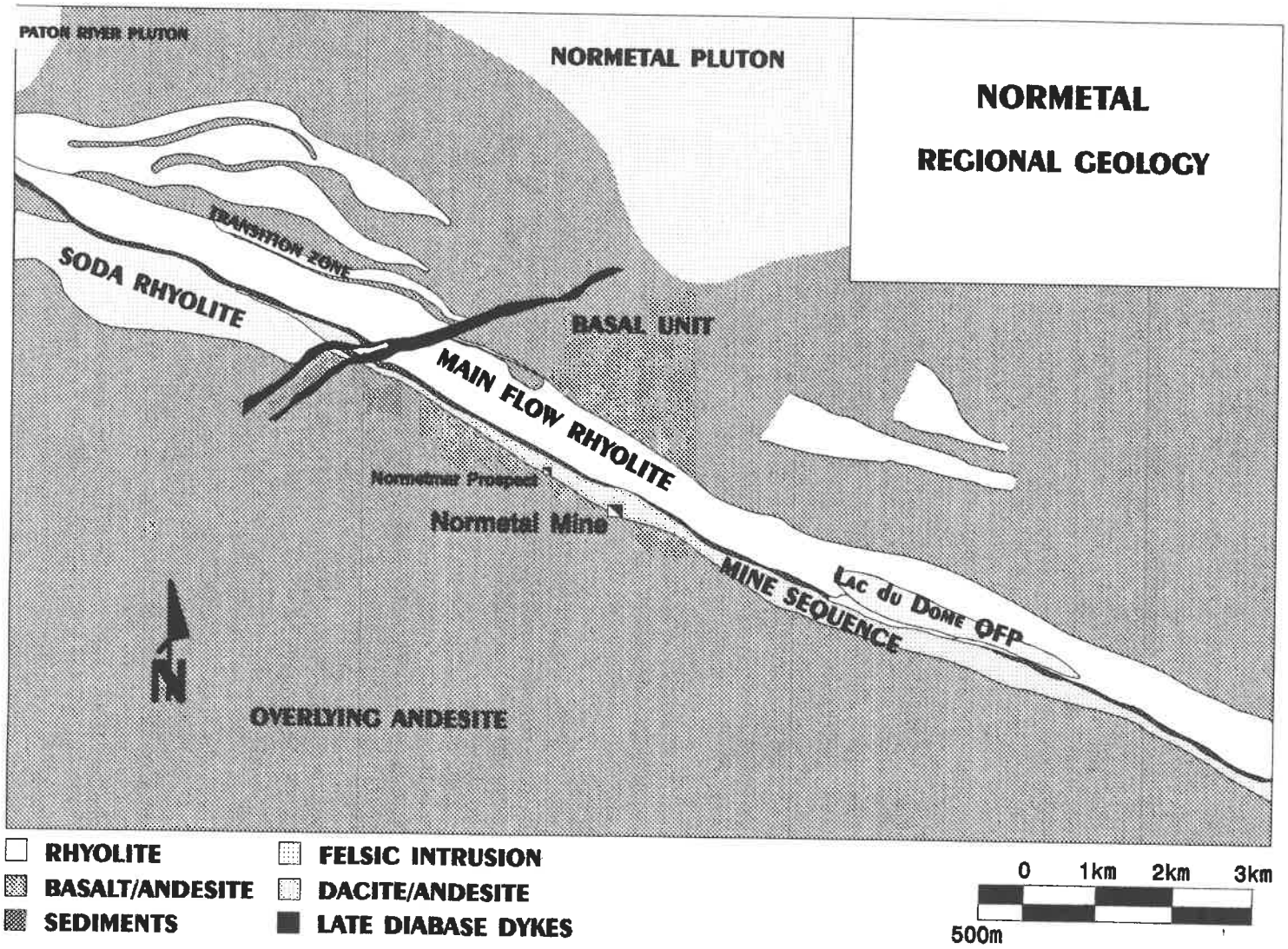

Figure 3: Generalized geologic plan map of the Normetal Mining camp.

lithological contrasts and their respective variations in effective permeabilities, could in this way, be reduced.

The horizons selected for sampling were rhyolites directly underlying the sedimentary unit and the Mine Horizon itself. Rhyolites below the sediments (RBS) were sampled to verify a hypothesis that the sediments may have acted as a relatively impermeable horizon or aquitard which could have ponded fluids below it. If this were so, the sediments would have controlled the upward flow of convecting hydrothermal solutions and, as in sedex deposits, they may have effectively channeled the exhalation of hydrothermal solutions. The absence of these sediments directly below the mine is exceptional in the Normetal belt and supports this interpretation.

The Mine Horizon was also chosen for study due to its temporal relationship with ore, and to evaluate chemical variations within it. It was hoped then that compositional or isotopic variations in the RBS could explain variations observed in the Mine Horizon and might therefore permit a two-dimensional interpretation of fluid-flow paths in the Normetal camp.

A compilation of whole-rock data extending from throughout the belt, as well as individual analyses coincident with samples analyzed for either $\delta^{18}O$ or for microprobe

study was also used to help both in explaining variations in the above data as well as to observe chemical variations in whole-rock chemistry.

1.2 Whole-Rock Analyses

All whole-rock geochemical data presented in this thesis was provided by Cominco Ltd. Analyses were obtained by X-ray fluorescence of fused glass beads by Xral Ltd. Detection limits were approximately 0.01% for major elements and 10 ppm for trace elements. All whole-rock data have been recalculated to 100% volatile free. Hasik (1991), in a study of the petrography and geochemistry of Normetal rhyolites, re-analyzed trace elements for some 14 samples (previously analyzed by Xral Ltd.) at the Université de Montréal, and demonstrated a strong reproducibility for Zr and a fair reproducibility for Sr. Her study also showed that the Xral analyses of Rb tended to be high for values lower than 80 ppm (up to +30 ppm). Analyses of Y were generally high (10 to 30 ppm), as were values for Nb which show the lowest correlation factor ($R^2 = 0.47$).

1.3 Alteration Mineralogy and Mineral Chemistry

A total of 128 thin sections were prepared for this study. A short summary of descriptions is presented with the sample list in Appendix 18. Witness samples from these thin sections were stained to determine carbonate types according to the method described by Dickson (1965), permitting easy identification of calcite (stained red) vs. ankerite (dark

blue), and somewhat more arbitrarily, Fe-rich dolomite (stained pale blue). A few ankerites analyzed in this study are considered to be dolomites (3 out of 119 analyses). Slightly more numerous are pale blue-stained carbonates, some of which could be Fe-rich dolomites or ankerites (ankerite may range up to 0.25 Fe:Mg according to Deer et al., 1966). The small number of Fe-rich dolomites and the absence of a spatial association of these dolomites with mineralization or alteration does not justify further definition of this criterion, and Fe-rich dolomites are included with the ankerites.

Quantitative analyses were performed on 65 of the thin section using the École Polytechnique EDS microprobe. From these, 135 chloritoids, 119 ankerites, 81 chlorites, 44 sericites, 16 siderites, 8 calcites and 4 tourmalines were analyzed (Appendix 5 to 12). Silicates were analyzed with a beam current of 2.0 nA for 100 seconds. Carbonates were analyzed with a beam current of 1.5 nA and counted for 100 seconds. Data for chlorites, sericites and carbonates were recalculated using Minfile (Afifi and Essene, 1988). The absence of a suitable ankerite standard (i.e., a sample having known iron and magnesium contents) led to consistent overestimates of FeO and MgO as revealed by samples closing in excess of 100%. Therefore, data from carbonates should be considered as relative values in this study and by no means as absolute compositions. Also, insufficient data for tourmalines and the absence of an appropriate standard for this mineral does not permit generalizations to be made upon their compositions.

1.4 Oxygen Isotopes

All oxygen isotope analyses were performed by L. D. Hoy, Département de Génie Minéral, École Polytechnique. Oxygen was extracted from powdered whole-rock samples through reaction with BrF_5, using a similar method as that described by Clayton and Mayeda (1963). Values for $\delta^{18}O$ are reported relative to V-SMOW (Baertshi, 1976). Error estimates are $\pm 0.2‰$ based on repeated simultaneous analyses of the V-SMOW standard.

CHAPTER 2

GEOLOGY

2.1 Introduction

The following geological data are based mainly on internal Cominco reports by Tessier (1991a, 1991b) and Moore (1990). Field observations made by the author during the summer of 1991 also contributed to geological descriptions. Most of the 1991 summer field work was focussed on local alteration trends and their relationship to physical volcanology (i.e., the physical attributes and relationships between volcanic units or facies).

2.2 Regional Geology

The felsic to intermediate, Archean-age volcanic rocks at Normetal are located within the central part of the Abitibi greenstone belt within the Joutel-Normetal volcanic complex (Goodwin and Ridler, 1970). More precisely, they are situated within the Gale Group (Latulippe, 1976).

The volcanic rocks trend northwest, southeast (Fig. 3) and dip steeply to the north (Moore, 1990; Tessier, 1991a). Stratigraphic tops are generally interpreted as facing

south, implying an overturned volcanic pile. Evidence to support this attitude includes crude cross-bedding, in-filling of local depressions and large-scale clastic grading of individual beds. Such indicators of polarity are rare, but appear to support this interpretation (Tessier, 1991a), as does metal zonation within the deposit (Brown, 1948, Bertrand and Hutchinson, 1973).

This volcanic pile, including at least one local relatively small high-level felsic synvolcanic pluton, the Lac du Dome (LDD) intrusion, wraps around the edge of a large unnamed granodioritic pluton to the north, parts of which, if multistage, may post-date the overlying strata to the south. This large intrusion (Fig. 3) is referred to informally as the Normetal pluton (Tessier, 1991a).

The VMS deposits of the Normetal camp are hosted in the upper part of a transition zone (termed the Mine Sequence; see Fig. 3) lying between massive aphyric rhyolite and overlying andesites (Tessier, 1991a; Moore 1990). A silty to argillitic sedimentary unit separating underlying rhyolite from the Mine Sequence has been traced by geologists at Cominco for a number of kilometres on either side of the Normetal deposit and constitutes a valuable stratigraphic marker (see Fig. 4).

In addition to the footwall chlorite-magnetite alteration, a highly conformable sericite-chloritoid-chlorite-ankerite mineral assemblage characterizes the Mine Horizon

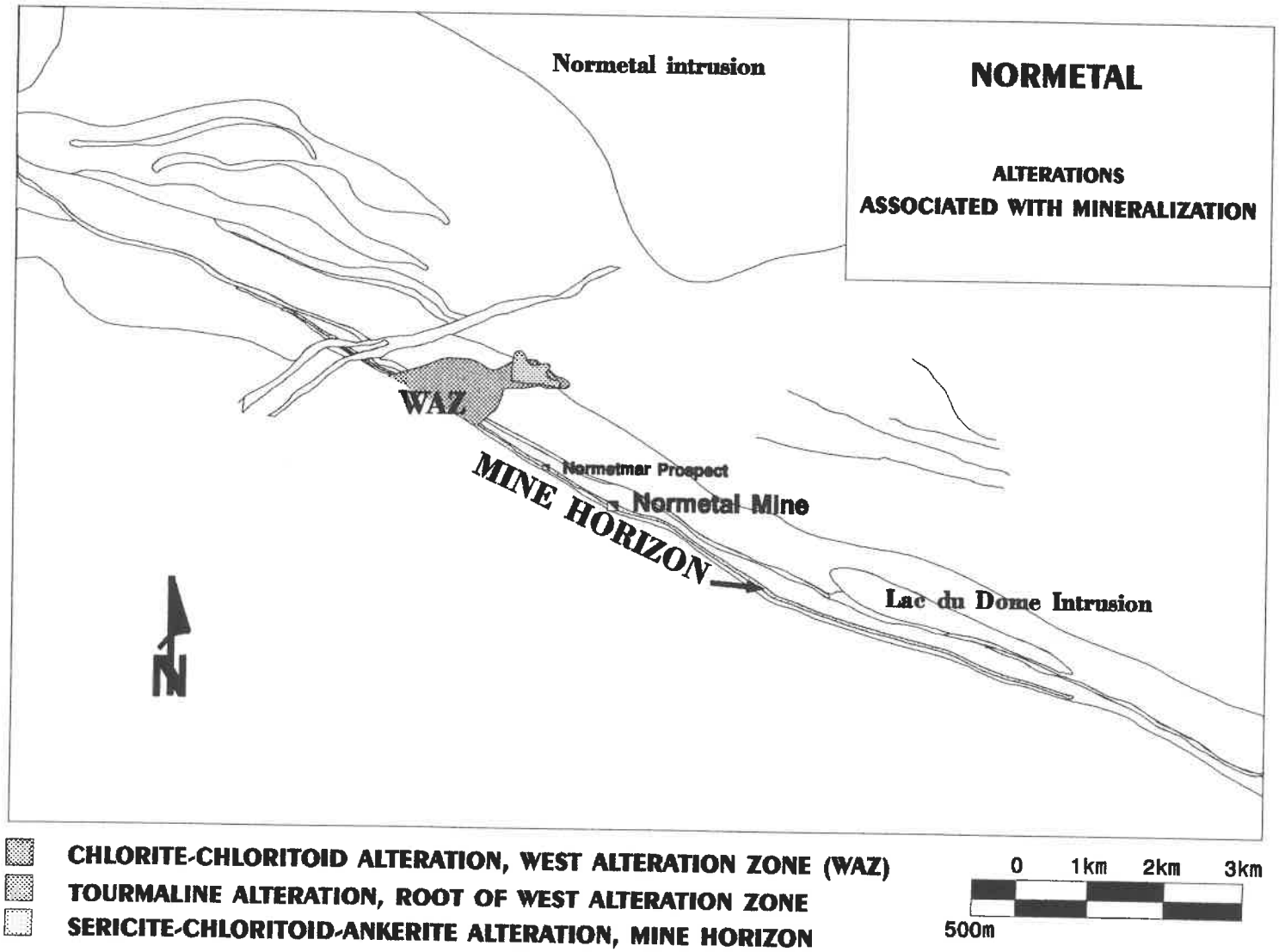

Figure 4: Dominant alterations associated with mineralization in the Normetal camp.

within the Mine Sequence. This horizon can be traced for greater than 10 kilometres on either side of the Normetal deposit. Extensive silicification and local tourmalinization are also dominant forms of alteration. Mapping of mineral isograds has enabled geologists at Cominco to define zones of conformable and of cross-cutting alteration, possibly of synvolcanic nature. Replacement of chloritoid by staurolite (at depths greater than 1525 m) is interpreted by Bertrand and Hutchinson (1973) as a transition from upper greenshist to amphibolite facies.

North-south flattening and steeply dipping elongation lineations of clasts is common throughout the region. This vertical stretching, locally reaching averaging geometrical ratios of 1:5:25 (Tessier, 1991a), is believed to be responsible for the geometry of the similarly elongate Normetal and Normetmar deposits.

2.3 The Normetal Deposit and Normetmar Prospect

Two deposits in the Normetal volcanic belt have physical and alteration characteristics common with the Mattabi-type subgroup of volcanogenic massive sulphide deposits, as described by Franklin et al. (1975), Morton and Franklin (1987) and Morton (1990). These deposits are the Normetal orebody, mined continuously from 1937 to 1975, and the much smaller, mostly sub-economic Normetmar prospect. The former produced some 11,140,778 tonnes grading 2.15% Cu, 5.12% Zn, 0.549 g/t Au, 45.25 g/t Ag and

666,838 tonnes of pyrite concentrate (Moore, 1990). The smaller Normetmar satellite lens yielded approximately 40,000 tonnes grading 9% Zn during 1990 (Tessier, 1991a). The Normetal deposit extended, downplunge, to a length of 2500 m, with a strike-length varying from 213 to 305 m and a thickness varying from 9 to 18 m (Tessier 1991a). Stringer chalcopyrite associated with intense chloritic alteration, as well as chlorite and magnetite (accompanied by garnet at depth) alteration on the north (footwall) side of the deposit, probably represent a feeder or pipe-like alteration zone (Sangster, 1972). These features imply proximal deposition (Moore, 1990). This alteration type is possibly the product of a channeled flow of hydrothermal fluids (probably modified seawater) driven convectively by an underlying heat source (Franklin et al., 1981). Broader, less well-defined sericitic and iron-carbonate mineral assemblages may represent semi-conformable alteration on a regional scale (Gibson et al., 1983; Groves, 1984; Morton and Franklin, 1987) produced by a large-scale hydrothermal reservoir. Clearly defined metal zoning within the deposit, with a predominance of copper to the north versus zinc to the south (Bertrand and Hutchinson, 1973), combined with intense alteration to the north of the deposit and an increasing level of differentiation in rhyolitic units toward the south (Cattalani and Bambic, 1991), suggests a southward younging direction.

2.4 Stratigraphy

The recognition of a sedimentary unit (Moore 1990) separating aphyric rhyolite

from the transition zone and hosting the Normetal and Normetmar deposits has been extremely helpful in establishing the stratigraphy on a regional scale, particularly in areas with little outcrop. This sedimentary unit had previously been recognized only sporadically and where so, it was described as dark tuff. The following descriptions of stratigraphic units are adopted directly from Tessier (1991a), and are defined in order from north to south, i.e., in the younging direction (see Fig. 2).

2.4.1 Basal Unit:

A basal unit consisting of locally amygdaloidal, massive and locally pillowed basaltic to andesitic flows, having a total minimum thickness of 1 km, forms the base of the volcanic pile. These flows are intruded to the north by the Normetal granodiorite pluton and to the northwest by the Paton River monzonite pluton. Minor local quartz or quartz-feldspar porphyritic units are interbedded with the basal unit. These porphyritic bodies are each less than 100 m thick.

2.4.2 Western rhyolites:

Two rhyolite units, each up to 1 km thick, lie some three to nine kilometres west of Normetal. These units probably represent deposits formed within a basin-like structure or small caldera. The lower rhyolite includes a thin (<50 m thick) intercalated mafic flow. Both rhyolites are quartz porphyritic with local feldspar phenocrysts, and are separated by

less than 200 m of massive and locally pillowed amygdaloidal andesite flows. Heterolithic lapilli tuffs and bedded crystal tuffs are observed at the top of the upper unit.

2.4.3 Eastern rhyolites:

Two rhyolite units occur to the east of Normetal. Both of these rhyolites, as well as those to the west (section 2.4.2), are hosted within the basal unit. Although these units resemble the previously described rhyolites that lie west of Normetal, no physical evidence has been found to correlate them. The stratigraphically lower of the eastern rhyolites is aphyric and lies some 4 to 5 km east of Normetal, with a thickness possibly reaching 600 m. The overlying rhyolite, occurring 1 to 10 km east of Normetal, is quartz porphyritic. This second rhyolite appears to reach a thickness of some 550 m. Although there are few quality exposures of these two rhyolites, those available show a greater component of fragmental facies or pyroclastics in comparison to those to the west.

2.4.4 Transition Zone:

Overlying the basal mafic unit is a transitional unit, consisting of intermediate flows interbedded with felsic rocks, which is referred to as the transition zone. This unit has been mapped over a distance of six km northwest of Normetal. Its thickness reaches some 500 m, including individual flows varying in thickness from 20 to 200 m. The intermediate component consists dominantly of massive to locally pillowed, amygdaloidal andesites interbedded with quartz and locally with quartz-feldspar porphyritic rhyolite flows.

Contacts between individual flows typically exhibit strong silicification and sericitization, and are commonly host to pyritic fragmental units reaching 15 m in thickness. These flows typically contain 5 to 15% nodular, fragmental, stringer and/or disseminated pyrite and may extend laterally up to 1 km.

2.4.5 The main rhyolite sequence:

This unit, with a total thickness ranging from 400 to 800 m, has been traced laterally over a distance of some 27 km overlying the previously described transitional zone. It has been divided into a lower (200 to 600 m thick) quartz porphyritic rhyolite, separated from the overlying aphyric rhyolite by a pyritic fragmental unit (3 to 4 m thick) known as the Jacmar horizon. The upper aphyric rhyolite is commonly referred to as the "super rhyolite" due to its high silica content (average 80% SiO_2). These rhyolites commonly display flow banding and autoclastic breccias. The aphyric rhyolite grades rapidly into a deformed lithic lapilli tuff and tuff breccia facies close to the Normetal deposit (between 500 m west and 1 km east of the deposit). The Jacmar horizon has been traced for only 500m along strike.

2.4.5 Argillites:

Thin pyritic and graphitic argillites have been recognized within the upper part of the aphyric rhyolite. These may contain up to 40% nodular pyrite, 15% graphite and/or minor quantities of sphalerite.

2.4.6 LDD intrusion:

This coarse-grained quartz-feldspar porphyritic intrusion was intersected by drilling in the upper part of the aphyric rhyolite east of Normetal. Ground magnetic data suggest an approximate thickness of 450 m for this intrusion, but its continuity at depth is still unknown. If its lenticular geometry reflects vertical elongation as is observed in many other geological entities of the Normetal camp, it may be of considerable volume. From its coarse-grained nature and its effects upon the Mine Horizon (discussed further below) the porphyry is believed to be a small high-level synvolcanic intrusion .

2.4.7 Main sediments:

A generally narrow band of silty to argillitic sediments, referred to as the "main sediments", is in direct contact with the underlying main rhyolite sequence. The thickness of the sediments averages around 50 m, but this thickness is believed to increase past some 8 km east of Normetal based on surface magnetic data. The sediments commonly grade from sandy siltstones composed of reworked rhyolitic material at the base, to mudstones or argillites up-section. Their presence suggests a significant time break between periods of volcanism. The sediments have proved to be of great value as a stratigraphic marker horizon. The unit appears to be continuous over the length of the main rhyolite sequence, with the exception of the area over the LDD intrusion some 2.5 to 6 km east of Normetal and in the footwall of the Normetal deposit.

2.4.8 Mine Sequence:

A transition zone composed of intermediate to felsic flows (many exhibiting fragmental textures, others appearing more massive) overlies the main sediments. This transition, referred to as the Mine Sequence, is host to the Mine Horizon located in the upper part of the Mine Sequence. The entire transition section reaches a thickness of some 350 m, and is intruded by a large number of diorite sills. The Mine Sequence generally consists of highly altered lapilli tuffs, tuffs, and tuff breccias which appear to be of a pyroclastic and/or epiclastic origin, and which also tend to be highly deformed such that primary textures are locally obliterated. The Mine Horizon is characterized by a quartz-sericite-chloritoid-ankerite assemblage. Intermediate tuffs commonly overlie the Mine Horizon.

2.4.9 Hangingwall felsic flows:

Some felsic flows have been recognized directly overlying the main sediments, interbedded with more intermediate flows of the Mine Sequence.

2.4.10 Hangingwall soda-rhyolite:

A large magnetic rhyolite body of distinctive sodic composition overlies the Mine Sequence between three and nine kilometres west of Normetal. In the absence of the Mine Sequence, the rhyolite, directly overlies the Main sediments. Recent data (personal

communication; Moore, 1992) suggest that this rhyolite, termed soda-rhyolite, may be intrusive. Also, smaller quartz-feldspar porphyritic rhyolite domes generally overlie but locally truncate the Normetal deposit (Brown, 1948). These rhyolites may be co-genetic with the soda-rhyolite (Moore, 1990).

2.4.11 Hangingwall andesites:

Some 800 m or more of massive, pillowed, amydaloidal and feldspar porphyritic andesites overlie the transition zone which is host to the Mine Sequence.

2.5 Cross-Cutting Alteration

Part of the mapping priorities set out by Cominco geologists included the mapping of specific minerals for the purpose of defining alteration isograds (Fig. 4). Other than the highly conformable Mine Horizon with its characteristic sericite-chloritoid-ankerite assemblage, a few other crosscutting alteration features were defined. Chloritoid and tourmaline occurrences proved to be quite useful in defining local isograds, compared to ankerite and sericite which are regionally pervasive.

A chlorite-rich alteration zone is directly associated with the immediate footwall (rhyolite) of the Normetal deposit and is described by Brown (1948), Bertrand and Hutchinson (1973) and Moore (1990). It is characterized by intense sericitization and chloritization associated with stringer chalcopyrite in the immediate footwall, as well as

lesser amounts of chloritoid and magnetite (accompanied by garnet at depth) alteration. An abundance of iron carbonate is also obvious from the rusty brown weathering of outcrops (Brown, 1948). The chlorite-rich alteration zone was unfortunately not sampled in this study due to absence of equivalent surface exposures. Intense structural flattening, with possibly associated minor transposition of stratigraphic units and generally minor mineralization in alteration zones (common for Mattabi-type deposits; Franklin, 1990), may account for the lack of distinct crosscutting footwall alteration in outcrops surrounding the Normetal mine.

The Normetmar prospect, on the other hand, clearly shows cross-cutting ankerite and chloritoid alteration, that cut the volcaniclastic and/or epiclastic horizons underlying the deposit, the sericitic felsic tuff/lappilli tuff hosting this small deposit, and continuing with lesser intensity into overlying andesites. A highly silicified, cherty felsic unit directly underlies the mineralized horizon.

A large alteration zone located between 1 and 3 km to the west of Normetal, known as the West Alteration Zone (WAZ) is also of interest to this study. Its root starts at the base of the transition zone and extends stratigraphically upwards towards the southwest through the Mine Sequence into the overlying andesite. It is characterized by abundant ankerite, sericite, local chloritoid occurrences and vein to stringer-like sulphides (including pyrite, sphalerite and chalcopyrite, in order of abundance) associated with

dark-green, relatively magnesium-rich chlorite. A tourmaline isograd was also defined along the base of this alteration zone. Like the alteration zone below the Helen siderite deposit of the Michipicoten area (Morton and Nebel, 1984), the WAZ tapers downward (i.e., similar geometry) and is similar in surface and dimensions. This large alteration zone has been considered as a possible crosscutting alteration zone for the Normetal deposit, but evidence given in further chapters shows that sufficient geochemical alteration exists directly below the Normetal deposit to explain its formation without the need to call upon a spatially separate and/or distant alteration zone.

CHAPTER 3

WHOLE-ROCK GEOCHEMISTRY

3.1 Introduction

In order to compare geochemical variations associated with proximity to the Normetal deposit, the methodology described by MacLean (1990) for mass change calculations was followed. It has been applied to the Phelps Dodge deposit by MacLean and Kranidiotis (1987), MacLean (1988), and by Cattalani et al. (1990a, b), as well as to selected areas of Normetal by Cattalani and Bambic (1991). This methodology permits the user to determine 1) the precursor composition of specific components (i.e., the original content of components at the reference state of alteration equivalent to that of least-altered samples), 2) a reconstructed composition (defined below), and 3) the net mass change.

Under conditions of mass loss or mass gain, ratios of so-called immobile elements are believed to remain relatively stable (MacLean 1990; Finlow-Bates and Stumpfl, 1981). If the precursor composition of a rock is known, it is relatively simple to calculate the net change in mass. To do this, we first find the reconstructed composition (see Fig. 5) by multiplying the concentration of the component in question in an altered rock by the ratio of the immobile monitor element in precursor vs. altered rock (MacLean 1990), i.e.,:

$$\left(\text{Reconstructed Composition} = \%\ \text{Component in altered rock} \times \frac{\%\text{Monitor Element in Precursor}}{\%\text{Monitor element in Altered Rock}}\right).$$

Finlow-Bates and Stumpfl (1981) showed that suites of altered rocks would plot along a straight line alteration path on TiO_2 vs. Zr graphs (Fig. 6). Movement on this path towards the origin represents dilution of immobile elements and therefore overall mass gain for an altered sample, or conversely, movement away from the origin indicates enrichment of immobile elements caused by overall mass loss during alteration.

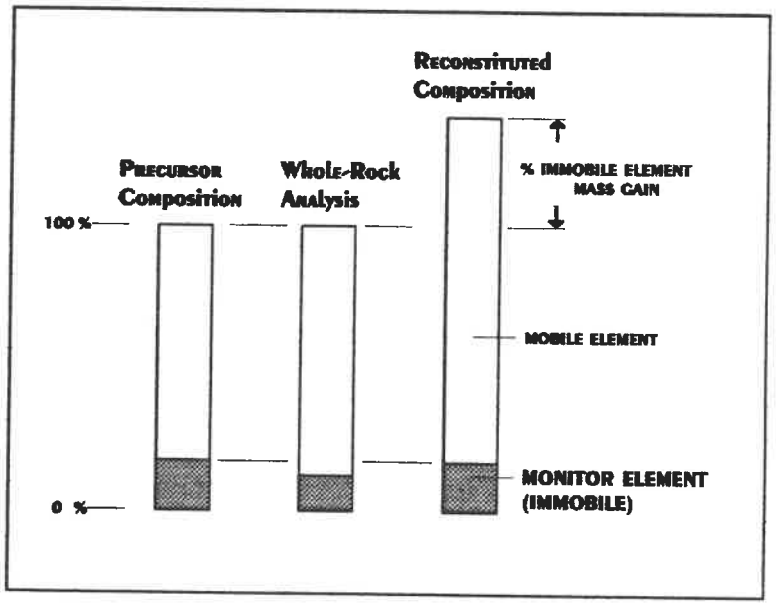

Figure 5: Graphic representation of calculations involved in reconstructing compositions after mass change, based on Maclean (1990).

When the original precursor of the altered rock is not known, or when dealing with multiple precursor systems, it may still be possible to apply this technique if the associated rocks show predictable fractionation trends. To follow this more complex procedure

requires a good knowledge of the fractionation trend of the rocks studied. Fractionation trends can be shown by plotting a compatible element against an incompatible element. While a compatible element crystallizes out in early minerals forming in a magma chamber, it should be depleted in later magma fractions, whereas an incompatible element is enriched in the residual liquid. Alteration paths trending toward the origin should transect this predictable fractionation trend at the precursor composition (Finlow-Bates and Stumpfl, 1981; MacLean and Kranidiotis, 1987; MacLean, 1990). This procedure provides us with the original precursor composition and allows for calculations of mass changes without exact prior knowledge of the original precursor.

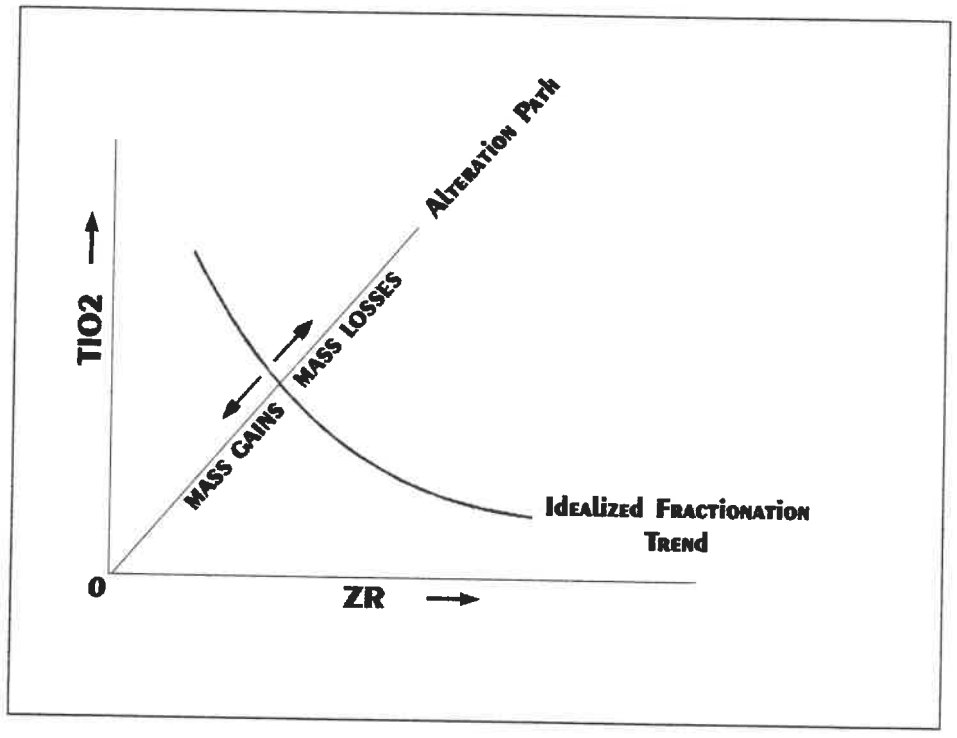

Figure 6: Plot of idealized fractionation trend on TiO_2 vs. Zr graph, showing alteration path, after Finlow-Bates and Stumpfl (1981).

In the application of the above procedures, verification that immobile elements are in fact consistently immobile is highly recommended. The possibility that so-called incompatible elements become compatible by over-saturation during magma fractionation requires that such elements be tested against other immobile elements (Cattalani and Bambic, 1991). However, once an immobile element has been verified as a reliable monitor element, fractionation trends for various mobile components can be confidently plotted against immobile monitor elements to determine their individual fractionation trends. Again, the alteration line through the origin of Figure 6 intersects the fractionation line at the precursor composition.

Having determined the reconstructed composition and the precursor composition, the mass change (in wt.% added or gained) is equal to the difference between the reconstructed composition and the precursor composition (MacLean, 1990; Fig. 5). It is important to remember that mass changes calculated in this way represent the sum of changes that may be incremental or related to multiple episodes of alteration and/or metamorphism. To alleviate these ambiguities, precursor compositions and mass changes have been plotted relative to proximity to the Normetal deposit to permit identification of those variations most directly associated to alteration and/or mineralization.

3.2 Regional Geochemistry

Most major-element rock classification diagrams are dependent on Na_2O, K_2O and

SiO_2 contents. Because these elements may be mobile during metamorphism and hydrothermal alteration, great care must be taken, if protoliths are to be identified, to select samples showing the least possible alteration. Least-altered samples of the rhyolite and dacites, stratigraphically beneath the sedimentary unit (see Appendix 2-1), and a compilation of least-altered Mine Sequence rocks (see Appendix 3-1), were first used to classify the rocks of this study. To improve the data base, calculated precursor compositions (see MacLean, 1990, and explanations above) were also used to help classify rocks according to their magmatic affinities (see Appendix 2-7 and 3-6).

All analyses clearly fall within the sub-alkaline series on diagrams of $Na_2O + K_2O$ vs. SiO_2 (Figs 7a and b). The division into tholeiitic vs. calc-alkaline series is more problematic, particularly for the Mine Sequence and Mine Horizon rocks which plot directly upon and/or to either side of the division for tholeiitic vs. calc-alkaline series on an AFM diagram (Figs. 8), indicating a transitional affinity. Felsic rocks underlying the sediments tended to be more differentiated and show calc-alkaline affinities, although a few samples plot in the transitional area.

From all data considered (including data for the LDD intrusion, Appendix 4-1), a generally linear trend is seen from tholeiitic to calc-alkaline affinities on an AFM diagram (Fig. 9), suggesting a possible co-magmatic origin for all of the rocks analyzed. Rocks of

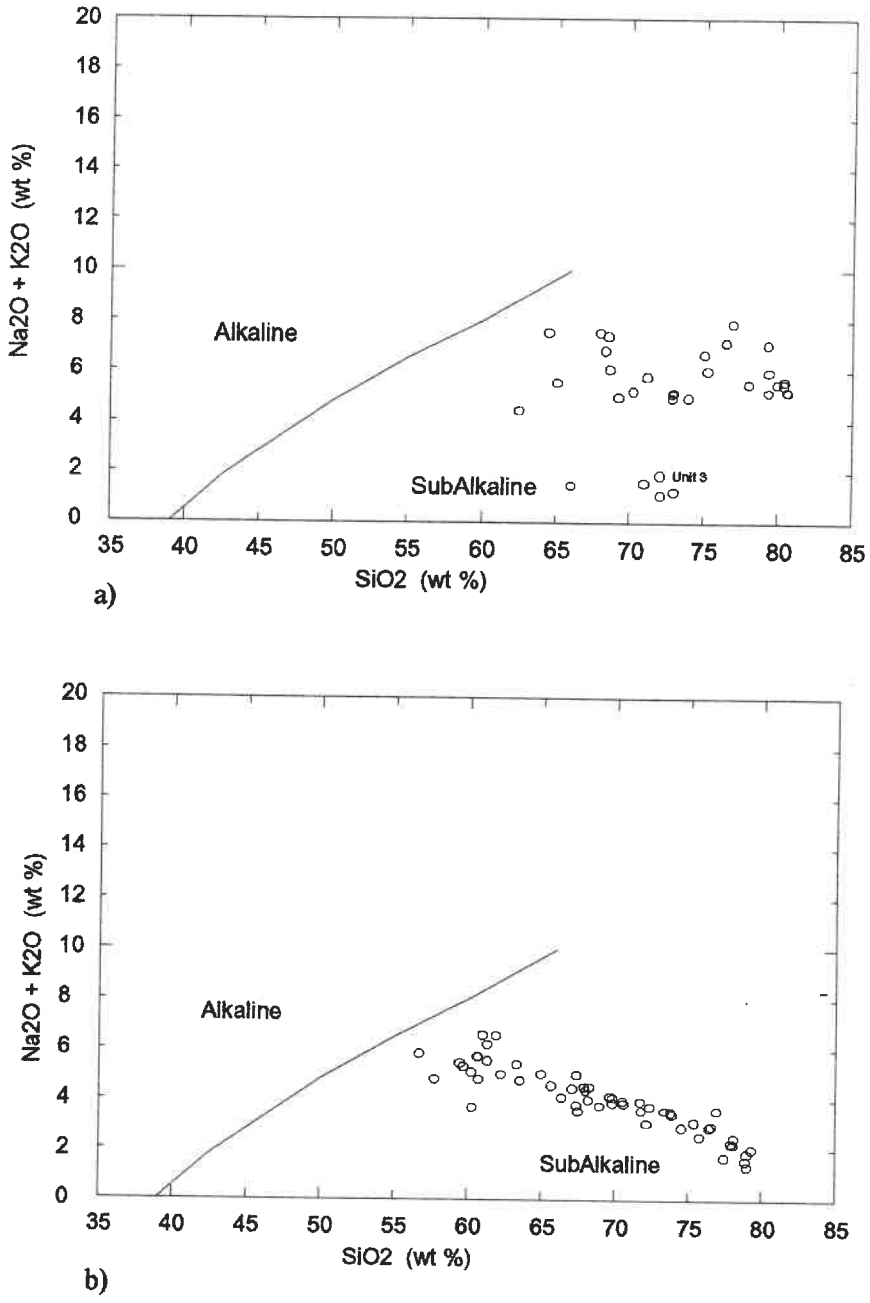

Figure 7: Plots of $Na_2O + K_2O$ (wt%) vs. SiO_2 (wt%) on alkaline and subalkaline fields (Irvine and Baragar, 1971) for a) combined felsic rocks underlying sediments and b) Mine Sequence, including the Mine Horizon.

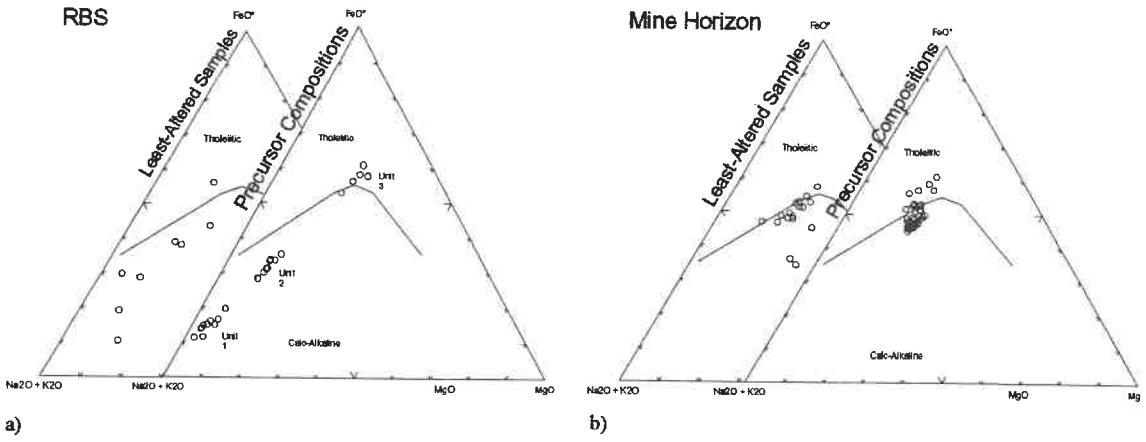

Figure 8: Ternary AFM plots on tholeitic and calc-alkaline fields (Irvine and Baragar, 1971), separated into least-altered and calculated precursor compositions for a) RBS and b) Mine Horizon. FeO recalculated by Newpet (Clarke, 1990).

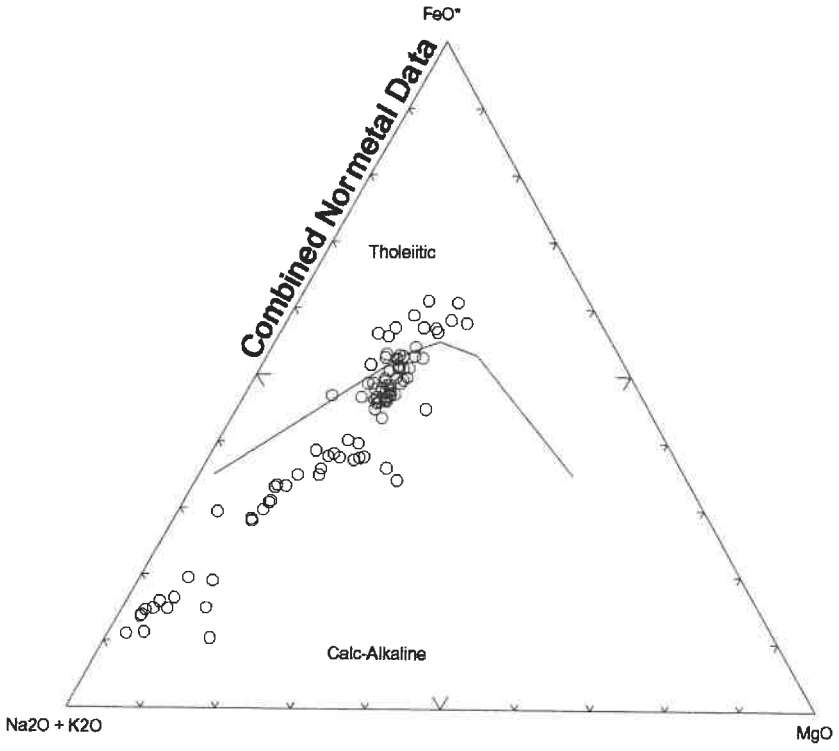

Figure 9: Ternary AFM plot of combined Normetal data onto tholeiitic and calc-alkaline fields (Irvine and Baragar, 1971).

the Mine Sequence (combined Mine Sequence and Mine Horizon precursors) show a much more linear plot on alkali ($Na_2O + K_2O$ vs. SiO_2) diagram (Fig. 7b) than do combined felsic rocks underlying the sedimentary sequence (Fig. 7a), i.e., Mine Sequence rocks show a more constant alkali depletion with increasing silica content. Combined felsic rocks underlying the sedimentary sequence (Figure 7a) plot both above and below the tight linear Mine Sequence set.

Classifications using high-field-strength (HFS) elements, such as Ti and Zr, which are believed to be relatively immobile during metamorphism or hydrothermal alteration (Finlow-Bates and Stumpfl, 1981; Lesher et al., 1986; MacLean and Kranidiotis, 1987; MacLean, 1990), may thus be more useful. Since Zr precursors are of questionable significance in this study (see section 3.4), only combined least-altered samples (Mine Sequence and felsic rocks underlying sediments) were plotted on a SiO_2 vs. Zr/TiO_2 diagram (Winchester and Floyd, 1977, Fig. 10). This diagram also shows a generally alkaline nature for most of the data, with only a few samples plotting as mildly alkaline trachyandesites and one as a commendite/pantellerite (sample 10811); silica depletion of a rhyolite could explain the anomalous position of this last sample. A wide range of Zr/TiO_2, with compositions ranging from andesites to highly siliceous rhyolites, suggests a high degree of differentiation for Normetal rocks, if these are indeed co-magmatic. A further series of diagrams showing rather well-defined fractionation trends for both the least-altered Mine Sequence rocks (Appendix 3-3), and for the least-altered RBS samples

(Appendix, 2-3), also support the earlier suggestion that both data sets represent, a least, separate co-magmatic series.

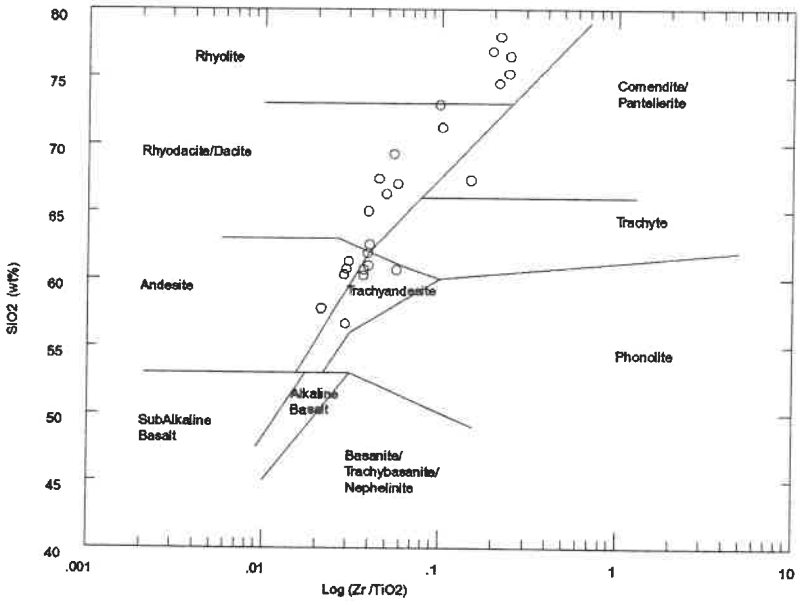

Figure 10: Plot of SiO2 vs. Log (Zr/TiO2) for combined least-altered samples on delimited fields for common volcanic rocks (Winchester and Floyd, 1977).

3.3 Lac du Dome (LDD) QFP Intrusion

The Lac du Dome quartz-feldspar porphyry intrusion east of Normetal, as for all other samples considered in this study, clearly falls within the sub-alkaline field (Appendix 4-2). It shows little alteration megascopically and can therefore be characterized using major elements. Its position on an AFM plot clearly indicates a calc-alkaline affinity (Appendix 4-3). The LDD intrusion is intermediate with respect to the largely transitional rocks of the Mine Sequence, and it is highly evolved with respect to mostly calc-alkaline felsic

rocks below the sediments. An apparent trend towards more felsic members to the east is also worthy of mention (Appendix 4-4), although this suggestion is statistically non-conclusive for the limited data set. Nevertheless, diamond drill hole 18 compositions are clearly rhyolitic, whereas those of drill holes 12, 14, 16 and 20 are tightly grouped in the dacitic field (Appendix 4-2).

3.4 Rhyolites Below Sediments (RBS)

Before undertaking mass-change calculations for these rocks, a selection must be made of so-called immobile elements. MacLean's method (1990) normally calls for a compatible element to be plotted against an incompatible element such as Zr. However, Zr, normally an incompatible element, may be compatible in highly evolved calc-alkaline suites (Watson and Harrison 1983; MacLean, 1990). Verification of Zr incompatibility must be carried out to be certain that its fractionation is predictable if it is to be used as a monitor of fractionation.

For this purpose, four graphs were constructed from data for RBS samples (Appendix 2-2) to show the fractionation trends of Zr and TiO_2 against Al_2O_3 and SiO_2. The first two graphs (Al_2O_3 vs. Zr, and SiO_2 vs. Zr) show a positive correlation for Al_2O_3 vs. Zr and a negative correlation for SiO_2 vs. Zr. These trends are contrary to expected trends if Zr is incompatible because Zr should increase with decreasing Al_2O_3 in this range

and should increase with increasing SiO_2 if it is incompatible. Graphs of Al_2O_3 vs. TiO_2 and SiO_2 vs. TiO_2 also show positive correlations between Al_2O_3 vs. TiO_2 and Al_2O_3 vs. TiO_2. Contrary to the previous graphs, these trends are normal for TiO_2 which is usually incompatible. Therefore, these data suggest that Zr behaved in a compatible way for these rhyolites and that zircon precipitation may have occurred in the RBS. For this reason, the Al_2O_3 vs. TiO_2 diagram, as opposed to the TiO_2 vs. Zr diagram, is used to evaluate reconstructed compositions for the RBS.

Having established the proper immobile element suite, the next step in evaluating mass changes is to determine primary fractionation trends so as to be able to identify or at least approximate precursor compositions. The compilation of least-altered samples from the RBS was used for this purpose (Appendix 2-1). Data from five samples from Cattalani and Bambic (1991), one sample from Hasik (1991) and two from the present study were used in this compilation (samples 10148, 10195, 10036, 10228, 10033, VH-90-07, 10752 and 21575, respectively). Least-altered samples were identified by Cattalani and Bambic (1991) as those with low K_2O, low LOI and "reasonably normal values of Na_2O, CaO, Fe_2O_3, MgO and SiO_2". Samples from Hasik (1991) and from this study were chosen from petrographic descriptions as having fresh or at least relict plagioclase. With these data, Al_2O_3, SiO_2, Fe_2O_3, MgO, CaO Na_2O, K2O and MnO vs. TiO2 diagrams were constructed (Appendix 2-3).

Fractionation trends for these components have best line fits trending towards the left for increasingly differentiated rocks (TiO_2-depleted magma). Precursor compositions of altered samples are found by finding the intersections of best line fits with lines passing through the origin and through points representing the compositions of given samples (Fig. 6). Fractionation trends are then traced upon similarly constructed graphs of altered samples. For compatible elements having fractionation trends converging towards the origin (Fe_2O_3, MnO, CaO and MgO), new graphs were constructed to eliminate errors due to the near parallel trends of narrowly intersecting lines (Appendix 2-4). These graphs were constructed using Al2O3/TiO2 for the horizontal axis. Because both Al_2O_3 and TiO_2 are considered to be relatively immobile, alteration trends, on these graphs, are represented by vertical lines (i.e., by constant Al_2O_3/TiO_2 ratios). Their precursor composition is therefore equal to the y intercept of the best line fit. For linear trends, formulas were obtained using regression analysis with standard spreadsheet software. Curved trends were solved by graphical analyses.

3.4.1 Results

Three populations are distinguishable within the RBS data plotted on an AFM diagram of precursor compositions (Fig. 8a). By plotting their various components against east-west coordinates, the three populations are again distinguishable (Fig. 11). The first population (unit 1), consisting mainly of samples close to the Normetal deposit and further westward, has a highly consistent composition (SiO_2 = 77.7 ± 1%; Al2O3 =

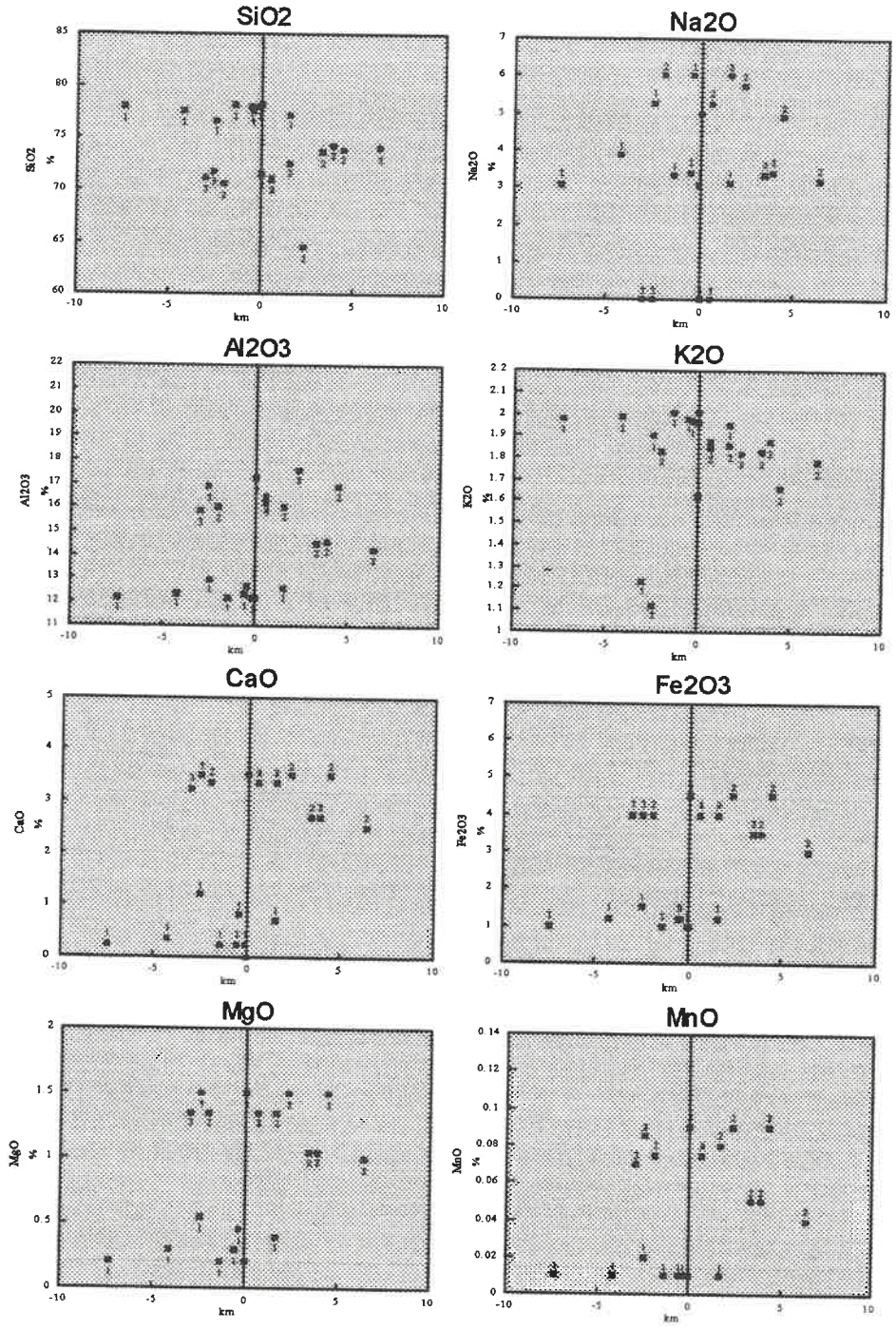

Figure 11: Plots of calculated precursor compositions for samples from the RBS; data labels refer to unit number; x-axis represents coordinates relative to the Normetal deposit at 0 km; coordinates increase towards the east and decrease towards the west.

12.4 ± 0.3%; Fe_2O_3 = 1.14 ± 0.35%) over a distance of at least 8 km. This consistent composition over such a large distance suggests emplacement by a uniform mechanism such as a widespread pyroclastic processes. This unit overlies both other less-clearly defined units (unit 2 to the east, and unit 3 proximally to the deposit to the west). Unit 2, unlike unit 1, appears to be laterally zoned, with silica increasing towards the east. Unit 3 may be related to unit 2, but it is essentially devoid of Na_2O and has highly variable K_2O values distinguishing it from unit 2 on the AFM diagram due to its lower alkali content. Unit 2 is the most consistently and progressively altered unit with respect to units 1 and 3 which show greater variabilities in mass changes (Fig. 12). This trend in unit 2 applies for Fe_2O_3, Na_2O, K_2O, CaO and MnO. SiO_2, on the other hand, shows a steady increase towards the Normetal deposit in unit 1.

The most striking trends observable, based on mass-change calculations for data from the RBS, are the intense silicification (up to 20% net silica gain with respect to its precursor) and potassium enrichment (>8% gain) with increasing proximity to the Normetal deposit. In fact, silica appears to be generally depleted at distances greater than three km from the deposit, suggesting a possible source for the silica addition near the ore deposit. Therefore the apparent silica depletion zone may represent a recharge zone. These trends are clearly distinguishable over distances on the order of km, consistent with modern concepts of the size of ore-forming systems for VMS deposition.

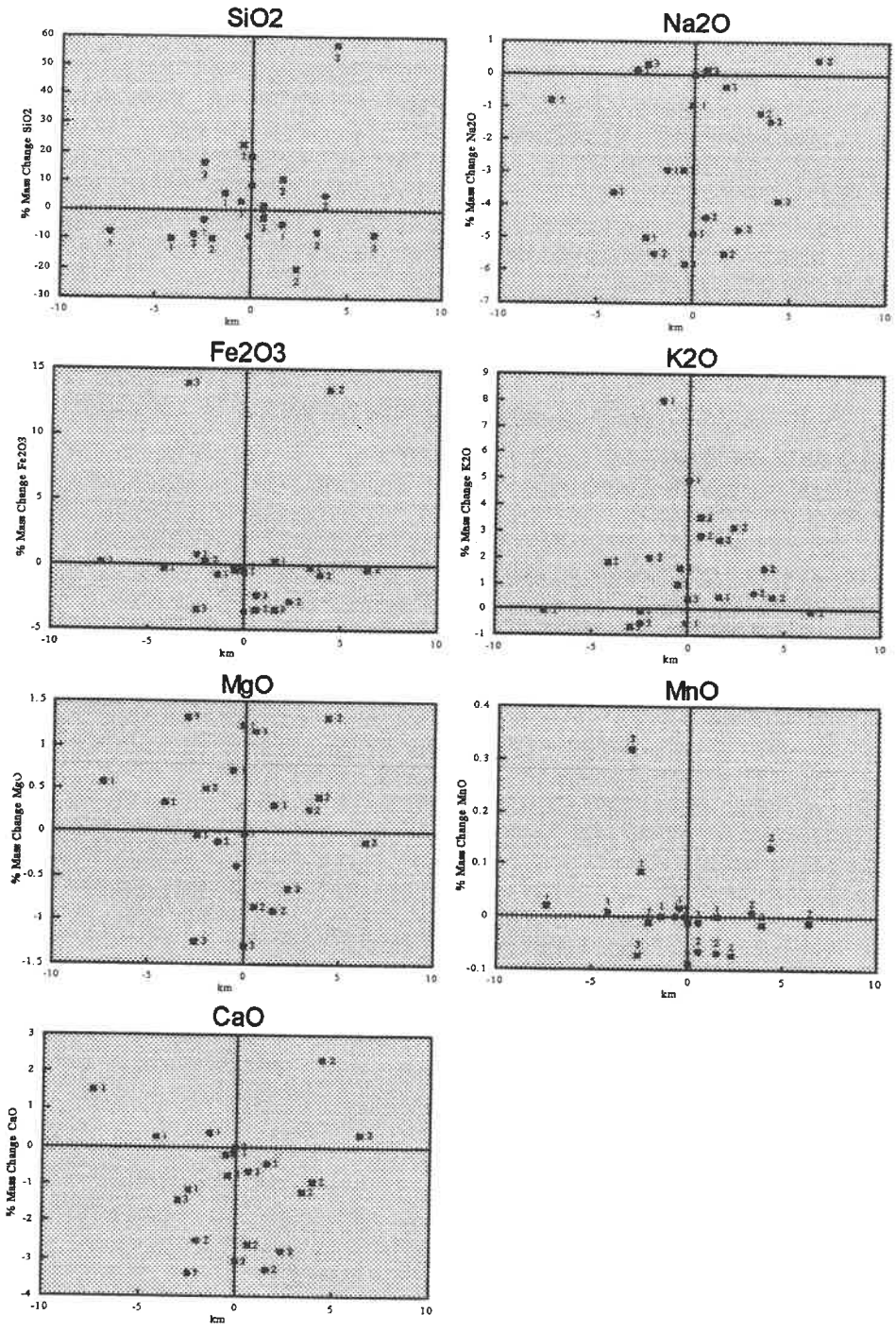

Figure 12: Plots of calculated mass changes in samples from the RBS; data labels refer to unit number; x-axis represents coordinates relative to the Normetal deposit at 0 km; coordinates increase towards the east and decrease towards the west.

The potassium enrichment curve is somewhat skewed, with abrupt increases from the west, as opposed to a gradual increase from the east. This skeweness is due in consistently increasing K_2O concentration unit 2 towards the mine from the east, with respect to more variable increases of unit 1 from the west.

Magnesium shows both higher-than-average and lower-than-average values in terms of mass changes with increasing proximity to the Normetal deposit. These data also show anomalously high values for MgO in cores from drill holes 5 and 6 (corresponding to the WAZ), and in cores from drill holes 99 and 1, and in surface sample T-90-19A (proximal to the Normetal deposit).

CaO and NaO appear to be variably but consistently depleted over the length of the RBS horizon. Sites of maximum CaO and Na_2O depletion are proximal to the Normetal deposit as well as in samples from drill hole 17 (WAZ). Unit 2 is notably more depleted in CaO than unit 1 (west). Sample No TS-48, from drill hole 14, shows a significant mass gain (silicification >50%), increased MgO, CaO and MnO, and Na_2O depletion. These highly anomalous deviations from the average may be due to the location of the sample directly over the LDD intrusion.

Iron becomes increasingly depleted in unit 2 with proximity to deposit from an eastward approach, whereas iron in unit 1 remains relatively constant with little mass gain

or loss. Exceptions include the anomalous increases in Fe_2O_3 noted in drill hole 5 (WAZ) and in drill hole 20 (LDD).

Manganese shows little variation near recognized mineralization or alteration other than a high 0.3% MnO gain in sample TS-72 located within the WAZ. Sample TS-72 (hole 25, WAZ) and sample TS-48 (hole 14, LDD) also display notable increases in MnO (>0.1%). Holes 1, 2 and 4 (all in unit 2) and surface sample VH-90-01 (Unit 3) show MnO depletion.

3.5 Mine Horizon

For the Mine Horizon, a compilation of data for least-altered samples of the Mine Sequence was carried out (Appendix 3-1) to identify fractionation trends and also, to verify the expected incompatibility of Zr. The fractionation trends established for the RBS were not used due to the possible time gap in volcanism marked by the intervening thick sequence of sediments. Potential least-altered samples were first chosen from diamond drill hole log descriptions. Samples were then selected on the basis of low LOI values and normal major-element compositions. Care was also taken to avoid samples directly overlying the LDD intrusion due to the possibility that large quantities of water may have been driven through overlying rocks by local thermal convection, possibly causing extensive local hydrothermal alteration.

Graphs for this data set were constructed using the same method as for data from the RBS described above (Appendix 3-2). Again, Zr fractionation was tested. For this data set, two dacites were found to plot within the andesite field on an Al_2O_3 vs. Zr diagram (indicating low Zr), whereas these samples plot within the dacite field or in a transitional field between rhyolites and andesites on an Al_2O_3 vs. TiO_2 diagram. These plots can be explained by simple depletion of Zr during fractionation. Data were also calculated separately based on a $Zr_{precursor}/Zr_{altered}$ ratios, leading to little variations in regional trends, but the data presented here were calculated from $Ti_{precursor}/Ti_{altered}$ to avoid possible error. The fractionation trends identified on the previous diagrams were then reproduced on similarly constructed diagrams representing altered Mine Horizon samples (Appendix 3-3). The apparent fractionation trends of the Mine Horizon appear to fit rather well with the previously interpreted trends suggesting co-magmatic differentiation of the Mine Horizon samples with those of the hosting Mine Sequence.

3.5.1 Results

Unlike rhyolites underlying the sediments, a wide range of precursor compositions (Fig. 13), suggests that, although the Mine Horizon is highly concordant, it obviously includes a wide range of distinct compositions and may therefore be of epiclastic nature. This heterogeneity does not present a problem for mass-change calculations as long as the epiclastic sediments were derived from a co-magmatic suite represented on composition diagrams by predictable magmatic fractionation trends as demonstrated above.

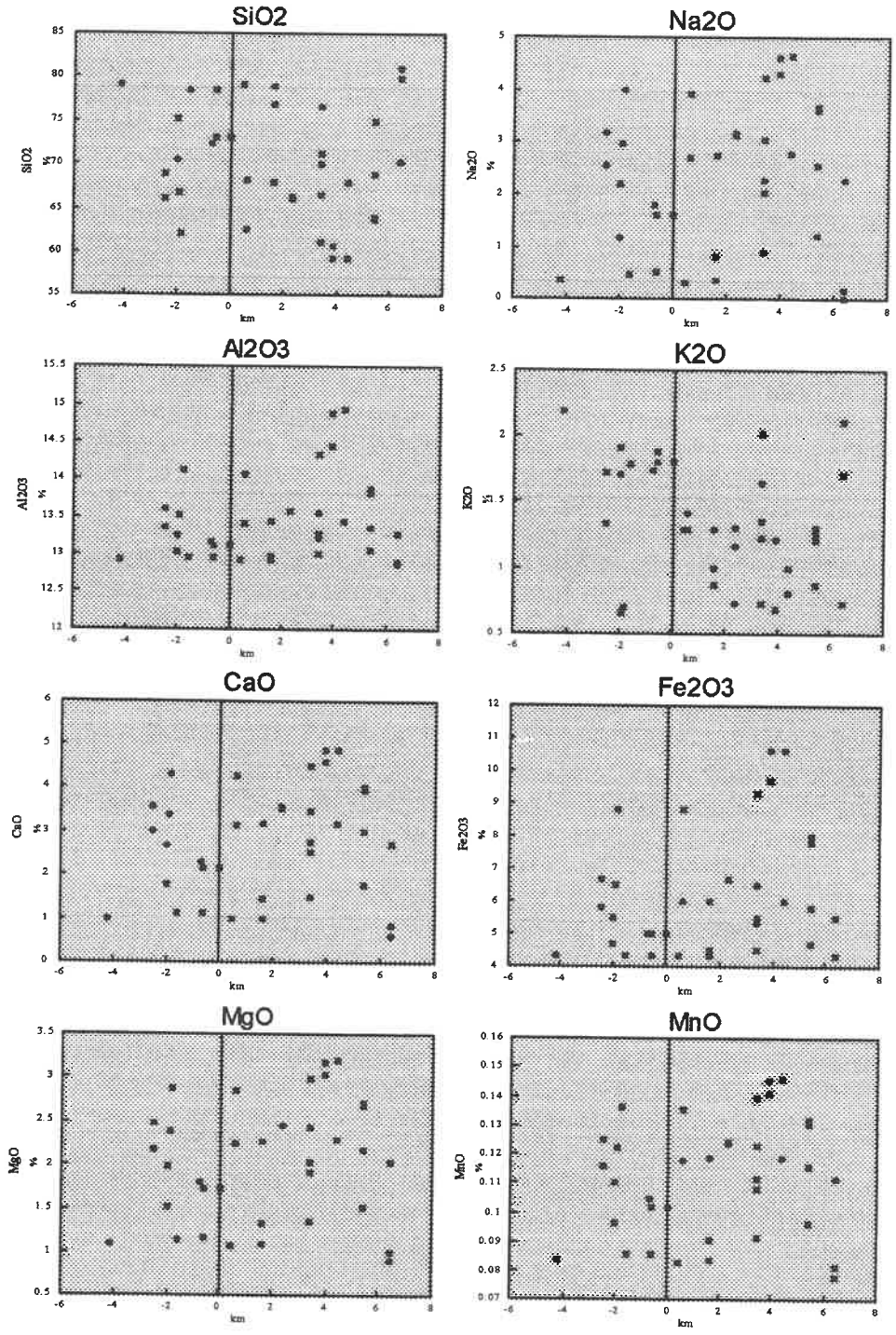

Figure 13: Plots of calculated precursor compositions for samples from the Mine Horizon; x-axis represents coordinates relative to the Normetal deposit at 0 km; coordinates increase towards the east and decrease towards the west.

Mass-change anomalies of various components within the Mine Horizon show much greater local variations compared to the RBS (Fig. 14). A net mass-change diagram and an almost identical SiO_2 mass-gain diagram clearly show SiO_2 as the main cause of significant mass gains and losses. Silicification greatly exceeding 10% was noted only in three samples: NMAR-90-05, a cherty sample, directly underlying the Normetmar deposit; TS-15 from drill hole 99; and TS-78 from drill hole 16. Nevertheless, SiO_2 gains of up to 10% occur near the Normetal deposit, and an increase in silica depletion (up to 20%), is noted at distances greater than 1 km from the deposit.

Fe_2O_3 clearly increases towards the Normetal deposit (up to 23% gain) and to the east of the LDD intrusion. Manganese mass variations show a high correlations with iron, with highest mass gains close to the Normetal deposit and to the east of the LDD. Magnesium is generally depleted, but high MgO is noted in both drill holes 99 and 28 (on either side of Normetal), as well as in drill hole 3 (1.6 km east of Normetal) and in drill hole 16 (overlying the LDD). Calcium is generally enriched significantly in the Mine Horizon, compared to the RBS which shows CaO depletion. High CaO gains are noted both in close proximity to the Normetal deposit and overlying the LDD. Inversely, values of highest calcium depletion also occur proximal to the Normetal deposit.

Sodium shows highest depletion values close to the LDD intrusion and in drill hole 17 within the WAZ. These trends are contrary to the RBS which show CaO and Na2O

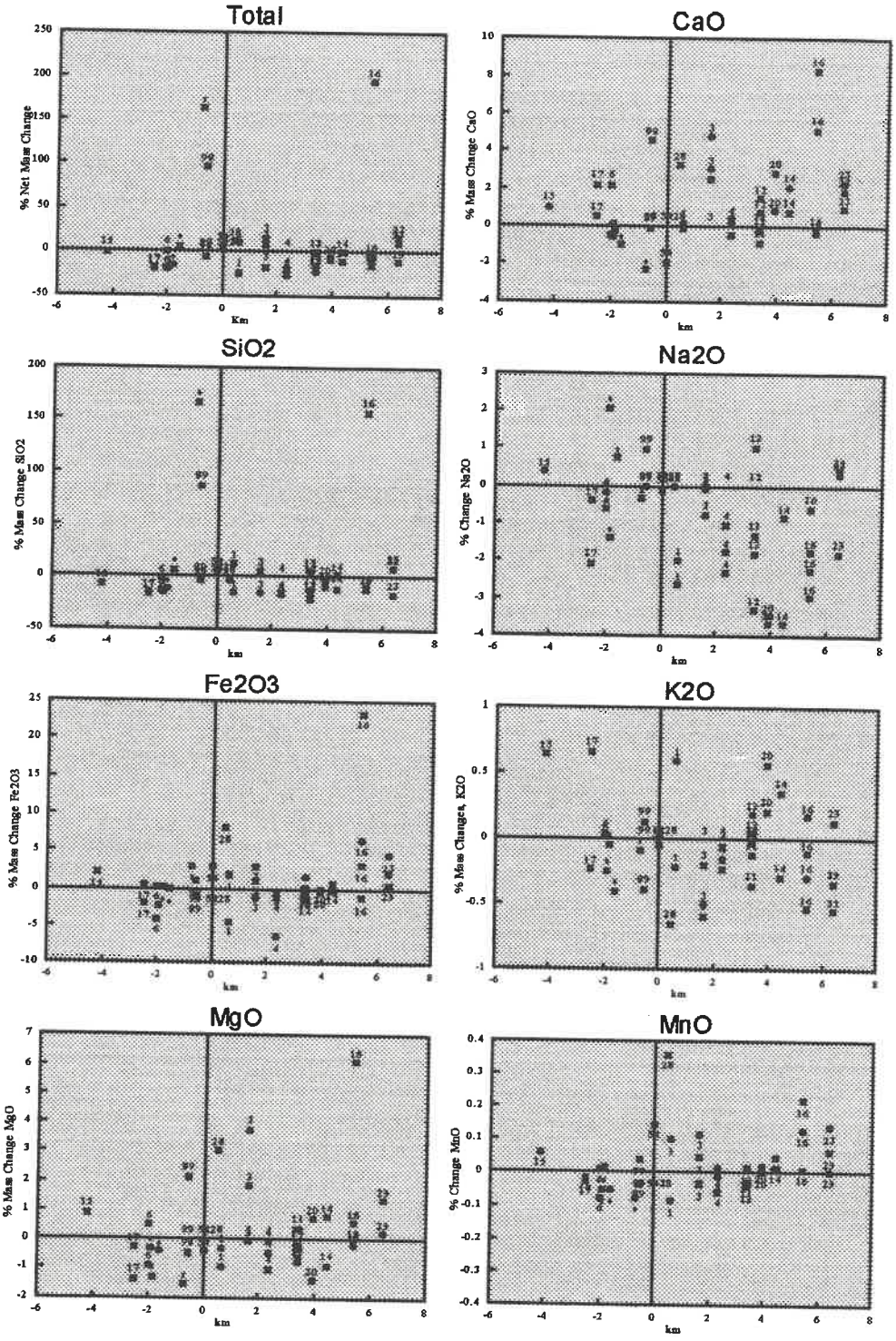

Figure 14: Plots of calculated mass changes in samples from the Mine Horizon. Data labels refer to drill hole number; x-axis represents coordinates relative to the Normetal deposit at 0 km; coordinates increase towards the east and decrease towards the west.

depletion in close proximity to the deposit. Potassium is highly variable, with highest mass-gain values above the LDD and west of Normetal in drill holes 17 and 15 (WAZ).

3.6 Discussion

Regionally increasing mass changes towards the Normetal deposit in the RBS, in terms of K_2O, Na_2O, SiO_2 and CaO, strongly suggest that regional fluid-flow patterns were focussed below the deposit. This interpretation is consistent with a VMS-type mineralization model which calls for convection of seawater driven by an underlying heat-source, with sulphide precipitation on the seafloor at points of exhalation (Sangster, 1972; Franklin et al., 1981).

The likelihood that variations in whole-rock data were produced by evolved seawater is supported by experimental studies by Hajash and Chandler (1981). They described the interaction of high-temperature seawater with rhyolite, andesite and other more mafic and ultramafic rocks. They found that leaching of K, Fe, Mn and Si occurred in rhyolites for temperatures between 200 and 500°C at a pressure of 1000 bars. Mg decreased in seawater during their experiments, whereas results for Na and Ca varied. Similar results were obtained for andesite. The pH of the solutions was found to vary primarily as a result of Mg-OH-silicate precipitation which significantly increases the H^+ concentration of the solution.

The first obvious observation that must be drawn from our data is the significant alteration of the Mine Horizon spatially associated with the LDD intrusion. This intrusion may have driven significant quantities of water through the Mine Horizon to produce the significant sodium depletion and the notable potassium enrichment that is observed in the Mine Horizon. Unfortunately, the timing of the intrusive's emplacement is uncertain and therefore these effects cannot definitively be concluded to have been produced by syn-volcanic hydrothermal convection.

A second possibility is that the alteration could be associated with the observed gap in the sediments above the intrusion which may inversely have permitted a draw-down of cold seawater. Increases in silicification, in iron concentrations, and in iron precipitates (notably oolitic siderite), as well as increases in magnesium and manganese to the east of the intrusion, suggest precipitation of exhalites and therefore a potential for VMS-type mineralization.

The inverse relationship between CaO and Fe_2O_3 depletion in the RBS and CaO and Fe_2O_3 enrichment in the Mine Horizon close to mineralization suggests that these components may have been mobilized by hydrothermal fluids from lower units and then precipitated by boiling or by mixing with cold seawater (Morton and Nebel 1984) at the seafloor (i.e., at the Mine Horizon). This deposition may have led to the observed local

occurrences of carbonate facies iron formations near the Normetmar deposit and to the east of the LDD intrusion.

Silica within the RBS is enriched below the Normetal deposit but is depleted at distances greater than 3 km. This observation could indicate a large hydrothermal reservoir below the sediments, if the silica precipitated below the deposit was derived from depleted distal portions of the same horizon. Iron shows a somewhat similar behavior as silica within this horizon. Magnesium in both horizons tends to be both enriched and depleted in increasing intensities near the deposit-although variations in magnesium within the Mine Horizon have five times the amplitude of those from the RBS. These proximal variations could imply either a highly focussed precipitation of Mg-OH silicates within previously depleted rocks or a local re-mobilization of magnesium.

Assuming that the Normetal deposit was produced by deposition from exhalations or from discharge of metal-rich hydrothermal solutions at/or near the seafloor (Mine Horizon), we can also assume that Fe_2O_3, which also shows mass gains proximal to the deposit, was also enriched by similar processes at the Mine Horizon. MnO, which shows a spatial distribution almost identical to Fe_2O_3 within the Mine Horizon, can therefore be assumed to have been added by the same mechanism, along with CaO which also appears to have a similar spatial distribution.

Areas of sodium depletion could also be easily explained by the passage of large quantities of water through the footwall rocks, effectively remobilizing this element. Two such areas of sodium depletion occurring on either side of the Normetal deposit (WAZ and LDD) could represent such areas of focussed circulation. It is interesting to note that areas showing enrichment in CaO, Fe_2O_3 and MnO do not show significant Na_2O depletion.

Silica, which is a common precipitate in the form of chert associated with VMS deposits, is also more commonly and intensely depleted in the WAZ and above the LDD intrusion, both interpreted as areas of high fluid circulation. This interpretation implies that fluids which reached the Mine Horizon through these two alteration zones differed from those that exhaled in close proximity to the Normetal deposit. Such differences could be due to different water-to-rock ratios, different temperatures, or to different residence times for these fluids within their hydrothermal reservoir.

The Mine Horizon rhyolite coinciding with the WAZ and the LDD intrusion are enriched in potassium which is commonly associated with sericitization. Sericite, on the other hand, clearly increases in abundance towards the Normetal deposit (Fig. 15). Interestingly, the RBS in these same areas are locally enriched in MgO, CaO, MnO and Fe_2O_3, in contrast to an inverse trend noted within the Mine Horizon. Such trends could also be explained by draw-down of fluids through a sediment gap or break. Na_2O depletion and K_2O enrichments would then be a product of alteration by cold seawater,

without enrichments in Fe_2O_3, MnO and MgO.

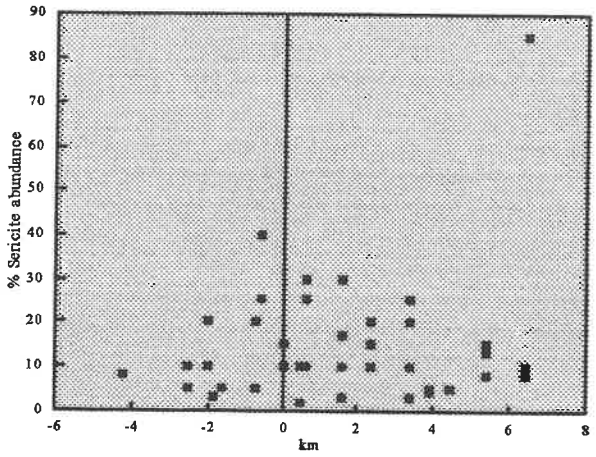

Figure 15: Plot of sericite abundances in samples from the Mine Horizon vs. east-west coordinates; x-axis represents coordinates relative to the Normetal deposit at 0 km; coordinates increase towards the east and decrease towards the west.

If these areas of mass exchange do represent areas of hydrothermal discharge, then possible reasons for not producing larger metal concentrations include an incapacity for further metal transport (e.g., due to mixing with cool in-situ seawater), and dilution by high water-to-rock ratios, resulting in in-situ precipitation within footwall rocks and/or dispersion of precipitates at the seafloor.

Increases in silicification, increases in iron magnesium and manganese concentrations, and occurrences of iron-formations, to the east of the LDD intrusion (similarly to trends observed in Mine Horizon proximal to the Normetal deposit) suggest significant precipitation of exhalites and therefore a high potential for VMS-type mineralization.

The methods applied here permit the user to evaluate the potential of individual elements as indicators of mineralization. These individual indicators may then be combined to form a single index of alteration. Large (1992), in a review of volcanic-hosted massive sulphide deposits, has presented an alteration index (MgO + K2O)/(Na_2O + CaO + MgO +K_2O)×100 based on raw whole-rock data. This index results in similar trends in mass-change graphs for K_2O as well as for absolute values of mass-change for CaO and Na_2O (Fig. 16).

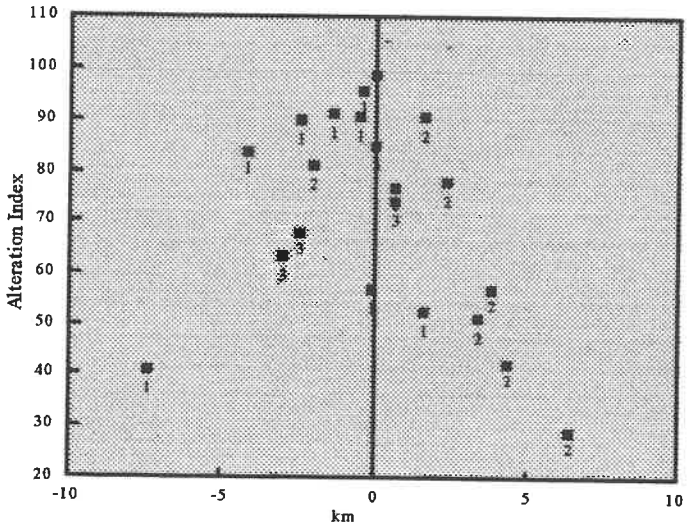

Figure 16: Plot of alteration index (MgO + K2O)/(Na_2O + CaO + MgO +K_2O)×100 (Large, 1992) vs. east-west coordinates for the RBS. Data labels refer to unit number; x-axis represents coordinates relative to the Normetal deposit at 0 km; coordinates increase towards the east and decrease towards the west.

CHAPTER 4

ALTERATION MINERALOGY AND MINERAL CHEMISTRY

4.1 Rhyolite Bellow Sediments

Samples taken from the RBS typically consist of massive aphyric rhyolite containing variable amounts of sericite (normally ranging up to 20% in thin sections)[1]. Samples for thin sections were chosen so as to show carbonate, if any was present, for later microprobe analysis. Carbonate abundances in these samples rarely exceeded 2%. A few samples located near the WAZ (Appendix 12-2) contained concentrations of chlorite and chloritoid reaching 15% and carbonate reaching 10%. Based on carbonate staining, the highest concentrations of carbonate (>5%) in the RBS also appear to coincide spatially with the WAZ. There is insufficient chloritoid and chlorite data from the RBS to permit a spatial interpretation of its compositional variations.

The 17 ankerites from the RBS analyzed by using the microprobe (Appendix 11-1), seem to show decreasing FeO and increasing MgO contents towards the Normetal deposit, with the exceptions of samples from drill holes 18 and 15 (the easternmost and westernmost drill holes, respectively), which show low FeO and high MgO. These trends lead to a notably decreasing FeO/(FeO+MgO) trend towards the deposit (Appendix 11-3).

---

[1] Thin section abundances are represented graphically in Appendix 13-1

Low values for this ratio are also noted in data from drill hole 18 to the east of the LDD intrusion. A relatively high concentration of MnO is noted in drill hole 1, 250 m from the eastern limit of the Normetal deposit.

MgO and K_2O increase significantly and consistently in sericite (17 analyses, Appendix 5), towards the Normetal deposit. FeO in sericite also increases consistently towards the deposit, although not in concentrations as high as seen in the rhyolites above the LDD intrusion. MgO is also high proximally to the LDD intrusion. No significant CaO concentrations are noted in any sericite analysis from the RBS. High K_2O and low Na_2O are noted in drill hole 12 directly above the LDD intrusion.

Iron and magnesium in sericites are problematic since these elements have trends opposite those of whole-rock analyses and calculated mass changes. Their trends may suggest that locally derived Mg- and Fe-rich fluids were produced by depletion of other preexisting minerals, coupled with simultaneous enrichments of sericites in these same elements. In other words, sericite may have acted as a local mineralogical sink for FeO and MgO. The LDD intrusion, on the other hand, is characterized by important variations in the increasing K_2O trend in sericites (with the exception of a large decrease at drill hole 12), suggesting a secondary alteration process or local variations in the intensity of alteration. No compositional variations in pre-alteration mineralogy are recognized for the

WAZ. Although occurrences of chlorite and chloritoid are rare in this horizon, these anomalous occurrences suggest locally distinct alterations.

In summary, regional variations in mineralogical compositions with increasing proximity to the Normetal deposit, for the RBS, are characterized by decreasing FeO/FeO+MgO in ankerites (also seen in whole-rock trends), and by consistent regional increases in FeO, MgO and K_2O in sericites (Appendix 5-4). Potassium enrichment in sericites probably reflects similar trends in mass-change associated with the breakdown of plagioclase to muscovite.

4.2 Mine Horizon

Mine Horizon samples show an increase in highly sericitized rocks towards the Normetal deposit (sericite increases up to 40%, Fig. 15), and minor increases in chlorite abundance (up to 5%, estimated from thin section observations); however, drill hole 99 directly west of the Normetal deposit shows high chlorite concentrations (17%). Although no samples from the immediate footwall of the Normetal mine workings were reviewed in this study, data from Moore (1990) suggest that a zone of highly chloritic alteration associated with stringer chalcopyrite directly underlies the deposit. Chloritoid abundances show little or no variation with respect to spatial distribution and vary from 2 to 12% directly east of the Normetal deposit (with the exception of a single sample having

40% chloritoid in drill hole 1). Few occurrences of carbonate with concentrations above a background high of 13% are noted, although occurrences of carbonate facies iron-formations are found to the east of the LDD intrusion, and in proximity to the Normetmar prospect.

Microprobe data for ankerites from the Mine Horizon near the Normetal deposit (91 analyses, Appendix 10) show significant regional increases in MnO as well as a highly focussed CaO depletion in drill hole 54 and in the WAZ. Other high MnO values occur in drill hole 20 overlying the LDD intrusion, and in drill holes 16 and 23 (the easternmost drill holes considered in this study). Both MgO and FeO show significant variability. Nevertheless, FeO increases both toward the Normetal deposit and above the LDD intrusion, whereas MgO decreases over the LDD intrusion. Assuming that these tendencies might indicate alteration, diagrams were constructed using MnO*25/FeO and MnO/(MnO+MgO) ratios, so as to emphasize these trends (Fig. 17). Values for MnO*25/FeO clearly increase towards the Normetal deposit from both eastward and westward directions over a distance of some four kilometres. These values increase again in drill holes 16 and 23. A single high MnO value in drill hole 20 also stands out above the LDD intrusion. Values for MnO/(MnO+MgO) are highest in drill hole 54 directly west of the Normetal deposit, in drill hole 1 directly east of Normetal, as well as above the LDD intrusion, and near the WAZ. These spatial associations suggest that the MnO/MgO in ankerite may be a useful indicator of intense fluid alteration whereas MnO/FeO appears to

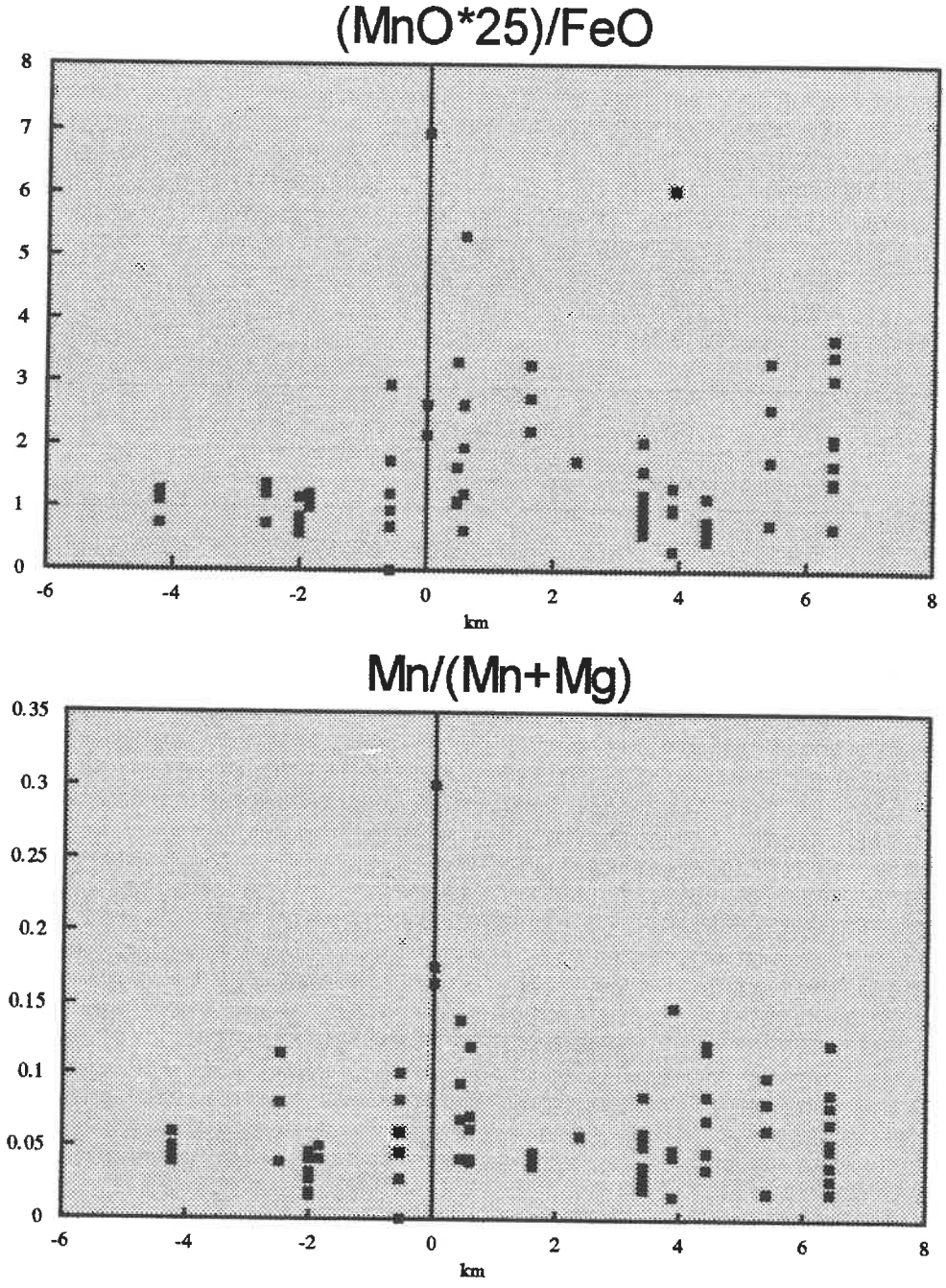

Figure17: Plots of compositional ratios in ankerites from the Mine Horizon vs. east-west coordinates; x-axis represents coordinates relative to the Normetal deposit at 0 km; coordinates increase towards the east and dercrease towards the west. a) (MnO×25)/FeO vs. position and b) MnO/(MnO+MgO) vs. position.

be more indicative of proximity to known mineralization.

Of 27 microprobe analyses of sericites from the Mine Horizon (Appendix 5), high K_2O and low Na_2O are noted in drill hole 1 directly east of the Normetal deposit. Other areas with both high K_2O and low Na_2O values are found east of the LDD intrusion. It should be noted that Na_2O is significantly higher in sericites from the Mine Horizon than in sericites from the RBS (average 3% vs. 0.5%). K_2O, on the other hand, is lower in the Mine Horizon than in the RBS, with lowest K_2O values coinciding with the LDD intrusion. These spatial associations suggest that paragonite may be the dominant species in the Mine Horizon, as opposed to muscovite in the RBS. The highest FeO and MgO contents are noted in drill hole 16 toward the east edge of the LDD intrusion. Calcium appears to show a minor decreasing trend from drill hole 16 toward the Normetal deposit (up to 0.4%, and decreasing to 0%), with a single high value occurring in drill hole 6 in the WAZ.

Microprobe data for chloritoids from the Mine Horizon (121 analyses, Appendix 8) clearly show striking increases in MnO close to the Normetal deposit (Fig. 18). FeO in chloritoids increases towards both the Normetal deposit and the LDD intrusion, although low values are noted in drill hole 54 directly west of the Normetal deposit (<100 m). MgO concentrations for drill hole 54 (<100 m west of the Normetal deposit), and for drill hole 28 (<100 m east of the Normetal deposit) show low values with increasing distance

from the Normetal deposit. There is also a trend of decreasing MgO towards the LDD intrusion. These trends result in sharp increases in MnO/(MnO+MgO) and in (MnO*50)/FeO values with proximity to the Normetal deposit (Fig. 19). FeO/(FeO+MgO) values seem to show a local high coinciding with the Normetal deposit as well as with the LDD intrusion and the WAZ.

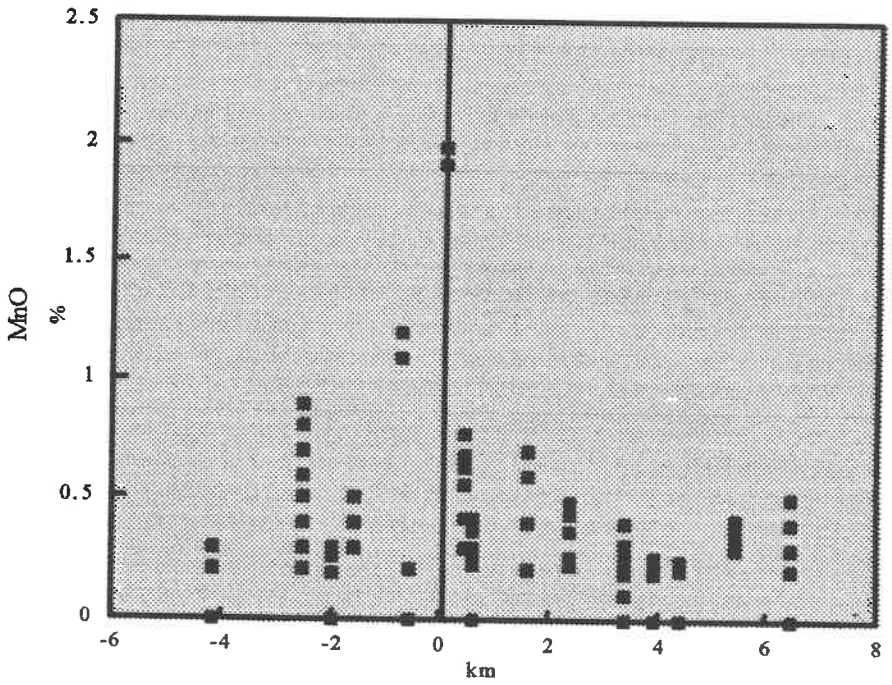

Figure 18: Plot of MnO concentrations in chloritoids from the Mine Horizon vs. east-west coordinates; x-axis represents coordinates relative to the Normetal deposit at 0 km; coordinates increase towards the east and decrease towards the west.

Microprobe analyses of chlorites (68 analyses, Appendix 6) show that they are Fe-rich overall (FeO/FeO+MgO approx. = 0.75), with slightly less Fe-rich chlorites (FeO/FeO+MgO approx. = 0.6) in drill hole 6 (coinciding with the WAZ) and in a surface

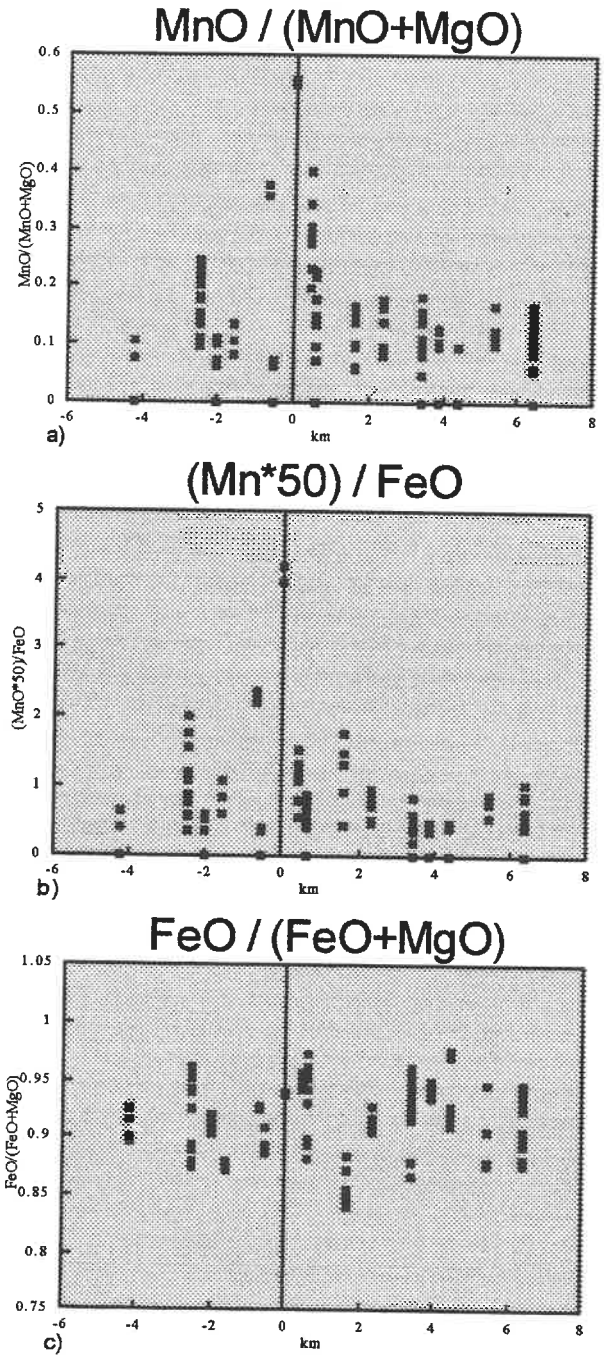

Figure 19: Plots of Compositional ratios of chloritoids from the Mine Horizon vs. east-west coordinates; a) MnO(MnO+MgO); b) (Mn×50)/FeO; and c) FeO/(FeO+MgO). X-axis represents coordinates relative to the Normetal deposit at 0 km; coordinates increase towards the east and decrease towards the west.

sample located 1.8 km east of Normetal. High MnO values in chlorite occur near the Normetal deposit, in drill hole 17 in the WAZ), and in drill hole 16 (east of the LDD intrusion). Therefore, MnO/(MgO+MnO) values increase upon approaching the Normetal deposit, with other notably high values also occurring in drill hole 17. High Na_2O contents in chlorite appear to be common further from the Normetal deposit.

In summary, compositional variations in ankerites, chlorites and chloritoids within the Mine Horizon show strong regional increases in MnO towards the Normetal deposit and as such they are also reflected in calculated mass gains. Chlorites appear to be richer in FeO near the Normetal deposit, sericites are significantly enriched in K_2O directly east of the Normetal deposit. Calcium depletion in ankerite may also indicate alteration with lowest calcium towards both the Normetal deposit and the WAZ. The WAZ is characterized by Mg-rich chlorite and relatively Fe-rich chloritoid. Variations spatially associated with the LDD intrusion are characterized by broad K_2O depletion in sericites (contrary to observed calculated mass change trends) and by minor MnO enrichments with respect to FeO in ankerite.

4.3 Compositions of Minerals Versus Whole-Rock Data

Shikazono and Kawhata (1987) present a correlation between the MgO/FeO of host rocks and the MgO/FeO of chlorites in propyliticly altered rocks. Although they

accept this correlation as being normal, they also observe significant deviations from this correlation in rocks from Kuroko and Neogene Cu-Pb-Zn vein-type deposits and attribute these deviations to intense hydrothermal alteration of fresh rocks. This suggestion leads to their assumption that Mg-rich chlorites precipitated from solutions with high proportions of Mg relative to Fe. Other factors that may cause such variations include influences by oxygen fugacity, pH and temperature.

Using their assumption that high MgO/FeO ratios may reflect the original MgO/FeO ratios of the fluid phase, a set of graphs of $(FeO/FeO+MgO)_{mineral}/(Fe2O3/Fe2O3+MgO)_{whole\text{-}rock}$ were plotted to test the dependence of mineralogy on whole-rock compositions (Fig. 20). Similarly, $(FeO/FeO+MgO)_{mineral}$ ratios were calculated against precursor compositions and against calculated mass changes. These diagrams can be interpreted as graphic representations of the stability of mineral phases with respect to the rocks or fluids in question; differences between precursor and final compositions can be attributed to mass changes.

Mass changes prove to be the most difficult to interpret due to the presence of both positive and negative mass changes. Data from sericite from the Mine Horizon and from the RBS, and data from ankerite (from the RBS), show little relationship to raw whole-rock, precursor or mass changes and are not discussed further.

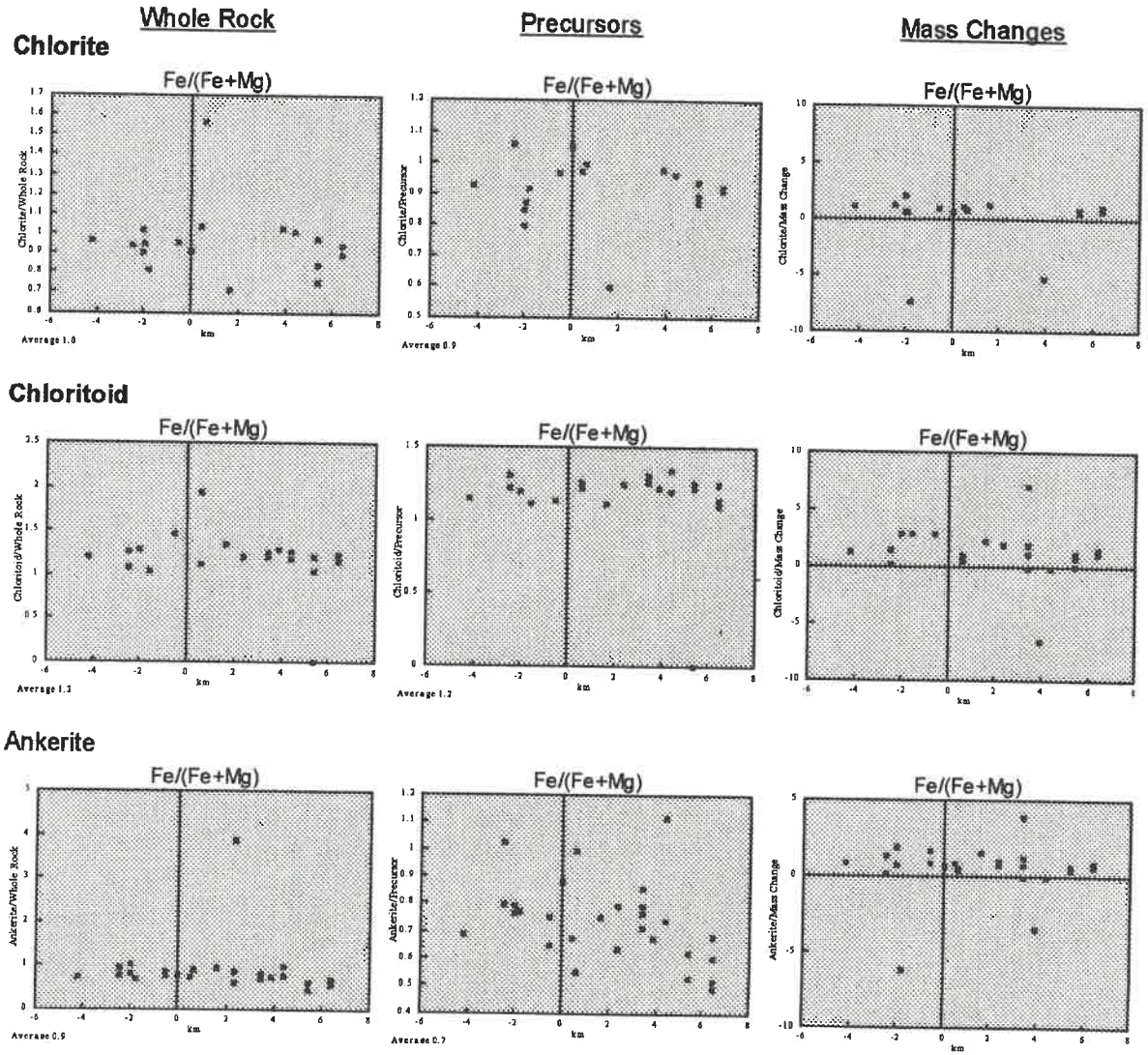

Figure 20: Plots of Compositional ratios of mineralogies vs. whole-rock compositions, prcursor compositions, and mass changes against east-west coordinates; x-axis represent coordinates rlative to the Normetal deposit at 0 km.

However, Mine horizon chlorites seem to show a significant dependence upon whole-rock data in terms of $(FeO/FeO+MgO)_{mineral}/(Fe2O3/Fe2O3+MgO)_{whole\text{-}rock}$, resulting in an average ratio of 1.0. Deviations from this average ratio are noted in drill hole 1 (a ratio of 1.6), proximal to the deposit, in samples coinciding with the WAZ (values > 0.8), in drill hole 2 (values > 0.6) east of the deposit and east of the LDD intrusion. These same trends or anomalies (although differing in magnitude), are also be noted for chlorites calculated against precursor compositions and mass changes. This observation may imply that alteration proximal to the Normetal deposit may have been produced by fluids with high FeO/MgO ratios in comparison with regional alteration. Inversely, the WAZ and the LDD may have been produced by relatively Mg-rich or Fe-poor fluids.

Interestingly, FeO/FeO+MgO ratios for chloritoid appear to be as dependent on whole-rock compositions as on calculated precursor compositions, both having an average ratio of 1.2. Such ratios may not in themselves be as important as variations from this average and as such it may be important to note that $(FeO/FeO+MgO)_{mineral}/(Fe2O3/Fe2O3+MgO)_{whole\text{-}rock}$ for chloritoid also gives an anomalously Fe-rich value proximal to the Normetal deposit. As well as indicating the dependence of various mineralogies on whole-rock chemistry, these graphics also serve to indicate the ability of certain mineral phases to concentrate particular elements for averages exceeding unity.

Ankerite compositions show their highest dependence on the Fe2O3/Fe2O3+MgO ratios of whole-rock composition, and to a lesser extent a dependence on calculated mass changes. A single anomalously FeO-rich whole-rock value is noted for ankerite (value of 4.0; see Fig. 20) in drill hole 4 between the LDD intrusion and the Normetal deposit vs. an average value of 0.9. The mass-change diagrams show negative anomalies in FeO/(FeO + MgO) both in the WAZ and near the LDD intrusion.

4.4 Discussion

In this section, the stoichiometric chemical compositions refer to the following minerals: albite = $NaAlSi_3O_8$, kaolinite = $Al_4Si_4O_{10}(OH)_8$, chlorite=$H_2(Fe,Mg)Al_2SiO_7$, paragonite = $NaAl_2AlSi_3O_{10}(OH)_2$, muscovite=$KAl_2(AlSi_3O_{10})(OH)_2$, Quartz = SiO_2, glauconite = $(K,Na,Ca)_{1.2-2}(Fe^{+3},Al,Fe^{+2},Mg)_4[Si_{7-7.6}Al_{1-0.4}O_{20}](OH)_4 \cdot n(H_2)$, and chloritoid = $H_2(Fe,Mg)Al_2SiO_7$,

Muscovite in least-altered samples (showing relict plagioclase) is interpreted to have formed through conversion of plagioclase to sericite (muscovite or paragonite) and quartz. Morton and Nebel (1984) suggest that (K-rich) interactions between evolved acidic seawater and albite might be responsible for producing such sericite-quartz alteration assemblages while depleting rocks in sodium, as follows:

$$3NaAlSi_3O_8 + 2H^+ + K^+ = KAl_3Si_3O_{10}(OH)_2 + 6SiO_2 + 3Na^+ \quad \text{(Lockwood, 1987)}$$

Although this reaction is feasible for the RBS below the Normetal deposit (Na_2O depleted, K_2O enriched in whole-rock), Mine Horizon rocks show regionally decreasing K_2O with proximity to the deposit. This is also the case for analyses of sericites which increase in abundance towards the deposit. These decreasing K_2O trends towards the Normetal deposit suggest that paragonite may be the alteration product of interactions between albite and seawater in the Mine Horizon, as follows:

$$3NaAlSi_3O_8 + 2H^+ = NaAl_2Si_3AlO_{10}(OH)_2 + 6SiO_2 + 2Na^{+2}$$

Thus, paragonite is the dominant sericite species in the Mine Horizon, except in closest proximity to the deposit where K-rich sericites (muscovite) are noted (drill hole No. 1). Again, such abrupt local variations probably resulted from locally distinct alteration. Were this reaction dominant, notable sodium depletion should also have resulted, but Na-depletion is not observed with any significance close to the Normetal deposit.

Regional-scale increases in sericite abundance within the RBS suggest that sericitic alteration may be related genetically to the Normetal deposit, with locally anomalous compositions proximal to the LDD intrusion suggesting that late alteration may have modified or been superimposed on an earlier alteration. These late fluids would have

resulted in Na-substitution for potassium, while adding Fe and Mg to the Al site (of glauconite?), as follows:

Muscovite + Na + (Fe, Mg) + 3 Quartz = Glauconite + K + Kaolinite(?)

Because Al_2O_3 is believed to be relatively immobile in these rocks, aluminum could be consumed in producing a secondary in-situ clay mineral (kaolinite?), as opposed to being mobilized and removed in solution.

These mineral compositions seem to correspond most closely to calculated precursor compositions and to raw whole-rock data rather than to mass changes, suggesting that sericite may have formed in the Mine Horizon from relatively isochemical reactions, possibly during early regional metamorphism or from late isochemical re-equilibration (retrograde alteration?). Samples showing relict plagioclase (least-altered samples) generally show disseminated, randomly oriented sericite and little reorganization of mineral assemblages (e.g., redistribution by pressure solution). The increase in sericitization near Normetal deposit, without significant stronger Na_2O depletion or K_2O enrichment, may not have occurred isochemically. Yet it did not produce significant departures from the whole-rock trends and therefore probably formed either early in the evolution of the rocks (synvolcanic alteration ± spilitization) or during later regional metamorphism. Due to initially low Na_2O compositions (i.e., calculated precursor compositions) proximal to the Normetal deposit, mass-losses (such as Na depletion) may

be below the detection limits. Alternatively, secondary fluids may have altered early sericite, locally emphasizing variations in precursor compositions and producing important local variations within these trends. Thus, high local concentrations of K_2O in sericites near the Normetal deposit in the Mine Horizon may have resulted from alteration by a secondary evolved K-rich fluid.

Chlorite compositions appear to correspond most strongly to mass-change calculations and to raw whole-rock data as opposed to precursor compositions, suggesting formation by secondary Fe- and/or Mg-rich fluids. In their study, Morton and Nebel (1984) suggest a secondary Fe, Mg, and Mn-rich fluid reacting with sericitic rocks or with primary albite, which could produce a chloritic alteration while depleting the sericite or feldspar in potassium according to the following reactions (Lockwood, 1987; Morton and Nebel, 1984):

$$\underset{\text{(sericite)}}{2KAl_3Si_3O_{10}(OH)_2} + 3Qtz + 15Fe^{2+} + 24H_2O = \underset{\text{(Fe-rich chlorite)}}{3Fe_5Al_2Si3O_{10}(OH)_8} + 2K^+ + 28H^+$$

$$\underset{\text{(Albite)}}{2NaAlSi_3O_8} + Fe^{2+} + 8H2O = \underset{\text{(Fe-rich chlorite)}}{Fe_5Al_2Si_3O_{10}(OH)_8} + 3SiO_2 + 8H^+ + 2Na^+$$

For Normetal rocks, these alterations might be reflected by the step-by-step reactions:

$$3NaAlSi_3O_8 + K^+ + 2H^+ + 7.5Fe^{2+} + 12H_2O = (K,xNa)Al_3Si_3O_{10}(OH)_2 + 6SiO_2 + 3\text{-}xNa^+$$

(Albite) (Sericite)

$$+ 7.5Fe^{2+} + 12H_2O = 0.5Fe_5Al_2Si3O_{10}(OH)_8 + 3SiO_2 + 14H^+ + K^+ + 3Na^+$$

(Fe-rich chlorite)

Alteration of albite with seawater could clearly have produced various amounts of sericite of variable Na-K composition, together with varying amounts of quartz and chlorite.

Shikazono and Kawhata (1987) suggest that the iron content of chlorites from Japanese epithermal mining districts may be higher in the discharge zones than within the recharge zones. This proposition supports an earlier suggestion by Mottl (1983) of high Fe^{2+}/Mg^{2+} in the discharge zone. Using thermochemical data, Shikazono and Kawhata proposed a model whereby fluids, initially in equilibrium with chlorite having the FeO/MgO ratio of average andesite and basalt at elevated temperatures, would precipitate chlorite with unusually high Fe/Mg ratios upon rapid ascension and decreasing temperature, without interacting with surrounding rocks. Inversely, they suggested that if a fluid was Mg-rich (e.g., seawater) or if the system were strongly water-dominated, then the chlorite would contain a high concentration of Mg even within the discharge zone. This model could explain the relatively high iron contents of chlorites proximal to the Normetal deposit if these chlorites were produced by highly evolved Fe-rich fluids. Using

this model, Mg-rich chlorites associated with the WAZ and in drill hole No. 2 might therefore represent products of a locally water-dominated system or products of recharge areas.

Spatial variations in chloritoid composition do not correspond well with calculated precursor data and clearly show even less correspondence with calculated mass changes, suggesting that chloritoid may have formed relatively late, probably as a product of regional metamorphism. There are also significant resemblances in the spatial distributions of chlorite and chloritoid compositions. It is probably reasonable to suppose then that chloritoid generally formed from re-equilibrium of chlorite during regional metamorphism as is also suggested by chloritoid overgrowths on chlorite.

Chloritoid, like ankerite, shows a strong regional correlation between MnO and proximity to the Normetal deposit as well as with proximity to the WAZ, and as such, the MnO composition of chloritoid appears to be a good regional pathfinder in mineral exploration. Even if chloritoid is a late, metamorphic mineral, it seems to be a good site for MnO concentration, and thus MnO analyses of chloritoid may be particularly well suited as a pathfinder in mineral exploration. This use of chloritoid and its MnO content may be particularly well illustrated in mass gains and losses. By analyzing mineralogies capable of concentrating MnO such as chloritoid, subtle variations may be still more easily distinguishable from background variations.

Furthermore, any sheared chloritoids grains may predate regional deformation and may therefore represent primary alteration products. Further studies should probably be attempted to focus on this generation of chloritoid in the hope of monitoring early alteration (e.g., syn-volcanic) events.

CHAPTER 5

OXYGEN ISOTOPES

5.1 Introduction

Taylor (1974) suggested that, because water was the dominant constituent of ore-forming fluids, the original source and history of fluids might best be interpreted by studying geochemical parameters of water molecules themselves. Since various rocks and natural waters show large variations in $^{18}O/^{16}O$, oxygen analyses of whole-rock samples and fluid inclusions have been used increasingly in recent years in studies on the nature and origins of hydrothermal fluids associated with the formation of massive sulphide deposits (Beaty et al. 1988; Hoy and Maclean 1991; Hoy, 1992; and many others). The technique has also demonstrated its potential as an exploration tool. Studies focussing on individual deposits commonly show well-centered bull's eye-type anomalies. For example:

The concentrically zoned alteration pipe of the Amulet "A" mine shows a systematic decrease in $\delta^{18}O$ values with increasing alteration towards the centre of the pipe relative to nearby rocks (Beaty and Taylor, 1982).

Hydrothermally altered rhyolites at the Kidd Creek deposit show an increasing regional $\delta^{18}O$ enrichment towards the deposit, with a sudden decrease in close proximity to the deposit (Beaty et al., 1988).

The Fukazawa Kuroko deposit, as well as other mineralized showings of the Hokuroku district, show a systematic decrease in $\delta^{18}O$ with proximity to the mines and with increasing alteration. These concentric halos commonly point to mineralization (Green et al., 1983).

It has also been suggested that $\delta^{18}O$ halos not only show larger areal extent and lesser variability than whole rock analyses, but are also well-preserved through metamorphism compared to major and trace-element distributions (Green et al., 1983). These characteristics are demonstrated by the high $\delta^{18}O$ gradients at Kidd Creek (Beaty et al. 1988) and by the persistence of original $\delta^{18}O$ values coincident with mineral alteration at the Amulet mine, through intense contact metamorphism (Beaty and Taylor, 1982). Studies of $\delta^{18}O$ may therefore be particularly useful in areas showing widespread alteration and little local variation in mineralogy, such as large Mattabi-like systems (e.g., Normetal).

Further mathematical modeling and regional studies, such as that of Hoy (1992), are focussed on the interpretation of water-to-rock ratios, temperature gradients and the effects of such variations on observable whole-rock isotopic re-equilibrium.

5.2 Principles of Oxygen Isotope Analyses

Oxygen is the most abundant element on earth and has three stable isotopes (Garlick, 1969):

$$^{16}O = 97.763\ \%$$
$$^{17}O = 0.0375\ \%$$
$$^{18}O = 0.1995\ \%$$

Because of the larger relative mass differences and abundances of ^{18}O and ^{16}O, only $^{18}O/^{16}O$ analyses are generally carried out.

Oxygen isotope data are commonly reported as $\delta^{18}O$ where:

$$\delta^{18}O = \left(\frac{R_{Sample}}{R_{Standard}} - 1\right) \times 1000,$$

where R_{sample} and $R_{standard}$ are the $^{18}O/^{16}O$ of a sample and a standard, respectively. This method permits us to quantify deviations relative to a well-defined well-mixed standard such as standard mean ocean water. A +8 value therefore represent a 8‰ (8 parts per thousand) enrichment in ^{18}O with respect to the standard.

Ocean water $\delta^{18}O$ is generally believe to have remained relatively constant throughout geological time (±1 per mil). This is explained by the oceans being buffered close to the 0 value by isotopic exchange reactions during thermal convection in

mid-oceanic rifts (Munha et al., 1986). For a complete review of $\delta^{18}O$ buffering at mid-oceanic ridges, see Gregory and Taylor (1981). This continuous process is believed to recycle the entire reservoir of oceanic water over a period of 5-30 m.y. at temperatures of approximately 300 °C. Evidence supporting this buffering process includes the abundance of $\delta^{18}O$ values close to 0 per mil found in many submarine massive sulphide deposits (Muehlenbachs and Clayton, 1972; Wenner and Taylor, 1973; Munha et al., 1986). For this reason, Standard Mean Ocean Water standards, SMOW or V-SMOW[1], are most commonly used. This is particularly true for VMS-type deposits where ocean water is generally believed to be the main source of hydrothermal ore-forming fluids.

Low water/rock ratios (i.e., rock-dominated systems) at elevated temperatures can result in significant $\delta^{18}O$ enrichments in the aqueous fluids, particularly if the water had a long exposure to elevated $\delta^{18}O$-rich rocks or had a relatively long migration distance (also reflected in relatively long residence times). Green et al. (1983) summarized this point well, and added that, even in water-dominated systems (high water/rock ratios), small quantities of water can be regarded as discrete packets of water in a larger system (see Spooner et al., 1977). For any given packet of water, the system is rock dominated and the chemical and isotopic characteristics of that packet are controlled by the enclosing rock. That is, for any packet of water, the time required to penetrate oceanic crust and then convect thermally to the site of exhalative mineral deposition, is typically in the range

[1] SMOW was defined by Craig (1961), V-SMOW by Baertshi (1976).

of 5,000 to 20,000 years (Spooner et al., 1977). Therefore, that packet must surely have interacted with more than its own weight of rock. Considering alteration in this way gives a much better idea of the progressive nature of change produced by alteration. This progressive change is the basis for models such as that of Hoy (1992) which begin with known initial isotopic compositions and examines the effects on a column of rock interacting with sequential packets of water and causing a progressive increase in the water/rock ratio as temperatures change.

5.3 Rhyolite Below Sediments (RBS)

Data for $\delta^{18}O$ from the RBS[1] (Appendix 14) appear to show a different average for the RBS with respect to the Mine Horizon on a frequency distribution plot (Fig. 21). The RBS samples spans the 12 to 16‰ range, whereas the Mine Horizon samples are represented by lower (10 to 12‰) values.

However a graph of $\delta^{18}O$ values displayed along east-west coordinates (Fig. 22) suggests a different distribution of populations. The first spans 13.6 to 16.1‰ and increases towards the Normetal deposit. Secondary occurrences deviate significantly from the first population, occurring over a broad region spatially associated with the WAZ

[1] It should be noted that no analysis of $\delta^{18}O$ was carried out for the RBS horizon above the LDD intrusion, due either to the absence of the marker sediments in drill cores (causing uncertainty in stratigraphic position) and/or because the RBS horizon was not intersected (as in drill hole 16).

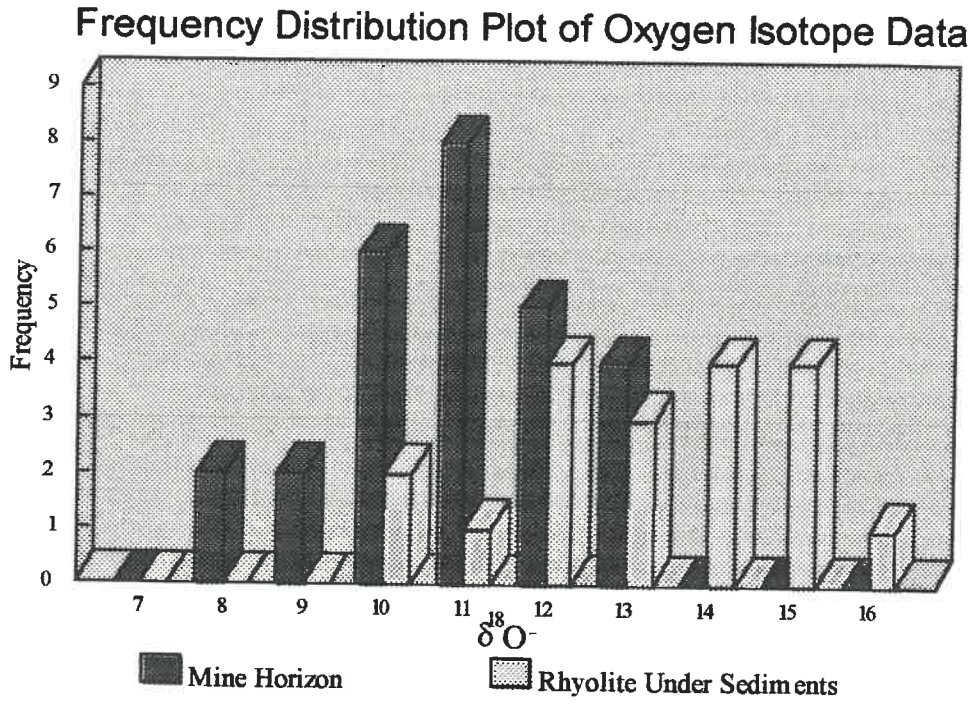

Figure 21: Frequency distribution plot of Normetal oxygen isotope data for both the Mine Horizon and the RBS.

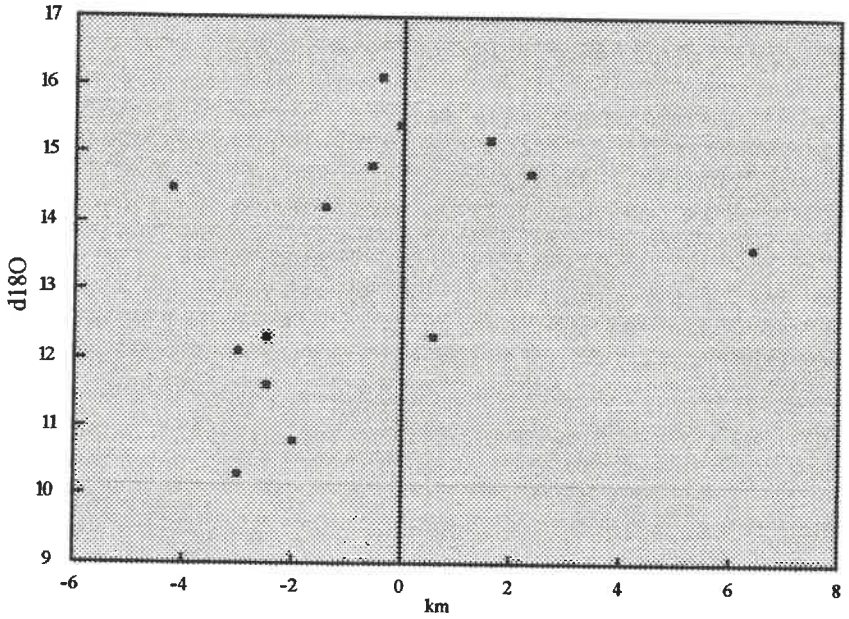

Figure 22: Plot of oxygen isotope data vs. east-west coordinates for the RBS; x-axis represents coordinates relative to the Normetal deposit at 0 km; coordinates increase towards the east and decrease towards the west.

(10.8 to 12.3‰). A second (12.3‰) with respect to the 13.6 to 16.1‰ population occurs in drill hole 1 proximal to the Normetal deposit.

Although in some other studies $\delta^{18}O$ has been found to be dependent on alteration mineralogy for formation under similar conditions (Maclean and Hoy, 1991; Beaty et al., 1988), data for the RBS (appendix 15-1) show no obvious correlation between $\delta^{18}O$ and quartz + matrix[1] or with chlorite. Only three of the six anomalous samples at the lower end of the $\delta^{18}O$ range have greater than 5% chlorite. Two of these samples are from drill hole 5, and the third is from drill hole 6 (all from the WAZ). The theoretical correlation is attributed to different isotopic fractionations between mineralogical species, producing differing $\delta^{18}O$ values under similar alteration conditions ($\delta^{18}O_{chlorite} < \delta^{18}O_{sericite} < \delta^{18}O_{albite} < \delta^{18}O_{quartz}$; Hoy, 1992).

5.4 Mine Horizon

As for the RBS (see above), $\delta^{18}O$ analyses from the Mine Horizon have not been found to show any obvious correlations with alteration mineralogies (Appendix 15-2). The absence of such a relationship may be due to the homogeneous distribution of mineralogical species within the Mine Horizon relative to the highly variable normative compositions of other studies (e.g., 0 - 80% normative chlorite at the Ansil deposit; Hoy,

[1] Matrix, being fine-grained, is believed to be dominantly quartz, but is of uncertain composition. It is calculated as 100-(sericite+carbonate+chlorite+chloritoid+feldspar), based on petrographic observations.

1992). Chloritoid, having formed late (post-deformation) in most cases, in the evolution of the host rocks and showing the lowest variations in abundances, is not considered to have produced any significant variations in $\delta^{18}O$. Therefore, the variations observed in $\delta^{18}O$ analyses in this study may better reflect variations due to fluid alteration than do other studies where $\delta^{18}O$ has been demonstrated to be dependent on mineralogy, particularly in studies where a mineralogical dependence was not considered and not compensated for in the interpretations of fluid origins.

Mine horizon $\delta^{18}O$ values show a well-defined mean in the 11 to 12‰ range (Fig. 21), with the highest value ($\delta^{18}O$=13.8‰, surface sample GR-90-42) west of Normetal (Fig. 23). Note that two other values exceed 13‰ east of the LDD intrusion. Values of

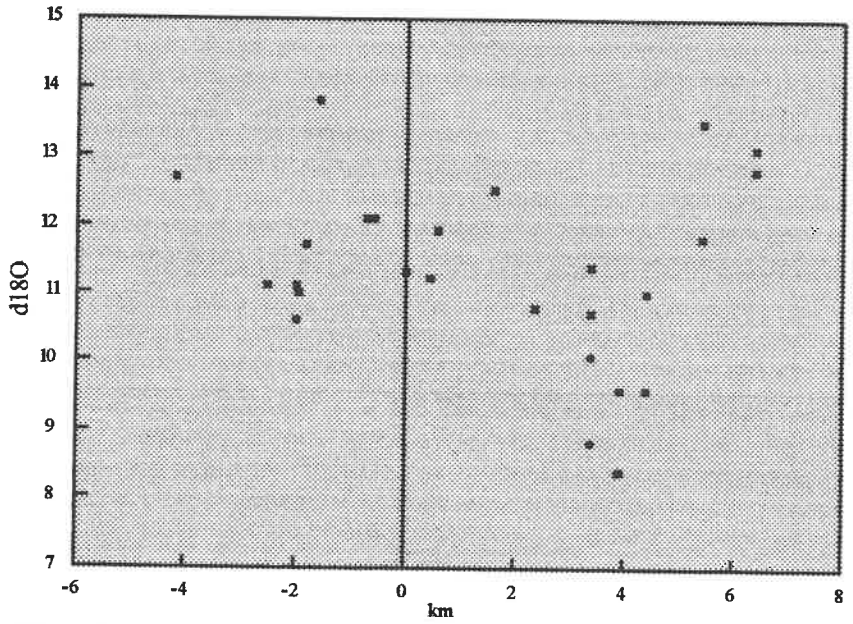

Figure 23: Plot of oxygen isotope data vs. east-west coordinates for the Mine Horizon; x-axis represents coordinates relative to the Normetal deposit at 0 km; coordinates increase towards the east and decrease towards the west.

$\delta^{18}O$ for samples proximal to the Normetal deposit show no significant variation from the mean. A broad region of lower than average $\delta^{18}O$ values 3 to 5 km east of Normetal clearly reflects different conditions of alteration spatially associated with the underlying LDD. Samples located proximal to the WAZ show little variation from the mean population, yet these samples returned $\delta^{18}O$ values approaching the lower limit of the main group of samples, with one value (10.6‰ in drill hole 6) surpassing it.

5.5 Normative Mineralogy

Calculations were undertaken to establish normative alteration mineralogy to further discriminate between variations in $\delta^{18}O$ associated with the isotopic compositions of alteration fluids from those associated with variations in mineralogy. Compositional averages for different mineralogical species were established separately for the RBS and for the Mine Horizon (Appendix 16 and 17). From these whole-rock analyses, all potassium was attributed to sericite, and other components were progressively removed according to their calculated average molar proportions. Calcium was attributed to ankerite, following the procedure used for potassium in sericite. Chlorite was calculated from the remaining FeO; normative albite was calculated from the remaining Al_2O_3, and quartz from the remaining silica, in that respective order. These normative calculations represent maximum mineral concentrations, and as such are dependent on all potassium having formed sericite and all calcium having formed ankerite. No allowance has been

made in these calculations for opaque minerals (e.g., magnetite), which might also contain some of the iron attributed to normative chlorite. Nevertheless, these calculations were undertaken not to obtain rigid normative compositions, but to test further whether variations in normative mineralogy might be responsible for observed variations in $\delta^{18}O$.

Normative calculations for sericite resulted in a positive correlation with observed petrographic abundances of sericite for both the Mine Horizon and for the RBS (Appendix 16-2 and 17-2). Ankerite data and chlorite data, on the other hand, clearly produced overestimates of observed abundances, suggesting that other mineralogical species may contain some calcium and iron, respectively. Quartz abundances tend to be high, although the normative quartz abundance is a cumulative product of abundance errors for all other calculated mineralogies.

Using the calculated normative values for sericite, ankerite, chlorite and quartz, diagrams were constructed (for the RBS and for the Mine Horizon, separately) against measured $\delta^{18}O$ values (Appendix 16-3). From these graphs, some Mine Horizon normative quartz and chlorite samples appear to increase and decrease respectively against increasing $\delta^{18}O$, as would be predicted by theoretical isotopic fractionation trends (see above), even though these graphs returned low R^2 values in regression analyses. Normative ankerite data demonstrates little or no correlation with $\delta^{18}O$. Yet based on theoretical data, the mineralogy (particularly the chlorite abundance) may have constrained

$\delta^{18}O$ to some extent, and may therefore be partially responsible for some of the lower $\delta^{18}O$ values in whole-rock analyses.

Nevertheless, by separating the RBS from the Mine Horizon, it was hoped that variations due to differences in mineralogical abundance could be further minimized. Six samples returned anomalously low $\delta^{18}O$ values for the RBS. Of these, five samples occur in close spatial proximity (WAZ), and two of those have little or no significant chlorite (normative or petrographic). The sixth anomalously low $\delta^{18}O$ value from the RBS is also devoid of chlorite. Therefore Mine Horizon isotopic data show little dependence on chlorite (normative or petrographic), with the lowest $\delta^{18}O$ values corresponding to samples nearly devoid of chlorite. These observations suggest that the isotopic composition of whole-rock samples was probably more dependent on the $\delta^{18}O$ of the fluid than on the existing mineralogy, or at least that the isotopic composition of the whole rock shows significantly lesser variability than do mineralogical abundances. Therefore, isotopic variations can not be attributed to mineralogical variations alone.

Projecting normative quartz abundances from the Mine Horizon to 100% on normative quartz vs. $\delta^{18}O$ plots (Hoy, 1992) suggests a $\delta^{18}O$ composition of 13 to 15‰ for quartz (Appendix 17-3). Projection of normative quartz abundances to 100% for the RBS implies an even higher $\delta^{18}O$ composition for quartz than for that of the Mine Horizon. This observation suggests that fluids responsible for alteration of the RBS either

had a greater temperature than those of the Mine Horizon or were more enriched in ^{18}O. Again, if the Mine Horizon represents the water/rock interface (seafloor) at time of ore deposition, it is normal to expect that alteration along this horizon would have been produced mainly by seawater. Therefore, having $\delta^{18}O$ lower in the Mine Horizon than in the RBS, might further indicate exposure to greater heat that produced more evolved (^{18}O-enriched) fluids. Using an assumed temperature < 200 °C for the Mine Horizon (seafloor) with estimated isotopic compositions of quartz at 13 to 15‰ (average in Mine Horizon) implies that the $\delta^{18}O$ of the alteration fluid was approximately 0 ± 3‰ (Fig. 23, from water/quartz fractionation equations). This would be consistent with alteration by seawater.

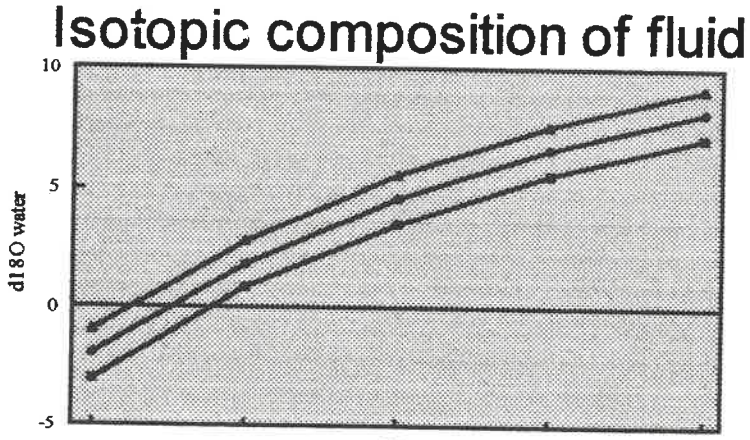

Temperature	150	200	250	300	350
d qtz=13	-3	1	4	6	7
d qtz=14	-2	2	5	7	8
d qtz=15	-1	3	6	8	9

Figure 24: Plot of isotopic composition of hydrothermal fluid (y-axis) vs. temperature(x-axis), varying according to estimated isotopic composition of quartz (based on normative calculations).

5.6 Discussion

Following the typical VMS model, and thus calling for deposition of massive sulphides at or near the water/rock interface (Sangster, 1972; Franklin et al., 1981), the lack of significant deviations in $\delta^{18}O$ values from the mean could be explained by a highly focussed discharge of hydrothermal fluids. Under such conditions, if no secondary draw-down of seawater occurred close to the Normetal deposit, deviations from the average would only be recorded in the immediate vicinity of fluid discharge. An absence of local draw-down might therefore imply that upwardly convected fluids originated either lower within the stratigraphy (possibly along regional aquifers) or at greater lateral distances. In terms of local deviations from the mean $\delta^{18}O$, only two such areas are recognized. Considering that seawater is believed to have remained constant at $\delta^{18}O = 0$ ($\pm$ 1‰), then areas of potential draw-down are limited to the zone overlying the LDD intrusion (lower than mean $\delta^{18}O$). The second area showing deviations from the mean occurs to the west of Normetal (showing higher than mean $\delta^{18}O$) and would represent either discharge of hotter fluids or discharge by more evolved fluids.

A second possible explanation for the absence of regional isotopic variations within the Mine Horizon might be that fluid draw-down occurred relatively homogeneously along the seafloor. Widespread diffuse downward percolation of fluids as

opposed to a more focussed discharge of heated hydrothermal fluids would not result in significant differential isotopic re-equilibration within the recharge zone.

Data representing the RBS suggests that temperatures may have been greater in close proximity to the Normetal deposit as would be expected from the typical VMS model. This observation is postulated from the regional increase in $\delta^{18}O$ near this deposit. Another factor which could create such a trend would be a progressively isotopically evolved (higher $\delta^{18}O$) fluid proximal to the Normetal deposit. A lower than average $\delta^{18}O$ value in drill hole 1, on the other hand, probably supports the first, heat-gradient hypothesis. Otherwise, two distinct fluids must be conceived to explain the observed variations. Therefore using the former model, the lower $\delta^{18}O$ values would result from locally water-dominated conditions. The regional implication of this model is that increasing $\delta^{18}O$ of whole-rock analyses might point to areas of high temperature flux, whereas proximal low values (drill hole 1) might represent areas of greater circulation proximal to mineralization (i.e., a water-dominated system). Inversely, areas such as the LDD intrusion which show only lower than average $\delta^{18}O$ values may not have convected equally evolved fluids. That is, the fluids may have had high temperatures or long residence periods (rock-dominated). It is worth mention that the Kidd Creek deposit also shows rapid reversal of $\delta^{18}O$ directly within the footwall and within areas of regionally, progressive ^{18}O enrichment (Beaty et al., 1988). The WAZ shows a coexistence of higher and lower than average $\delta^{18}O$ values of this type.

CONCLUSIONS

The results of the present study suggest that the best indicators of mineralization in the Mine Horizon are: 1) (MnO × 25)/FeO in ankerites (Fig. 19), 2) MnO/(MnO + MgO) in chloritoids and in chlorites (Fig. 18); and 3) MnO and Fe_2O_3 mass-gains in whole-rock (Fig. 14). In the RBS, the best indicators of overlying mineralization are: 1) SiO_2 and K_2O mass gains (Fig. 12); 2) CaO and Na_2O mass losses; 3) Large (1992) alteration indices (MgO + K2O)/(Na2O + CaO + MgO + K2O) without mass-change considerations which shows consistent increase towards the Normetal deposit (Fig. 16); and 4) coexistence or reversals from high $\delta^{18}O$ to low $\delta^{18}O$ with respect to average $\delta^{18}O$.

Due to the time and costs involved in microprobe analyses and to the still greater costs and tediousness in performing $\delta^{18}O$ analyses, whole-rock analyses complemented by mass-change calculations remain, in this study, the most cost-effective approach to the identification of indicators of VMS-type mineralization. Nevertheless, quantitative microprobe and $\delta^{18}O$ analyses clearly demonstrate their potential as guides to mineralization.

More specifically, the whole-rock geochemistry, quantitative mineralogy and oxygen isotope data studied here lead us the following general conclusions:

1) Assuming that seawater is the dominant source of fluids (Franklin et al., 1981), and that this seawater has been heated and circulated by an as yet undetermined heat source (the Normetal pluton? i.e., a synvolcanic intrusion; Campbell et al., 1984) which became metalliferous by wall-rock reactions, then oxygen isotopic data suggest limited areas of high fluid-flow (low $\delta^{18}O$) and others of relatively higher temperature (high $\delta^{18}O$) in the Normetal camp (Figs. 22 and 23). Of these, a regionally increasing trend in $\delta^{18}O$ in the RBS near the Normetal deposit, is believed to represent locally high temperatures (proximal to the exhalative vent). This evidence, combined with abundant whole-rock alteration below the deposit, and characteristic metal zonations within the deposit strongly supports a typical VMS model for emplacement of massive sulphide deposits (Franklin et al., 1981; Franklin, 1990; see Fig. 25).

2) It is interesting to note that another region of higher than average fluid circulation occurs over the LDD intrusion. Like the area near the Normetal deposit, this zone also coincides with a significant gap in the footwall sediment horizon, but unlike the former, the subvolcanic intrusion in this case directly underlies the sediment gap at shallow stratigraphic depths. The local absence of sediments in this case might in fact be due to a paleotopographic high spatially related to the intrusion, if the intrusion predated or was coeval with the sediments. If, on the other hand, the intrusion postdated the sediments, then a possible explanation for their local absence could be the presence of a small caldera overlying the intrusion. The absence of highly laminated tuffs, coarse breccias and other

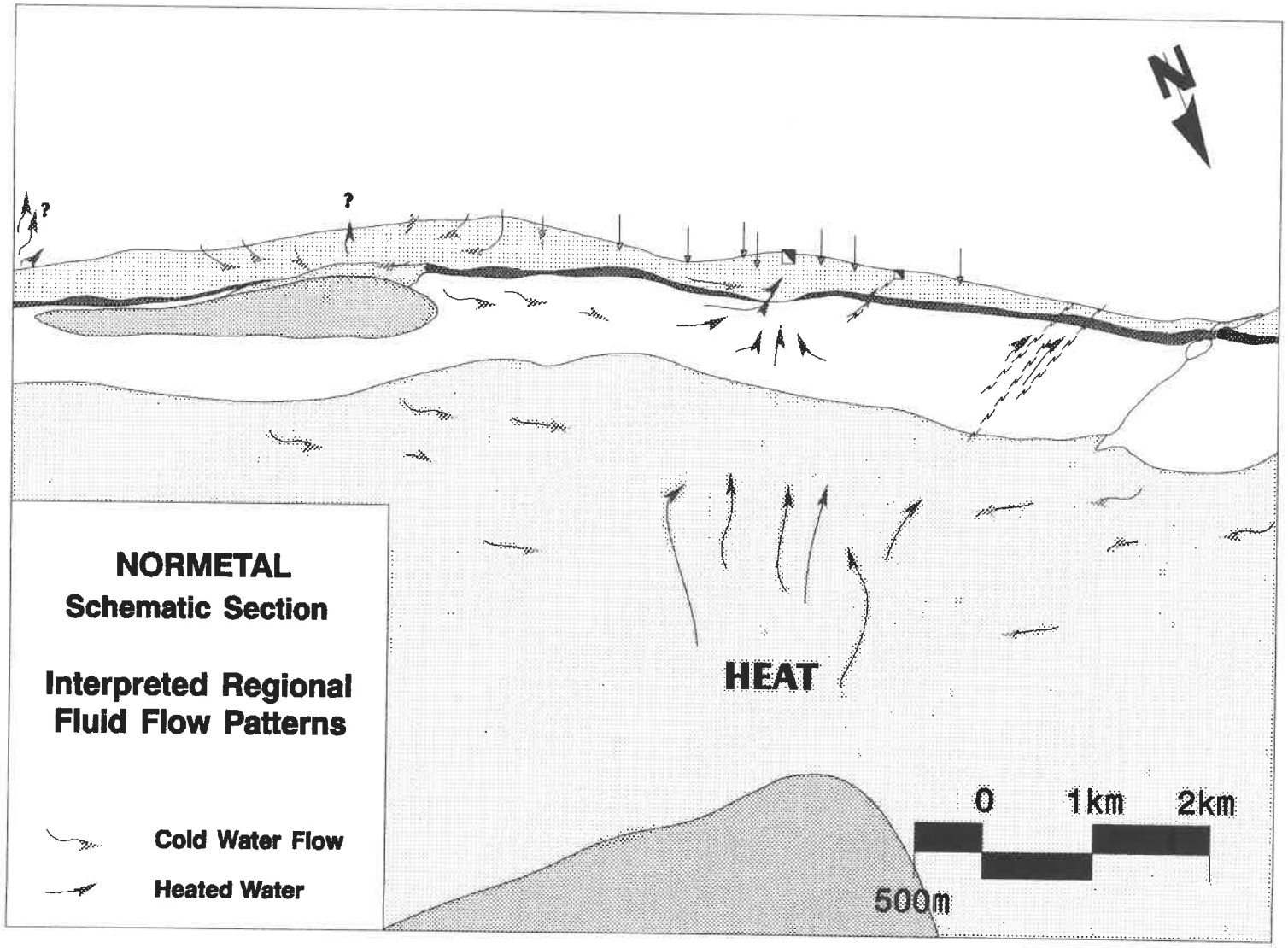

Figure 25: Regional schematic section of the Normetal camp and interpreted fluid-flow patterns.

such indicators of proximity tend to favour the first hypothesis. As such, the interpreted high circulation of fluid, inferred from lower than average $\delta^{18}O$ values, could have been produced by the draw-down of fluids driven by a larger, deeper heat source.

3) In comparing fluids which may have been driven by the LDD intrusion to those plutons which would have produced the Normetal deposit (the Normetal pluton?), it may be significant to consider the relative depths of the intrusion with respect to the seafloor. If the LDD pluton and the Normetal pluton had intruded beneath the same horizon (Mine horizon), then clearly the LDD intrusion would have been capable of circulating water only at shallow depths. This difference in the depth of circulation would have reduced the time of residence of potential ore-forming fluids in the underlying strata and could therefore have reduced their potential to dissolve metals within the hydrothermal reservoir.

4) Mineralization at the Normetal deposit cannot be clearly attributed to a specific directly underlying heat source. It has been suggested that the Normetal pluton could represent such a synvolcanic heat source (personal communication, M. Richard, 1991), but recent data suggesting an incompatibility between the ages of the pluton and the overlying volcanics may not support this interpretation (personal communication, D. Moore, 1992). Nevertheless, it is possible that parts of the Normetal pluton accompanied or postdated the overlying volcanics, whereas other portions may have predated it. If a major portion of the Normetal pluton were coeval with the volcanics, then such a heat

source would have been large and would have convected fluids to a much greater depth than the much smaller LDD intrusion. With respect to the LDD intrusion, deeper penetration of potential ore-forming fluids associated with the larger Normetal intrusion would also imply the existence of a much larger hydrothermal reservoir and also a greater evolution of the hydrothermal fluids.

5) Using this model, the sedimentary horizon, with a notable gap underlying the Normetal deposit, could have played a much greater role in controlling fluid flow, than would be the case for the overlying the LDD intrusion. Considering the sediments as a regional aquitard, any break or gap in the sediments (synvolcanic faults or paleo-topographic highs) would be a potential area for upward hydrothermal circulation and exhalation and therefore a potential site for VMS-type mineralization, particularly if these openings across the sediment horizon coincided with underlying areas of anomalous heat flux (again, favoring the coexistence of higher and lower than average $\delta^{18}O$ as indicator of potential mineralization, i.e., wave-shaped $\delta^{18}O$ patterns).

6) Another area of interest in terms of fluid circulation is the WAZ. Oxygen isotopic data from this zone clearly suggests that it was a site of significant fluid flow (low $\delta^{18}O$ values), as does the observed cross-cutting alteration mineralogy (chloritoid-chlorite-sericite-ankerite). A single high $\delta^{18}O$ value directly east of the alteration zone may indicate high temperatures or more evolved fluids, but the abundance

of disseminated and stringer mineralization within the alteration zone is sufficient to assume that circulation of mineralizing fluids had taken place. Such alteration in the absence of a gap in the sediments may be explained by faulting (syn-volcanic?). The same explanation is assumed to apply to the Normetmar mineralization.

7) Calculated mass gains and mass losses provide support for a regional model with a deep heat source. A zone of significant sodium, manganese, calcium and iron depletion is noted below the sediments and proximally to the Normetal deposit (Fig. 26). Inversely, the Mine horizon proximally to the Normetal deposit is significantly enriched in most of the same elements, with the exception of sodium. These trends suggest that the fluids responsible for deposition of sulphides may have evolved and derived many of their metallic constituents from below the sedimentary horizon. Only minor mass losses are found proximal to the Normetal deposit within the Mine Horizon. Silica is enriched or less depleted close to the Normetal deposit below the sediments, compared to rocks distal to the Normetal deposit at the same stratigraphic level. Cherts overlying the Normetal deposit and proximal to Normetmar testify to the silica-rich nature of the convected hydrothermal fluids. This distribution of silica mass-gains and mass-losses would suggest that the fluids reached silica saturation at greater distances or at colder temperatures than observed below the Normetal deposit (i.e., prior to reaching it), while at the same time the fluids were progressively enriching source rocks in potassium (possibly by conversion of plagioclase to muscovite).

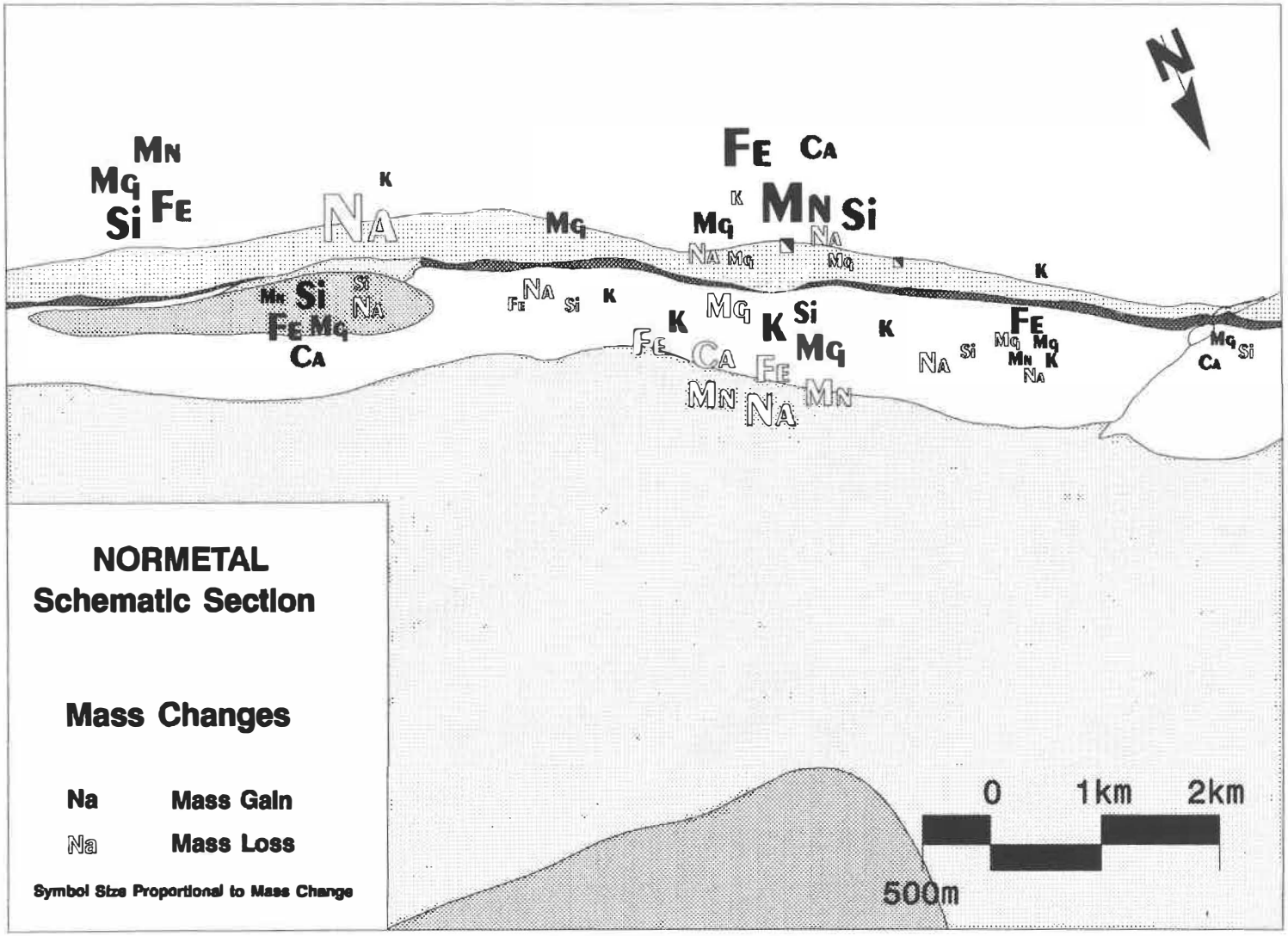

Figure 26: Graphic representation of mass changes on a regional schematic section of the Normetal camp.

8) In reviewing the mass-change data proximal to the LDD intrusion, it is interesting to note that observed mass changes reflect a mirror image of those noted proximal to the Normetal deposit. The Mine horizon overlying the LDD shows a broad halo of lower than average $\delta^{18}O$ values which is also notable for an equally large halo of sodium depletion and minor potassium enrichment. On the other hand, the RBS horizon is locally enriched in silica, iron, magnesium, calcium and minor amounts of manganese. A possible explanation for these opposite trends proximal to the LDD intrusion is that downward convected fluids caused in-situ precipitation of dissolved constituents of heated fluids at lower stratigraphic levels by mixing with cooler seawater, thereby impeding the precipitation of exhalative sediments at the seafloor. Alternatively, the observed alteration may represent fluid draw-down through the sediment gap over the LDD intrusion due to a deeper heat source (e.g., the Normetal pluton?). A combination of both these effects is also possible.

9) Similar mass-change trends are observed at the WAZ, but unlike the LDD intrusion, the WAZ is also characterized by significant amounts of disseminated and stringer sulphides and by a coexistence of low and high $\delta^{18}O$ values. If the sediments acted as an aquitard, the absence of a sedimentary break above this zone would therefore imply that faulting (syn-volcanic?) would be necessary for upward migration of these fluids.

10) Observed mass losses in Fe_2O_3, CaO, MgO and MnO from the RBS correspond strongly to similar compositional gains in the Mine Horizon proximal to the Normetal deposit, strongly suggesting alteration by a CO_2-rich fluid[1]. This interpretation supports an earlier suggestion that siderite may be an indicator of hydrothermal discharge and therefore a guide to potential VMS-type mineralization. Therefore, compositional variances in carbonates might also be proportional to temperature and fluid evolution. Highest temperatures are assumed to have underlain the Normetal deposit, based on the increasing intensity of mass losses below the sediments near the Normetal deposit, and based on the increasing trend of $\delta^{18}O$ towards the Normetal deposit in the Mine Horizon. Highest intensities of convection are assumed to coincide roughly with areas of greatest heat flux.

11) Chlorite also appears to concentrate manganese, which clearly seems to be one of the best pathfinders to alteration and mineralization within the Normetal volcanics. As such, it reflects the presence of both the Normetal deposit and the WAZ alteration, as well as indicating potential areas for alteration or mineralization east of the LDD intrusion. The lowest FeO/MgO ratios (Mg-rich) in chlorites occur both at the WAZ and some 1600 m east of Normetal, possibly implying different fluids in these areas with respect to those which circulated proximally to the Normetal deposit.

---

[1] FeO, MgO, CaO and MnO are all dominant components of ankerite and siderite.

12) Chloritoid data emphasizes the increases in MnO towards the Normetal deposit. This observation is believed mainly to reflect variations in whole-rock trends based on the abundant occurrence of undeformed chloritoids which clearly formed after deformation. These late chloritoids should be discounted in future studies to obtain more convincing evidence on syn-volcanic alteration. Nevertheless, chloritoid may concentrate MnO with respect to whole-rock contents and may therefore register more subtle variations.

13) These data and observations clearly demonstrate that a well-planned systematic sampling of specific units underlying a potentially mineralized horizon is an effective way to evaluate fluid-flow systematics at a regional scale.

14) Ankerites from the RBS appear to increase in magnesium and manganese while decreasing in iron towards the Normetal deposit. Ankerites from the Mine Horizon also show clearly increasing MnO with proximity to the Normetal deposit. FeO, MgO, MnO and CaO in ankerite potentially may show more subtle variations then the same components in whole-rock analyses, particularly where clear fractionation trends are difficult to establish. Although the apparent concentrations of elements from microprobe analyses of carbonates were somewhat questionable due to the difficulty of calibration, trends in apparent concentration should generally be significant and useful.

15) Areas with lower than average $\delta^{18}O$ values are believed to represent areas of broad-scale fluid circulation of cold seawater or at least broad areas of circulation of large volumes of moderately heated fluids, producing highly water-dominated environments. A single lower than average $\delta^{18}O$ value noted in drill hole 1 in the RBS proximal to the Normetal deposit and occurring within a regionally increasing $\delta^{18}O$ trend suggests a water-dominated area within regions of high heat flux. Other such environments should clearly be favoured targets for potential VMS type mineralization. The proximity of this anomaly to the Normetal deposit and a similarly observed effect at the Kidd Creek deposit support this interpretation.

REFERENCES CITED

AFIFI, A.M., and ESSENE, E.J., 1988. Minfile: A microcomputer program for storage and manipulation of chemical data on minerals. American Mineralogist, v.73, p. 446-448.

BAERTSHI, 1976. Absolute ^{18}O content of standard mean ocean water. Earth Planet. Letters, v. 31, p. 341.

BEATY, D.W., TAYLOR, H.P. Jr and Coad, P.R. 1988. An oxygen isotope study of the kidd creek, ontario, volcanogenic massive sulfide deposit: evidence for a high ^{18}O ore fluid. Economic Geology, v. 83, no 1, p. 1-17.

BEATY, D.W. and TAYLOR, H.P. Jr., 1982. Some petrologic isotopic relationships in the amulet mine, noranda, quebec, and their bearing on the origin of Archean massive deposits. Economic Geology, v. 77, p.95-108.

BERTRAND, C. and HUTCHINSON, R.W., 1973. Metamorphism at the Normetal mine, Northwestern Quebec. Geology and Ore Deposits, v. 76, p. 226-234.

BROWN, W.L., 1948. Normetal Mine, *in* Structural Geology of Canadian Ore Deposits. Canadian Institute of Mining and Metallurgy Special Vol. 1, p. 683-693

CAMPBELL, I.H., LESHER, C.M., Coad, P., Franklin, J.M., Gorton, M.P. and Thurston, P.C., 1984. Rare-Earth element mobility in alteration pipes below massive cu-zn sulfide deposits. Chemical Geology, v. 45, p.181-202.

CATTALANI et BAMBIC, 1991. Lithogeochemistry and alteration, Perron and Desmeloizes townships, Quebec. Internal Report Submitted to Cominco Ltd. 74 pages.

CATTALANI et al, 1990a. La métallogénie des sulfures massifs: Les mines Horne et Quemont, district de Noranda, Québec. Ministère de l'Énergie et des Ressources, report ET 90-07.

CATTALINI et al, 1990b. Géologie et géochimie du gisement d'Ansil, district de Noranda, Québec. Ministère de l'Énergie et des Ressources, report MB 90-26, p 160.

CLARK, 1990. NEWPET. Memorial University of Newfoundland, Department of Earth Sciences, Centre for Earth Resources Research software.

CLAYTON and MAYEDA, 1963. The use of bromine pentafluoride in the extraction of oxygen from oxides and silicates for isotopic analysis. Geochim. Cosmochim. Acta, v. 27, p. 43-52.

CRAIG, 1961 Isotopic composition and origin of the Red Sea and Salton Sea geothermal brines. Science, v. 154, p. 1544-1548.

DEER, W.A., HOWIE, R.A., and ZUSSMAN, J., 1966. An Introduction to the Rock Forming Minerals, Longman Group Ltd., London, 528 pages.

DEPTUCK, R., SQUAIR, H. and WIERZBICKI, V., 1982. Geology of the Detour zinc-copper deposits, Brouillan township, Quebec. *in* Precambrian Sulphide Deposits, H. S. Robinson Memorial Volume, eds. R. W. Spence and J .M. Franklin, Geological Association of Canada. Special Paper 25.

DICKSON, 1965. A modified staining technique for carbonates. Nature, v. 205, no. 4971, p. 587.

FINLOW-BATES, T. and STUMPFL, E.F., 1981. The behavior of the so-called immobile elements in hydrothermally altered rocks associated with volcanogenic submarine-exhalative ore deposits: Mineralium Deposita, v.16, p. 319-328.

FRANKLIN et al, 1981. Volcanic-associated massive sulfide deposits. Economic Geology, 75th Anniv. Vol., p. 485-627.

FRANKLIN, 1990. Volcanic-associated massive sulphide deposits, *in* Gold and base-metal mineralization in the Abitibi Subprovince, Canada, with emphasis on the Quebec segment, Short Course Notes, eds. Ho, S.E, Robert, F. and Groves, D.I., The University of Western Australia, Publication No. 24, p. 211-241.

FRANKLIN, J.M., KASARDA, J. and POULSEN, K.H., 1975. Petrology and chemistry of the alteration zone of the Mattabi massive sulfide deposit. Economic Geology, v. 70, p. 63-79.

GARLICK, H. 1969. The stable isotopes of oxygen, *in* Wedepohl, K.H., ed. Handbook of Geochemistry, 8B., Springer.

GIBSON, H.L., WATKINSON, D.H. and COMBA, C.D.A., 1983. Silicification: hydrothermal alteration in an Archean geothermal system within the Amulet Rhyolite Formation, Noranda, Quebec. Economic Geology, v. 78, p. 954-971.

GOODWIN, A.M. and RIDLER, R.H., 1970. The Abitibi orogenic belt. Can. Geol. Surv. Paper 70-40, p. 1-28.

GREEN, G.R., OHMOTO, H., Date, J. and TAKAHASHI, T., 1983. Whole-rock oxygen isotope distribution in the Fukazawa-Kosaka area, Hokuroku district, Japan, and its potential application to mineral exploration. Economic Geology, Monograph 5, p 395-411.

GREGORY, R.T. and TAYLOR, H.P., 1981. An oxygen isotope profile in a section of Cretaceous oceanic crust, Samail Ophiolite, Oman: evidence for ^{18}O buffering of the oceans by deep (5 > km) seawater-hydrothermal circulation at mid-ocean ridges. Journal of Geophysical Research, v. 86, p. 2737-2755.

GROVES, D., 1984. Stratigraphy, lithology, and hydrothermal alteration of volcanic rocks beneath the Mattabi massive sulfide deposit, Sturgeon Lake, Ontario: M.S. thesis, Univ. Minnesota, Duluth, 115 p.

HAJASH, A. and CHANDLER, G.W., 1981. An experimental investigation of high-temperature interactions between seawater and rhyolite, andesite, basalt, and peridotite: Contr. Mineralogy Petrology, v.78, p.240-254.

HASIK, V., 1991. Pétrographie et géochimie des unités rhyolitiques de la bande felsique de Normétal. B.Sc. thesis, Université de Montréal, 56 pages.

HOY, L.D., 1992. Regional evolution of hydrothermal fluids in the Noranda district, Quebec: evidence from $\delta^{18}O$ alteration zones around volcanogenic maasive sulfide deposits. Economic Geology (in press).

IRVINE, T.N. and BARAGAR, W.R.A., 1971. A guide to chemical classification of the common rocks. Canadian Journal of Earth Sciences, v. 8, p. 523-548.

LARGE, R.R., 1992. Australian volcanic-hosted massive sulfide deposits: features, styles, and genetic models. Economic Geology, v. 87, p. 471-510.

LATULIPPE, M., 1976. Excursion géologique, Val d'Or, Malartic. Ministère des Richesses naturelles du Québec, DP-367, 124 pages.

LESHER, C.M., GOODWIN, A.M., CAMPBELL, I.H. and GORTON, M.P., 1986. Trace-element geochemistry of ore-associated and barren, felsic metavolcanic rocks in the Superior Province, Canada. Canadian Journal Of Earth Sciences, v. 23, p. 222-237.

LOCKWOOD, M.B., 1987. The petrogenetic and economic significance of chloritoid in the Wawa greenstone belt. M.Sc. Thesis, Carlton University, Ottawa, 221 pages.

MACLEAN, W.H., 1990. Mass change calculations in altered rock series. Mineralium Deposita, v. 25, p. 44-49.

MACLEAN, W.H. and KRANIDIOTIS, P., 1987. Immobile element as monitors of mass transfer in hydrothermal alteration, Phelps Dodge massive sulfide deposit, Matagami, Quebec: Economic Geology, v.82, p. 951-962.

MACLEAN, W.H., 1988. Rare earth elements mobility at constant inter-REE ratios in the alteration zone at the Phelps Dodge massive sulfide deposit, Matagami, Quebec: Mineralium Deposita, v.23, p. 231-238.

MACLEAN, W.H. and HOY, L.D., 1991. Geochemistry of hydrothermally altered rocks at the Horne Mine, Noranda, Quebec. Economic Geology, v. 86, p. 506-528.

MORTON, R.L. and FRANKLIN, J.M., 1987. Two-Fold Classification of Archean Volcanic-Associated Massive Sulfide Deposits. Economic Geology, v. 82, p. 1057-1063.

MORTON, R.L., 1990. Volcanogenic massive sulfide deposits: classification based on the physical volcanology of the host rocks, *in* Program with Abstracts, 8th IAGOD Symposium, 12-18th August 1990, Ottawa, p. A14-A15.

MORTON, R.L. and NEBEL, M.L., 1984. Hydrothermal alteration of felsic volcanic rocks at the Helen siderite deposit, Wawa, Ontario. Economic Geology, v. 79, p. 1319-1333.

MOORE, D.W., 1990. Geological summary of Normetal mine based on review of historical mine level plans. Internal report to Cominco Ltd, 7 pages.

MOTTL, M.J., 1983. Metabasalts, axial hot springs, and the structure of hydrothermal system at mid-ocean ridges. Geological Society of America Bulletin, v. 94, p. 161-180.

MUEHLENBACHS, K. and CLAYTON, R.N. 1972. Oxygen isotope studies of fresh and weathered submarine basalts. Canadian Journal of Earth Sciences, v. 9, p. 172-184.

MUNHA, J., BARRIGA, F.J.A.S. and KERRICH, R., 1986. High ^{18}O ore-forming fluids in volcanic-hosted base metal massive sulfide deposits: geologic, $^{18}O/^{16}O$, and D/H evidence from the Iberian pyrite belt; Crandon, Wisconsin, and Blue Hill, Maine. Economic Geology, v. 81, p. 530-552.

SANGSTER, D., 1972. Precambrian Volcanogenic Massive Sulphide Deposits in Canada: A Review. Geol. Surv. Can. Paper 72-22, 44 pages.

SHIKAZONO, N. and KAWAHATA, H., 1987. Compositonal differences in chlorite from hydrothermally altered rocks and hydrothermal ore deposits. Canadian Mineralogist, v. 25, p. 465-474.

SPOONER, E.T.C., BECKINSALE, R.D., ENGLAND, P.C. and SENIOR, A., 1977. Hydration, 18O enrichment and oxidation during ocean floor hydrothermal alteration of ophiolitic metabasic rocks from E. Liguria, Italy. Geochim. Cosmochim. Acta, v. 41, p. 857-871.

TAYLOR, H.P. Jr., 1974. The application of oxygen and hydrogen isotope studies to problems of hydrothermal alteration and ore deposition. Economic Geology, v. 69, p. 843-883.

TESSIER, A., 1991a. The Norcom/Normetal Projects: May 1990 to May 1991 Progress Report. Internal report to Cominco Ltd., 47 pages.

TESSIER, A., 1991b. Norcom/Normetal Properties: Report on Alteration Lithogeochemistry. Internal report to Cominco Ltd.

VALIQUETTE, G., MARCOTTE, D., MELLINGER, M., SMYTH, E., WEBBER, G.R. and DESCHAMPS, F., 1978. Recherche des métallotectes dans la région de Normétal: MERQ, DPV-582, 236 p.

VALIQUETTE, G., MELLINGER, M. and GAGNON, Y., 1980. Lithogéochimie des roches volcaniques de la région de Normétal: MERQ, DPV-310, 90 p.

WATSON, E.B., and HARRISON, T.M., 1983. Zircon saturation revisited: temperature and composition effects in a variety of crustal magma types. Earth Planet. Sci. Lett., V. 64, p. 295-304.

WENNER, D.B. and TAYLOR, H.P., 1973. Oxygen and hydrogen isotope studies of the serpentinization of ultramafic rocks in oceanic environments and continental ophiolite complexes. American Journal of Science, v. 273, p. 207-239.

WINCHESTER, J.A. and FLOYD, P.A., 1977. Geochemical discrimination of different magma series and their differentiation products using immobile elements, Chem. Geol., v. 20, p. 325-343.

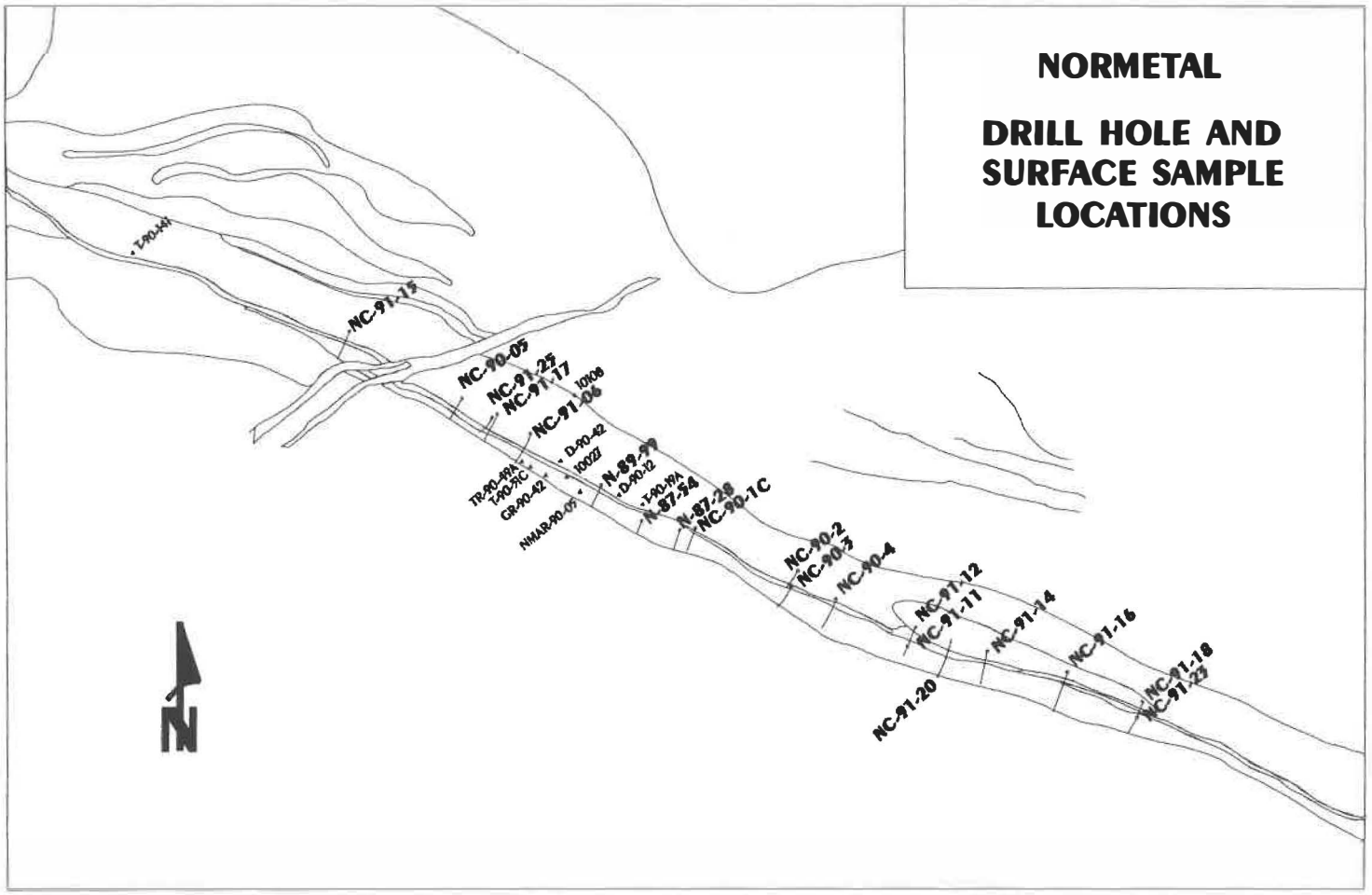

/ DIAMOND DRILL HOLE

· SURFACE SAMPLE

Appendix 1

Drill hole and surface sample locations.

Appendix 2

Whole-rock data and plots for samples from the RBS.

Appendix 2-1
Data for least-altered samples; RBS.

Sample	SiO2	Al2O3	TiO2	Fe2O3	MnO	MgO
10148	60.31	15.62	1.24	9.89	0.15	2.33
10195	65.04	14.86	0.90	7.40	0.11	3.06
10752	78.15	13.65	0.13	1.49	0.00	0.77
VH-90-07	83.84	9.87	0.15	0.58	0.00	0.69
21575	71.21	15.44	0.36	2.99	0.03	0.98
10036	72.92	13.49	0.69	4.49	0.04	1.68
10228	69.26	15.27	0.59	4.51	0.07	1.43
10033	75.27	12.73	0.21	3.04	0.06	0.49

Sample	CaO	Na2O	K2O	P2O5	LOI	Zr	Y
10148	5.45	3.78	0.92	0.31	7.7	296	44
10195	2.90	3.69	1.87	0.17	4.54	214	35
10752	0.24	2.91	2.63	0.02	1.85	169	96
VH-90-07	1.09	2.36	1.38	0.04	1.96	160	39
21575	3.07	3.92	1.87	0.12	3.16	215	47
10036	1.54	3.53	1.41	0.21	2.39	408	54
10228	3.70	3.58	1.40	0.19	4.08	193	23
10033	2.12	4.37	1.68	0.03	3.31	305	57

Data normalized to 100%, volatile free.

Appendix 2-2
Plots of fractionation trends (RBS).

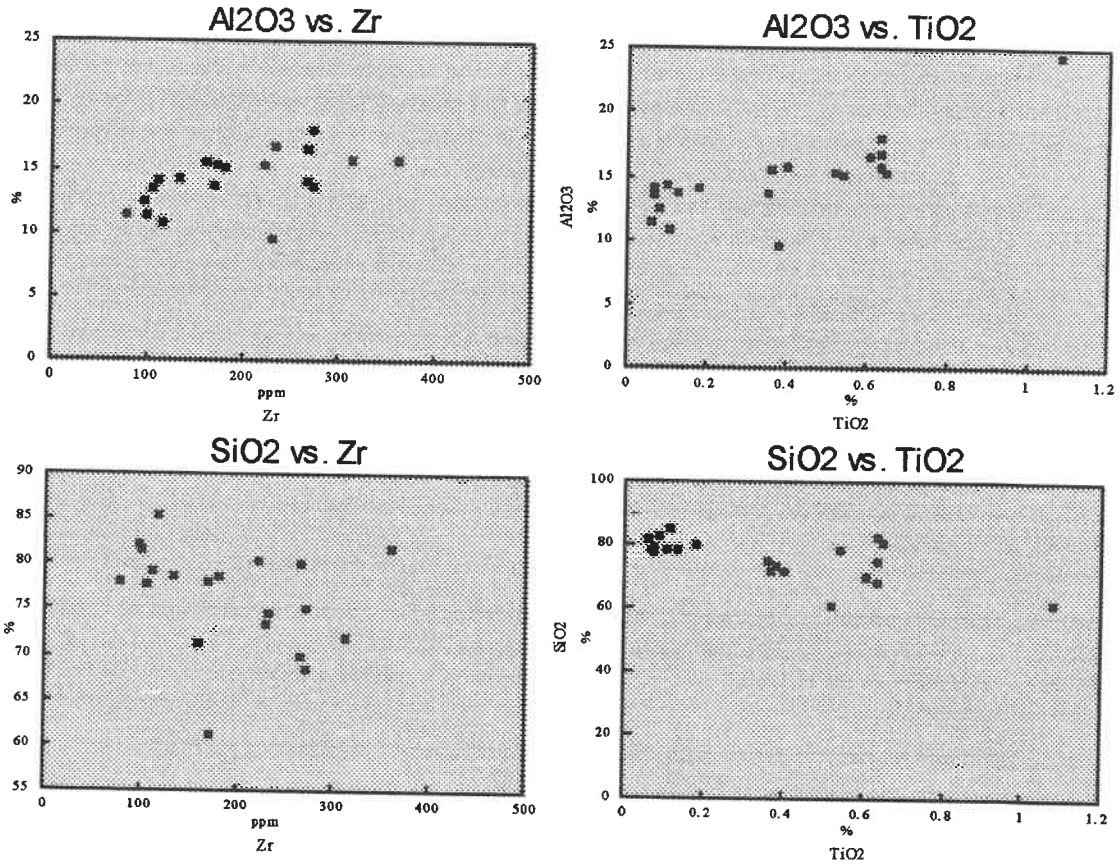

Appendix 2-3
Plots of fractionation trends for least-altered samples (RBS).

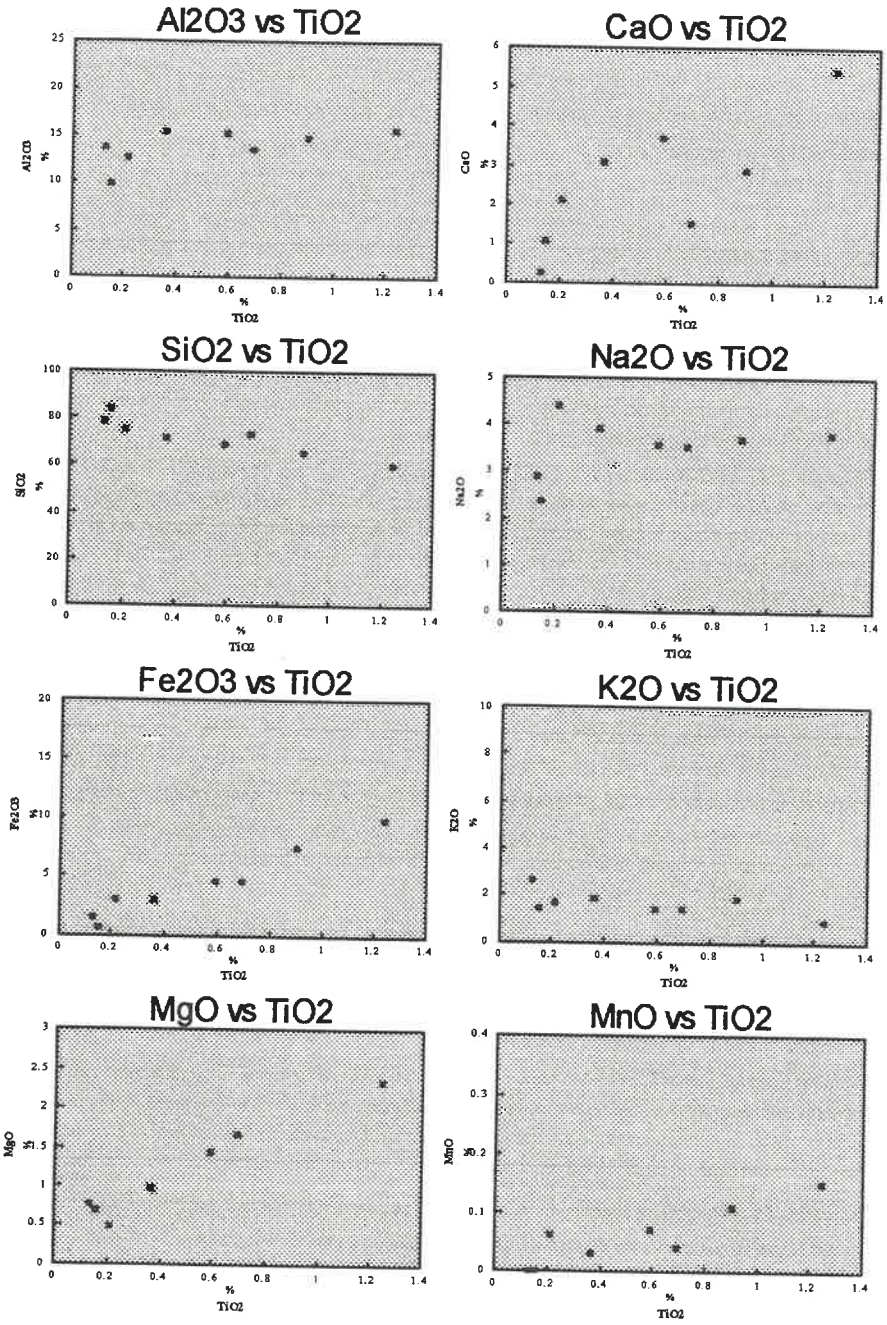

Appendix 2-4
Plots of fractionation trends for least-altered samples (RBS).

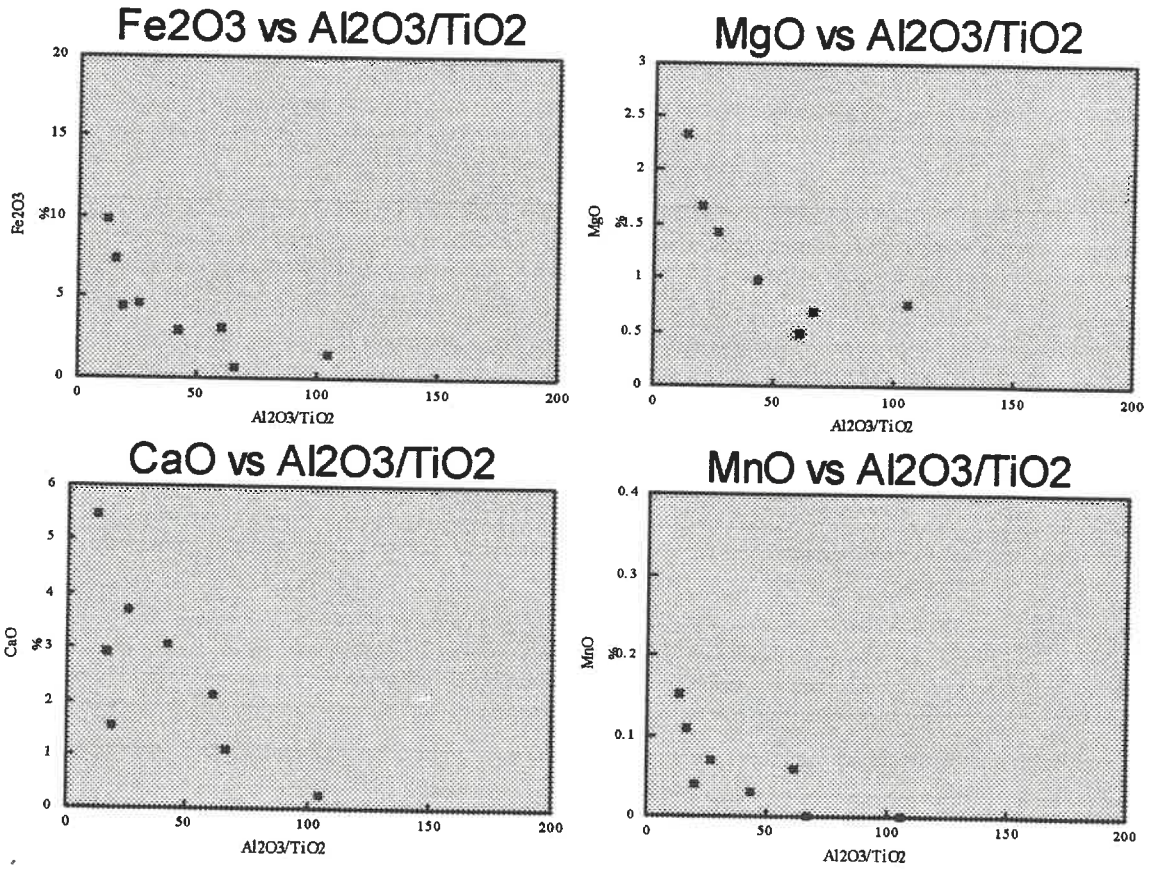

Appendix 2-5
Whole-rock data (RBS).

Sample	DDH	SIO2	AL2O3	CAO	MGO	NA2O	K2O	FE2O3	MNO	TIO2	P2O5
D-90-12	S	85.16	10.80	0.00	0.06	0.13	3.05	0.66	0.02	0.11	0.02
D-90-42	S	78.03	11.32	0.57	0.08	0.37	9.30	0.24	0.01	0.06	0.02
T-90-141	S	77.63	13.47	1.94	0.84	2.47	2.16	1.37	0.03	0.07	0.02
T-90-19A	S	79.11	13.98	0.10	1.63	2.42	1.66	1.00	0.01	0.07	0.01
VH-90-01	S	80.46	15.41	0.37	0.18	0.00	1.85	0.89	0.00	0.65	0.19
VH-90-05	S	81.38	11.41	0.01	0.18	0.09	6.49	0.35	0.00	0.06	0.03
TS-36	1	74.65	16.81	0.73	0.50	0.88	4.77	0.68	0.01	0.64	0.33
TS-37	1	69.92	16.55	2.73	2.56	0.14	5.50	1.78	0.06	0.61	0.15
TS-38	2	78.51	15.17	0.05	0.43	0.45	4.29	0.51	0.01	0.54	0.04
TS-39	2	78.00	13.63	0.24	0.77	2.90	2.63	1.66	0.01	0.13	0.02
TS-41	4	61.57	24.50	1.00	1.18	1.34	6.90	2.35	0.02	1.08	0.06
TS-72	5	61.11	15.30	1.73	2.59	0.13	0.58	17.40	0.38	0.52	0.26
TS-42	6	68.33	18.01	0.94	2.09	0.59	4.30	4.97	0.07	0.64	0.07
TS-47	12	71.88	15.80	1.61	1.43	2.33	2.67	3.73	0.06	0.40	0.08
TS-48	14	73.29	9.46	3.25	1.58	0.58	1.23	10.03	0.12	0.38	0.06
TS-51	15	78.47	14.27	0.72	0.74	0.28	4.39	0.98	0.02	0.10	0.03
TS-58	17	81.91	15.75	0.10	0.22	0.27	0.55	0.50	0.01	0.64	0.05
TS-63	18	71.21	15.44	3.07	0.98	3.92	1.87	2.99	0.03	0.36	0.12
TS-66	20	75.06	13.73	1.66	1.38	1.85	3.24	2.63	0.03	0.36	0.05
TS-85	25	80.02	14.16	0.05	0.57	0.25	2.06	2.55	0.11	0.18	0.04
TS-82	99	82.02	12.52	0.00	1.03	0.43	3.00	0.88	0.01	0.08	0.02

Sample	CR	RB	SR	Y	ZR	NB	BA	LOI
D-90-12	103	53	16	37	119	13	186	1.47
D-90-42	219	122	31	84	80	28	374	0.85
T-90-141	135	116	81	99	107	27	618	1.93
T-90-19A	113	62	92	78	112	28	372	2.23
VH-90-01		47	40	32	224	11		2.04
VH-90-05		97	48	43	100	15.6		0.68
TS-36	27	71	29	22	235	18	301	2.39
TS-37	15	85	13	54	268	20	248	5.54
TS-38	49	110	60	17	182	15	439	1.93
TS-39	73	102	72	96	169	23	399	1.85
TS-41	62	171	71	101	670	36	573	3.39
TS-72	283	30	43	20	172	10	199	3.77
TS-42	155	121	107	37	272	27	702	3.23
TS-47	46	106	62	54	315	17	439	3.23
TS-48	138	43	-10	42	232	21	209	3.54
TS-51	79	103	26	59	135	34	517	1.93
TS-58	175	31	-10	66	361	25	164	2.08
TS-63	110	44	134	12	162	17	340	3.16
TS-66	79	124	48	40	273	32	597	3.54
TS-85	118	60	10	76	267	22	498	2.16
TS-82	17	80	71	45	99	38	331	2.08

Data normalized to 100%, volatile free.

Appendix 2-6
Plots of major elements vs. monitor elements (RBS).

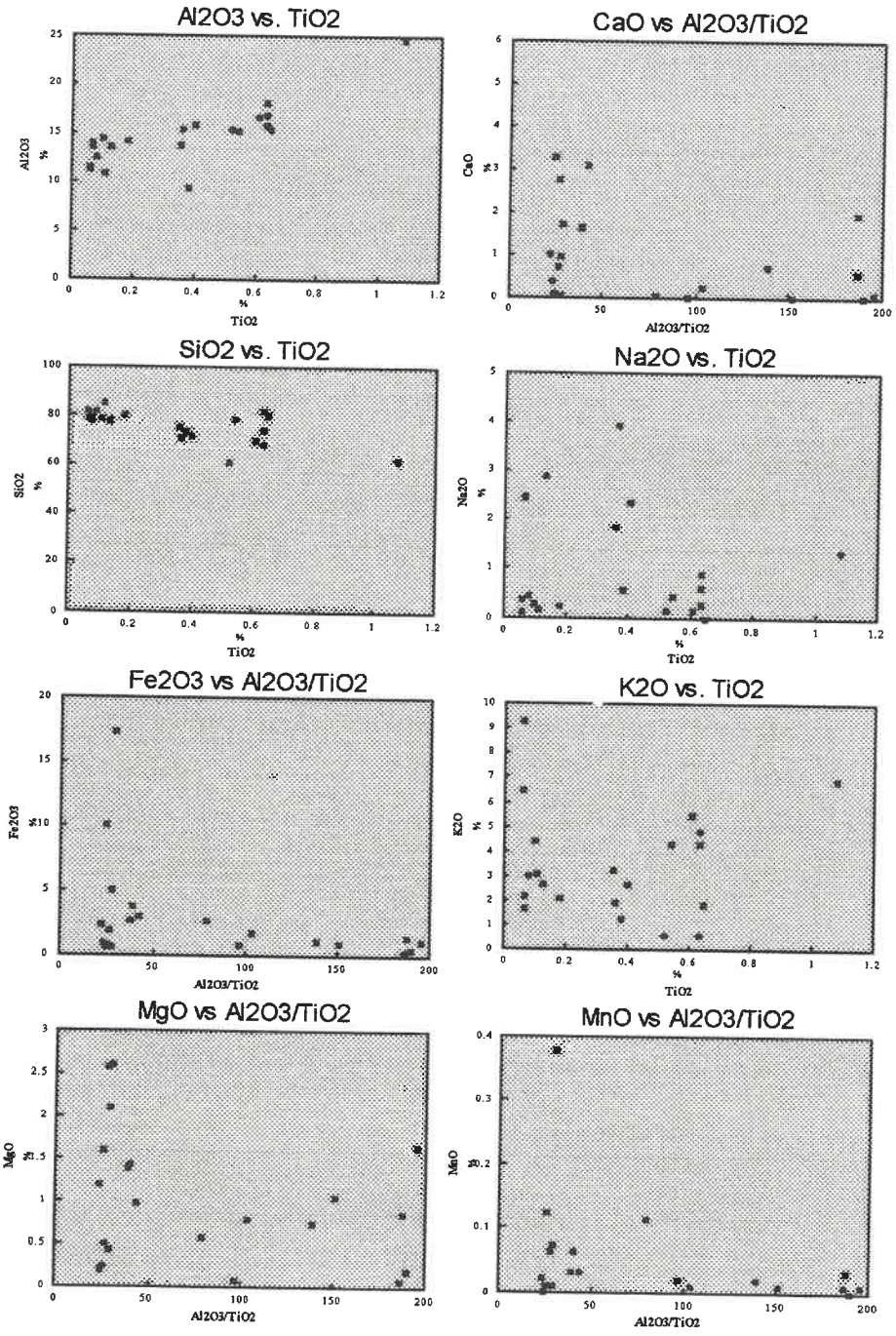

Appendix 2-7
Calculated precursor compositions (RBS).

Sample	DDH	SIO2	AL2O3	CAO	MGO	NA2O	K2O	FE2O3	MNO	TIO2
Unit 1										
D-90-12	s	77.6	12.7	0.8	0.45	6.0	2.0	1.2	0.01	0.1
D-90-42	s	78.1	12.2	0.25	0.2	3.3	2.0	1	0.01	0.1
T-90-141	s	78.0	12.2	0.25	0.2	3.1	2.0	1	0.01	0.1
T-90-19A	s	78.0	12.2	0.25	0.2	3.1	2.0	1	0.01	0.1
TS-51	15	77.6	12.4	0.35	0.3	3.9	2.0	1.2	0.01	0.1
TS-82	99	77.9	12.3	0.25	0.3	3.4	2.0	1.2	0.01	0.1
TS-39	2	77.2	12.6	0.7	0.4	3.1	2.0	1.2	0.01	0.1
TS-85	25	76.7	13.0	1.2	0.55	5.3	1.9	1.5	0.02	0.2
VH-90-05	s	78.2	12.2	0.01	0.2	5.0	2.0	1	0.01	0.1
Average		**77.70**	**12.41**	**0.45**	**0.31**	**4.01**	**1.97**	**1.14**	**0.01**	**0.09**
Unit 2										
TS-36	1	71.2	16.4	3.35	1.35	5.3	1.8	4	0.08	0.6
TS-38	2	72.5	16.0	3.35	1.35	6.0	1.9	4	0.08	0.6
TS-41	4	64.5	17.6	3.5	1.5	5.7	1.8	4.5	0.09	0.8
TS-42	6	70.5	16.0	3.35	1.35	6.0	1.8	4	0.08	0.6
TS-47	12	73.6	14.5	2.7	1.05	3.4	1.8	3.5	0.05	0.4
TS-48	14	74.0	16.9	3.5	1.5	4.9	1.7	4.5	0.09	0.7
TS-63	18	74.1	14.2	2.5	1	3.2	1.8	3	0.04	0.3
TS-66	22	74.4	14.6	2.7	1.05	3.4	1.9	3.5	0.05	0.4
Unit 3										
TS-33	5	71.1	15.8	3.25	1.35	0.0	1.2	4	0.07	0.5
TS-37	1	71.0	16.2	3.35	1.35	0.0	1.9	4	0.08	0.6
TS-58	17	71.8	16.9	3.5	1.5	0.0	1.1	4	0.09	0.7
VH-90-01	s	71.5	17.2	3.5	1.5	0.0	1.6	4.5	0.09	0.7
Average		**71.37**	**16.54**	**3.40**	**1.43**	**0.00**		**4.13**	**0.08**	**0.64**

Appendix 2-8
Calculated mass changes (RBS).

Sample	SIO2	AL2O3	CAO	MGO	NA2O	K2O	FE2O3	MNO
D-90-12	22.6	0.0	-0.8	-0.4	-5.8	1.6	-0.4	0.0
D-90-42	5.9	0.0	0.4	-0.1	-2.9	8.0	-0.7	0.0
T-90-141	-7.7	0.0	1.5	0.6	-0.8	-0.0	0.2	0.0
T-90-19A	-9.1	0.0	-0.2	1.2	-1.0	-0.5	-0.1	-0.0
VH-90-01	18.4	0.0	-3.1	-1.3	0.0	0.4	-3.5	-0.1
VH-90-05	8.8	-0.0	0.0	-0.0	-4.9	4.9	-0.6	-0.0
TS-36	1.8	0.0	-2.6	-0.9	-4.4	2.8	-3.3	-0.1
TS-37	-2.4	0.0	-0.7	1.2	0.1	3.5	-2.3	-0.0
TS-38	10.4	-0.0	-3.3	-0.9	-5.5	2.7	-3.5	-0.1
TS-39	-4.9	0.0	-0.5	0.3	-0.4	0.5	0.3	-0.0
TS-41	-20.3	0.0	-2.8	-0.7	-4.8	3.1	-2.8	-0.1
TS-72	-8.0	0.0	-1.5	1.3	0.1	-0.6	14.0	0.3
TS-42	-9.8	0.0	-2.5	0.5	-5.5	2.0	0.4	-0.0
TS-47	-7.6	0.0	-1.2	0.3	-1.2	0.6	-0.1	0.0
TS-48	56.9	0.0	2.3	1.3	-3.9	0.5	13.4	0.1
TS-51	-9.5	-0.0	0.3	0.3	-3.6	1.8	-0.4	0.0
TS-58	15.9	0.0	-3.4	-1.3	0.3	-0.5	-3.5	-0.1
TS-63	-8.3	0.0	0.3	-0.1	0.4	-0.0	-0.2	-0.0
TS-66	5.4	-0.0	-0.9	0.4	-1.4	1.6	-0.7	-0.0
TS-85	-3.5	0.0	-1.2	-0.0	-5.0	-0.0	0.8	0.1
TS-82	2.8	0.0	-0.3	0.7	-3.0	1.0	-0.3	0.0

Appendix 3

Whole-rock data and plots for samples from the Mine Horizon.

Appendix 3-1
Data for least-altered samples (Mine Horizon).

Sample	DDH	SIO2	AL2O3	CAO	MGO	NA2O	K2O	FE2O3	MNO	TIO2	P2O5	LOI
10345	5	76.55	12.10	1.59	1.69	1.31	1.64	4.71	0.11	0.27	0.03	2.54
10352	5	67.45	15.90	4.96	1.85	1.82	1.74	5.54	0.08	0.54	0.12	3.85
10353	4	67.06	15.97	3.73	1.87	3.26	1.21	6.17	0.08	0.53	0.11	2.77
10793	4	57.76	15.88	5.43	3.83	4.65	0.17	10.65	0.17	1.22	0.24	4.47
10794	4	60.26	15.64	4.49	2.99	4.68	0.42	9.87	0.15	1.23	0.27	2.93
10795	4	60.69	15.15	4.20	3.25	5.64	0.09	9.41	0.10	1.20	0.26	4.62
10799	4	60.65	16.06	3.57	3.02	3.83	1.89	9.50	0.12	1.07	0.30	5.77
10808	4	61.28	15.22	3.66	2.71	6.10	0.10	9.41	0.17	1.11	0.24	3.62
10811	4	67.33	14.56	3.55	2.60	1.19	2.61	7.43	0.15	0.50	0.09	5.31
19408	11	61.91	15.76	4.05	4.50	6.30	0.26	6.42	0.08	0.62	0.09	2.62
19409	11	60.99	16.05	4.74	4.08	5.16	1.43	6.69	0.14	0.63	0.10	5.47
19955	23	66.34	12.57	3.33	2.97	3.15	0.96	9.32	0.18	0.91	0.28	3.31
19956	23	60.73	14.85	5.95	3.09	3.96	0.86	9.17	0.16	1.03	0.21	3.23
19957	23	60.29	14.66	6.12	3.33	2.80	0.89	10.36	0.13	1.17	0.25	2.54
19958	23	56.70	15.81	4.33	3.67	3.93	1.91	11.86	0.16	1.36	0.26	2.62
19963	23	74.54	10.58	4.16	2.45	0.40	2.51	4.86	0.14	0.32	0.04	6.77
21331	23	76.91	13.11	0.43	1.01	0.39	3.19	4.51	0.06	0.34	0.04	3.31

Sample	CR	RB	SR	Y	ZR	NB	BA
10345	73	50	97	74	398	20	295
10352	54	39	188	17	147	-10	176
10353	77	42	101	20	183	17	187
10793	20	-10	133	31	156	32	130
10794	48	14	146	29	273	29	175
10795	29	18	99	35	267	-10	93
10799	25	57	87	48	364	20	322
10808	18	14	75	28	205	24	78
10811	31	54	40	75	447	33	302
19408	239	18	194	15	145	10	136
19409	214	29	78	23	148	11	467
19955	75	27	65	34	272	32	318
19956	45	23	121	39	184	34	153
19957	46	34	203	38	203	16	190
19958	34	68	129	30	240	33	307
19963	47	50	42	85	412	19	330
21331	89	55	23	76	402	25	527

Data normalized to 100%, volatile free.

Appendix 3-2
Plots of fractionation trends for least-altered samples (Mine Horizon).

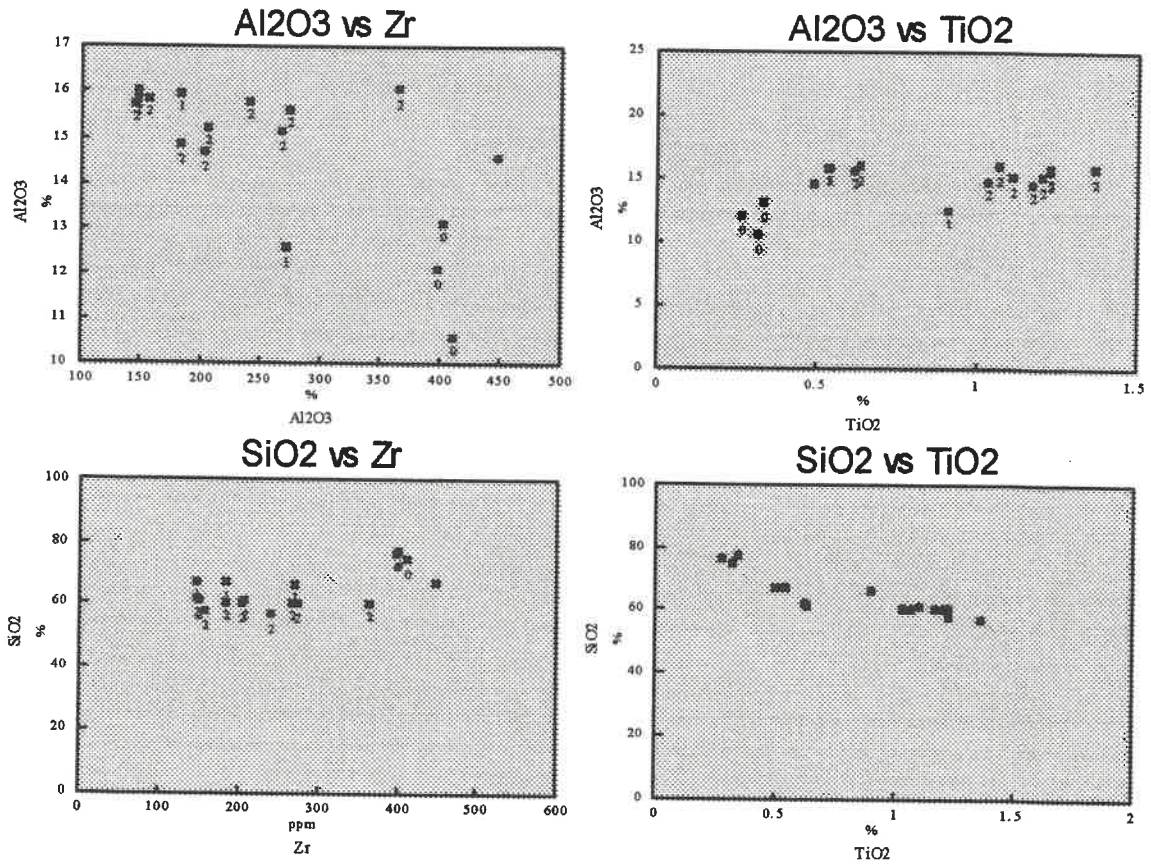

Data labels refer to rock type; Rhyolite 0, Dacite 1, Andesite 2.

Appendix 3-3
Plots of fractionation trends for least-altered samples (Mine Horizon).

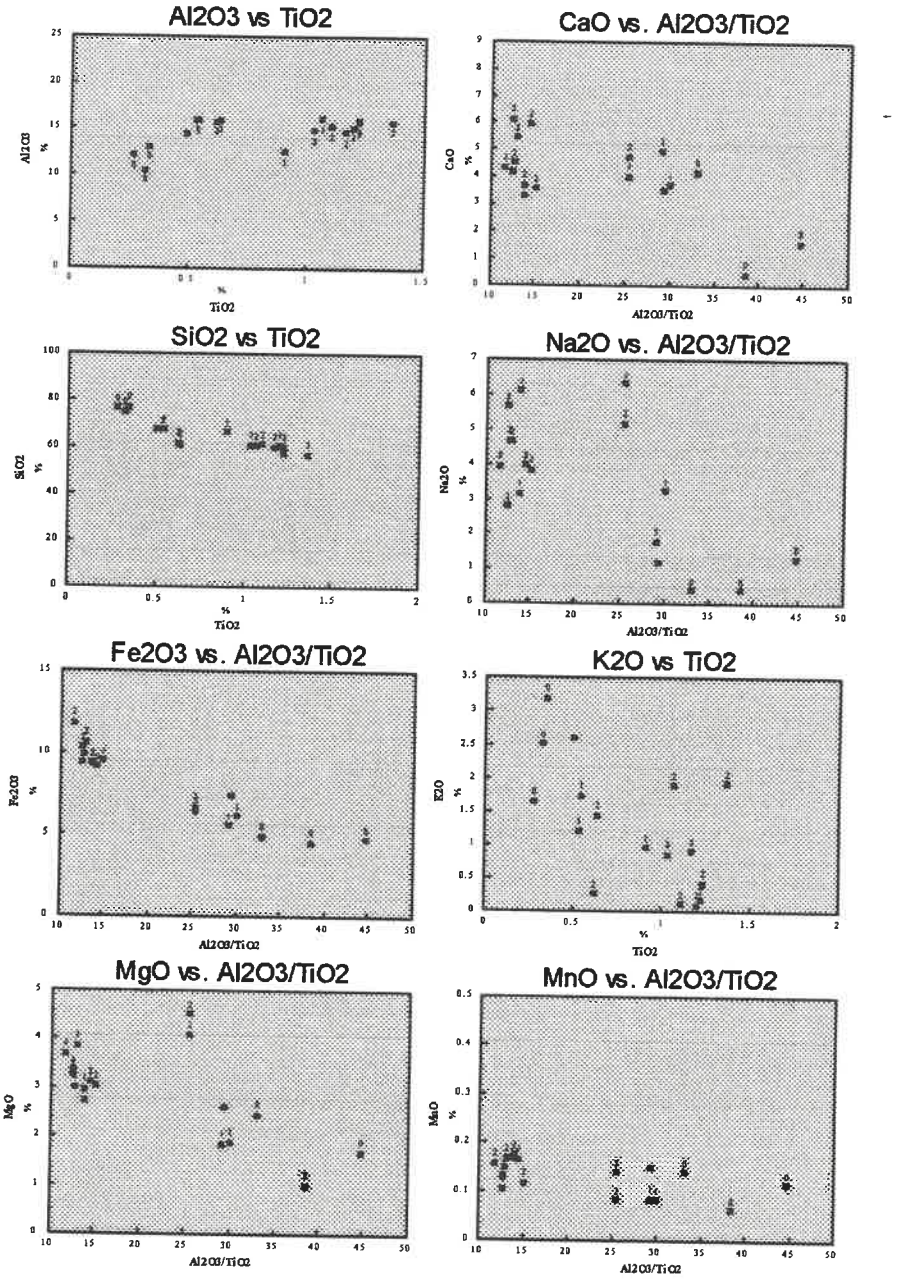

Appendix 3-4
Whole-rock data (Mine Horizon).

Sample	DDH	SIO2	AL2O3	CAO	MGO	NA2O	K2O	FE2O3	MNO	TIO2	P2O5	LOI
GR-90-42	s	80.36	12.19	0.10	0.67	1.15	1.31	3.86	0.03	0.29	0.03	2.39
NMAR-90-05	s	90.54	4.98	0.00	0.09	0.54	0.63	3.02	0.01	0.15	0.03	1.54
T-90-31C	s	60.58	16.80	4.84	1.85	3.08	0.78	10.60	0.18	0.96	0.34	4.54
TR-90-49A	s	64.47	16.66	3.46	2.55	6.22	0.51	5.20	0.08	0.68	0.16	3.16
TS-18	1	67.94	12.83	3.76	1.71	1.15	1.83	9.64	0.22	0.71	0.19	7.54
TS-19	1	69.94	17.83	4.37	2.53	0.93	1.44	2.16	0.04	0.67	0.09	6.16
TS-22	3	63.20	16.22	7.47	2.65	2.39	1.33	5.91	0.10	0.62	0.11	11.2
TS-24	3	72.30	11.16	5.01	4.18	0.28	0.36	6.24	0.17	0.26	0.03	7.7
TS-40	3	74.84	11.95	3.64	2.90	0.69	0.34	5.17	0.13	0.30	0.04	4.62
TS-28	4	63.39	17.63	4.63	2.55	1.04	1.62	8.08	0.18	0.75	0.13	7.93
TS-29	4	64.38	17.19	4.99	3.01	1.73	0.64	7.06	0.14	0.73	0.12	7.7
TS-30	4	69.51	18.77	4.18	1.94	2.85	1.41	0.34	0.09	0.79	0.11	7.08
TS-43	6	72.34	16.82	2.82	1.34	1.96	2.23	1.79	0.04	0.56	0.12	4.93
TS-44	6	72.84	12.92	3.94	1.98	1.01	1.91	4.88	0.11	0.35	0.07	5.77
TS-45	11	64.83	16.95	2.90	2.96	0.95	1.95	8.72	0.11	0.54	0.09	5.77
TS-74	11	74.88	13.28	1.90	1.68	0.96	0.87	5.79	0.08	0.45	0.09	4.16
TS-46	12	65.98	14.52	5.30	2.41	0.92	0.78	8.82	0.15	0.91	0.22	8.08
TS-47	12	71.88	15.80	1.61	1.43	2.33	2.67	3.73	0.06	0.40	0.08	3.23
TS-76	12	64.50	16.07	5.86	1.99	1.46	1.57	7.58	0.16	0.67	0.13	8.85
TS-50	14	61.20	14.97	5.66	3.96	0.94	1.16	10.63	0.16	1.15	0.16	9.23
TS-77	14	65.47	15.30	6.03	1.57	2.20	0.81	7.71	0.19	0.59	0.14	8.85
TS-52	15	72.33	13.11	2.01	2.00	0.72	2.87	6.46	0.15	0.30	0.04	3.77
TS-53	16	64.21	16.62	4.35	3.13	0.84	1.71	8.02	0.17	0.84	0.11	7.23
TS-54	16	59.86	13.98	8.50	2.07	0.82	0.97	12.85	0.35	0.51	0.08	11.7
TS-55	16	60.27	15.75	4.33	3.70	1.51	0.86	12.36	0.30	0.78	0.14	8.7
TS-78	16	78.94	4.43	3.44	2.59	0.21	0.26	9.58	0.40	0.12	0.03	7.47
TS-59	17	67.83	16.98	4.44	1.02	2.72	1.40	4.77	0.11	0.61	0.10	3.39
TS-60	17	59.65	16.68	7.08	2.70	1.34	2.93	8.65	0.13	0.72	0.13	9.54
TS-64	20	62.83	15.57	5.84	1.75	0.65	1.91	10.01	0.15	1.01	0.27	8.23
TS-65	20	55.80	16.25	8.44	4.20	1.25	0.97	11.48	0.18	1.23	0.20	12.2
TS-67	23	73.44	14.58	1.81	1.25	0.44	2.54	5.46	0.09	0.32	0.05	3.31
TS-68	23	70.34	11.97	4.17	3.04	0.41	0.35	9.03	0.22	0.40	0.06	6.47
TS-80	23	76.77	11.13	2.72	2.02	0.44	1.01	5.50	0.13	0.25	0.03	5.16
TS-81	23	76.77	11.13	2.72	2.02	0.44	1.01	5.50	0.13	0.25	0.03	5.16
TS-08	28	68.35	11.59	3.80	3.67	0.26	0.57	11.05	0.40	0.27	0.04	7.23
TS-83	54	74.92	12.42	0.21	1.22	1.42	1.67	7.47	0.24	0.36	0.06	4
TS-12	99	74.11	13.96	2.21	1.32	1.69	2.14	4.01	0.07	0.41	0.06	3.62
TS-15	99	84.34	6.62	2.90	1.69	0.77	0.73	2.71	0.06	0.16	0.02	3.93

Data normalized to 100%, volatile free.

Appendix 3-4, (Continued).

Sample	CR	RB	SR	Y	ZR	NB	BA
GR-90-42	84	38	61	62	413	28	253
NMAR-90-05	158	21	35	28	154	-10	106
T-90-31C	67	32	109	55	320	27	264
TR-90-49A	128	23	196	17	168	23	174
TS-18	27	51	130	53	327	14	414
TS-19	69	45	122	22	210	19	270
TS-22	33	22	242	10	122	10	215
TS-24	51	24	30	72	334	31	137
TS-40	111	11	43	70	389	33	116
TS-28	0	42	68	13	144	23	197
TS-29	97	17	51	35	155	-10	128
TS-30	104	45	207	18	169	17	215
TS-43	49	52	149	23	166	23	233
TS-44	130	46	109	85	374	15	232
TS-45	51	53	60	75	547	23	249
TS-74	77	20	41	61	281	0	156
TS-46	129	27	54	41	247	28	171
TS-47	46	106	62	54	315	17	439
TS-76	45	46	125	29	183	14	284
TS-50	47	41	54	0	133	21	178
TS-77	121	29	195	40	173	19	277
TS-52	88	62	24	73	428	34	420
TS-53	277	55	130	36	145	17	214
TS-54	53	22	68	14	137	19	166
TS-55	30	41	84	32	149	14	191
TS-78	115	16	19	10	98	25	82
TS-59	82	39	266	21	142	10	320
TS-60	192	80	129	12	139	27	624
TS-64	51	45	71	38	355	25	271
TS-65	39	17	66	18	165	17	163
TS-67	167	70	56	78	569	48	420
TS-68	202	26	78	40	388	44	333
TS-80	85	29	44	55	418	18	139
TS-81	85	29	44	55	418	18	139
TS-08	64	25	14	47	369	22	94
TS-83	35	37	29	59	339	25	232
TS-12	45	67	69	71	397	37	430
TS-15	119	38	26	44	230	-10	143

Appendix 3-5
Plots of major elements vs. monitor elements (Mine Horizon).

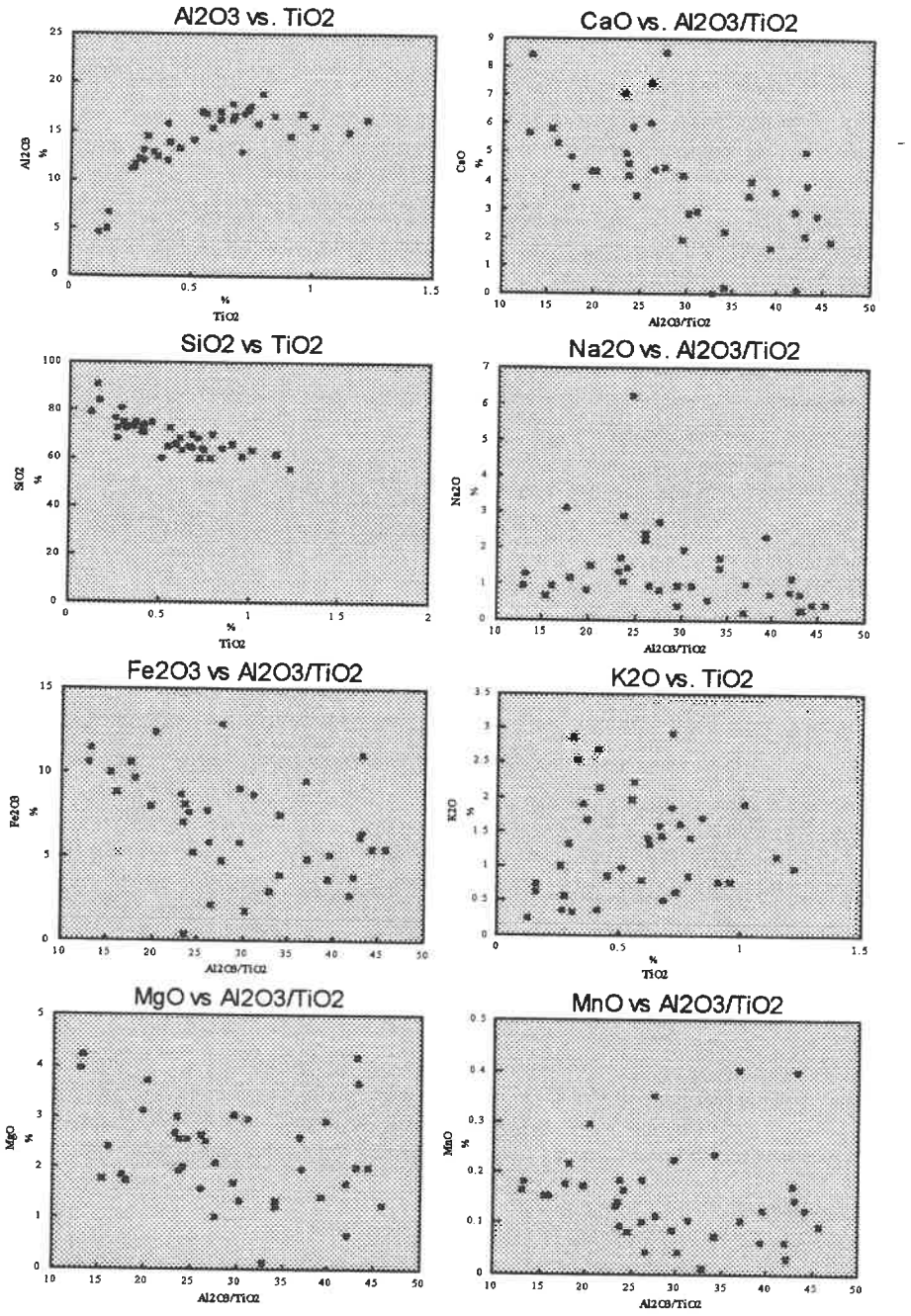

Appendix 3-6
Calculated precursor compositions (Mine Horizon).

Sample	DDH	SIO2	AL2O3	CAO	MGO	NA2O	K2O	FE2O3	MNO	TIO2
GR-90-42	s	79	12.9	1.1	1.1	0.5	1.8	4.3	0.09	0.3
NMAR-90-05	s	72	13.2	2.3	1.8	1.8	1.7	5	0.10	0.4
T-90-31C	s	62	14.1	4.3	2.9	4.0	0.7	8.8	0.14	0.8
TR-90-49A	s	67	13.5	3.4	2.4	3.0	0.7	6.5	0.12	0.6
TS-18	1	62	14.1	4.2	2.8	3.9	1.4	8.8	0.14	0.8
TS-19	1	68	13.4	3.1	2.2	2.7	1.3	6	0.12	0.5
TS-20	1	68	13.4	3.1	2.2	2.7	1.3	6	0.12	0.5
TS-22	3	68	13.4	3.2	2.3	2.8	1.3	6	0.12	0.5
TS-24	3	79	12.9	1.0	1.1	0.4	1.0	4.3	0.08	0.3
TS-25	3	79	12.9	1.0	1.1	0.4	1.0	4.3	0.08	0.3
TS-40	3	77	13.0	1.4	1.3	0.8	0.9	4.5	0.09	0.3
TS-28	4	66	13.6	3.5	2.4	3.1	1.3	6.7	0.12	0.6
TS-29	4	66	13.6	3.5	2.5	3.1	0.7	6.7	0.12	0.6
TS-30	4	66	13.6	3.5	2.4	3.1	1.2	6.7	0.12	0.6
TS-43	6	71	13.2	2.7	2.0	2.2	1.7	5.5	0.11	0.4
TS-44	6	75	13.0	1.8	1.5	1.2	1.9	4.7	0.10	0.4
TS-45	11	71	13.2	2.5	1.9	2.0	1.6	5.3	0.11	0.4
TS-74	11	70	13.3	2.7	2.0	2.3	1.2	5.5	0.11	0.4
TS-46	12	61	14.3	4.5	3.0	4.2	0.7	9.3	0.14	0.9
TS-47	12	77	13.0	1.5	1.4	0.9	2.0	4.5	0.09	0.3
TS-76	12	67	13.5	3.4	2.4	3.1	1.4	6.5	0.12	0.6
TS-50	14	59	14.9	4.9	3.2	4.6	0.8	10.6	0.15	1.1
TS-77	14	68	13.4	3.2	2.3	2.8	1.0	6	0.12	0.5
TS-52	15	79	12.9	1.0	1.1	0.4	2.2	4.3	0.08	0.3
TS-53	16	64	13.9	4.0	2.7	3.7	1.3	8	0.13	0.7
TS-54	16	69	13.4	3.0	2.2	2.6	1.2	5.8	0.12	0.5
TS-55	16	64	13.8	3.9	2.7	3.6	0.9	7.8	0.13	0.7
TS-78	16	75	13.0	1.8	1.5	1.2	1.3	4.7	0.10	0.4
TS-59	17	69	13.4	3.0	2.2	2.5	1.3	5.8	0.12	0.5
TS-60	17	66	13.6	3.6	2.5	3.2	1.7	6.7	0.12	0.6
TS-64	20	61	14.4	4.6	3.0	4.3	1.2	9.7	0.14	0.9
TS-65	20	59	14.9	4.9	3.2	4.6	0.7	10.6	0.15	1.1
TS-67	23	81	12.9	0.6	0.9	0.0	2.1	4.3	0.08	0.3
TS-68	23	70	13.3	2.7	2.0	2.3	0.7	5.5	0.11	0.4
TS-80	23	80	12.9	0.8	1.0	0.2	1.7	4.3	0.08	0.3
TS-81	23	80	12.9	0.8	1.0	0.2	1.7	4.3	0.08	0.3
TS-08	28	79	12.9	1.0	1.1	0.3	1.3	4.3	0.08	0.3
TS-83	54	73	13.1	2.1	1.7	1.6	1.8	5	0.10	0.4
TS-12	99	73	13.1	2.1	1.7	1.6	1.9	5	0.10	0.4
TS-15	99	78	12.9	1.1	1.2	0.5	1.8	4.3	0.09	0.3

Appendix 3-7
Calculated mass changes (Mine Horizon).

Sample	DDH	SIO2	AL2O3	CAO	MGO	NA2O	K2O	FE2O3	MNO	TIO2	P2O5	LOI
GR-90-42	s	80.36	12.19	0.10	0.67	1.15	1.31	3.86	0.03	0.29	0.03	2.39
NMAR-90-05	s	90.54	4.98	0.00	0.09	0.54	0.63	3.02	0.01	0.15	0.03	1.54
T-90-31C	s	60.58	16.80	4.84	1.85	3.08	0.78	10.60	0.18	0.96	0.34	4.54
TR-90-49A	s	64.47	16.66	3.46	2.55	6.22	0.51	5.20	0.08	0.68	0.16	3.16
TS-18	1	67.94	12.83	3.76	1.71	1.15	1.83	9.64	0.22	0.71	0.19	7.54
TS-19	1	69.94	17.83	4.37	2.53	0.93	1.44	2.16	0.04	0.67	0.09	6.16
TS-22	3	63.20	16.22	7.47	2.65	2.39	1.33	5.91	0.10	0.62	0.11	11.2
TS-24	3	72.30	11.16	5.01	4.18	0.28	0.36	6.24	0.17	0.26	0.03	7.7
TS-40	3	74.84	11.95	3.64	2.90	0.69	0.34	5.17	0.13	0.30	0.04	4.62
TS-28	4	63.39	17.63	4.63	2.55	1.04	1.62	8.08	0.18	0.75	0.13	7.93
TS-29	4	64.38	17.19	4.99	3.01	1.73	0.64	7.06	0.14	0.73	0.12	7.7
TS-30	4	69.51	18.77	4.18	1.94	2.85	1.41	0.34	0.09	0.79	0.11	7.08
TS-43	6	72.34	16.82	2.82	1.34	1.96	2.23	1.79	0.04	0.56	0.12	4.93
TS-44	6	72.84	12.92	3.94	1.98	1.01	1.91	4.88	0.11	0.35	0.07	5.77
TS-45	11	64.83	16.95	2.90	2.96	0.95	1.95	8.72	0.11	0.54	0.09	5.77
TS-74	11	74.88	13.28	1.90	1.68	0.96	0.87	5.79	0.08	0.45	0.09	4.16
TS-46	12	65.98	14.52	5.30	2.41	0.92	0.78	8.82	0.15	0.91	0.22	8.08
TS-47	12	71.88	15.80	1.61	1.43	2.33	2.67	3.73	0.06	0.40	0.08	3.23
TS-76	12	64.50	16.07	5.86	1.99	1.46	1.57	7.58	0.16	0.67	0.13	8.85
TS-50	14	61.20	14.97	5.66	3.96	0.94	1.16	10.63	0.16	1.15	0.16	9.23
TS-77	14	65.47	15.30	6.03	1.57	2.20	0.81	7.71	0.19	0.59	0.14	8.85
TS-52	15	72.33	13.11	2.01	2.00	0.72	2.87	6.46	0.15	0.30	0.04	3.77
TS-53	16	64.21	16.62	4.35	3.13	0.84	1.71	8.02	0.17	0.84	0.11	7.23
TS-54	16	59.86	13.98	8.50	2.07	0.82	0.97	12.85	0.35	0.51	0.08	11.7
TS-55	16	60.27	15.75	4.33	3.70	1.51	0.86	12.36	0.30	0.78	0.14	8.7
TS-78	16	78.94	4.43	3.44	2.59	0.21	0.26	9.58	0.40	0.12	0.03	7.47
TS-59	17	67.83	16.98	4.44	1.02	2.72	1.40	4.77	0.11	0.61	0.10	3.39
TS-60	17	59.65	16.68	7.08	2.70	1.34	2.93	8.65	0.13	0.72	0.13	9.54
TS-64	20	62.83	15.57	5.84	1.75	0.65	1.91	10.01	0.15	1.01	0.27	8.23
TS-65	20	55.80	16.25	8.44	4.20	1.25	0.97	11.48	0.18	1.23	0.20	12.2
TS-67	23	73.44	14.58	1.81	1.25	0.44	2.54	5.46	0.09	0.32	0.05	3.31
TS-68	23	70.34	11.97	4.17	3.04	0.41	0.35	9.03	0.22	0.40	0.06	6.47
TS-80	23	76.77	11.13	2.72	2.02	0.44	1.01	5.50	0.13	0.25	0.03	5.16
TS-81	23	76.77	11.13	2.72	2.02	0.44	1.01	5.50	0.13	0.25	0.03	5.16
TS-08	28	68.35	11.59	3.80	3.67	0.26	0.57	11.05	0.40	0.27	0.04	7.23
TS-83	54	74.92	12.42	0.21	1.22	1.42	1.67	7.47	0.24	0.36	0.06	4
TS-12	99	74.11	13.96	2.21	1.32	1.69	2.14	4.01	0.07	0.41	0.06	3.62
TS-15	99	84.34	6.62	2.90	1.69	0.77	0.73	2.71	0.06	0.16	0.02	3.93

Appendix 4

Whole-rock data and plots for samples from the LDD intrusion.

Appendix 4-1
Whole-rock data (LDD intrusion).

Sample	DDH	SIO2	AL2O3	CAO	MGO	NA2O	K2O	FE2O3	MNO	TIO2	P2O5	LOI
19159	12	65.6	15.6	4.17	2.59	4.94	0.82	5.54	0.07	0.58	0.16	3.39
19258	14	66.5	15.9	3.51	2.55	4.30	1.08	5.33	0.08	0.62	0.15	2.47
19259	14	65.7	16.0	4.03	2.66	3.66	1.71	5.42	0.07	0.63	0.17	3.08
19261	14	66.3	15.9	4.56	1.88	4.38	1.37	4.77	0.05	0.60	0.16	2.93
19262	14	66.2	16.0	4.25	1.99	4.15	1.39	5.20	0.07	0.60	0.15	2.77
TS-61	18	77.7	13.2	0.63	0.89	3.32	2.59	1.34	0.02	0.26	0.05	1.54
19472	18	72.9	14.5	2.91	1.42	0.29	4.09	3.49	0.08	0.28	0.04	4.93
19473	18	74.4	13.8	2.34	1.52	2.29	1.64	3.67	0.09	0.27	0.04	3.7
19799	20	66.2	16.0	4.47	2.06	4.20	0.90	5.37	0.05	0.59	0.16	1.93
19800	20	64.5	15.4	6.42	2.32	2.69	2.42	5.47	0.09	0.57	0.15	6.39

Sample	CR	RB	SR	Y	ZR	BA	Cu	Pb	Zn	Mn	Ag
19159	73	33	207	0	175	203	15	6	26	292	0
19258	81	36	214	16	174	349	26	8	148	242	0
19259	81	32	174	0	189	397	56	10	72	269	0
19261	81	38	230	15	154	311	4	21	85	241	0
19262	69	39	219	12	180	332	17	11	46	314	0
TS-61	68	157	164	47	222	967	na	na	na	na	na
19472	25	102	15	57	227	384	7	na	29	374	0
19473	39	103	100	48	220	366	7	na	32	509	0
19799	116	32	258	0	173	240	4	6	27	147	0
19800	70	55	119	19	153	410	27	3	51	360	1

Data normalized to 100%, volatile free.

Appendix 4-2
Major element discrimination plots (LDD intrusion).

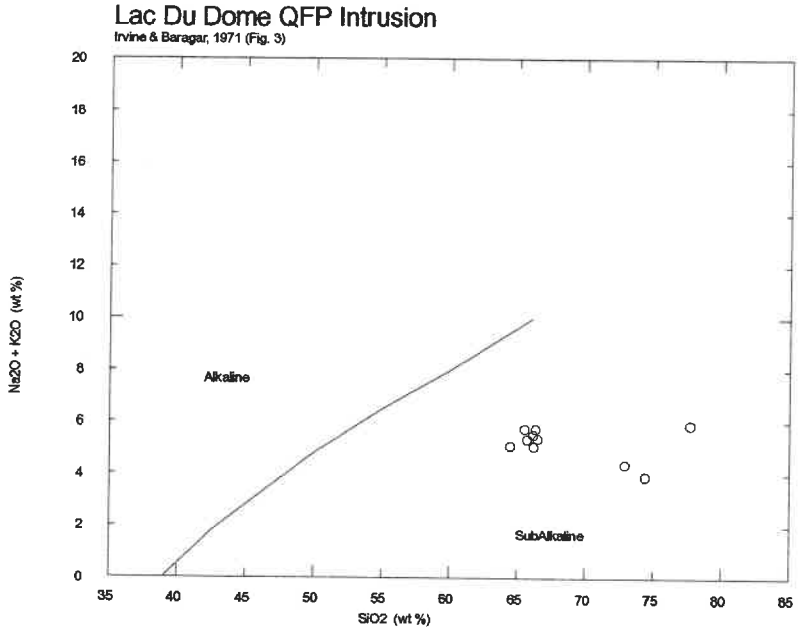

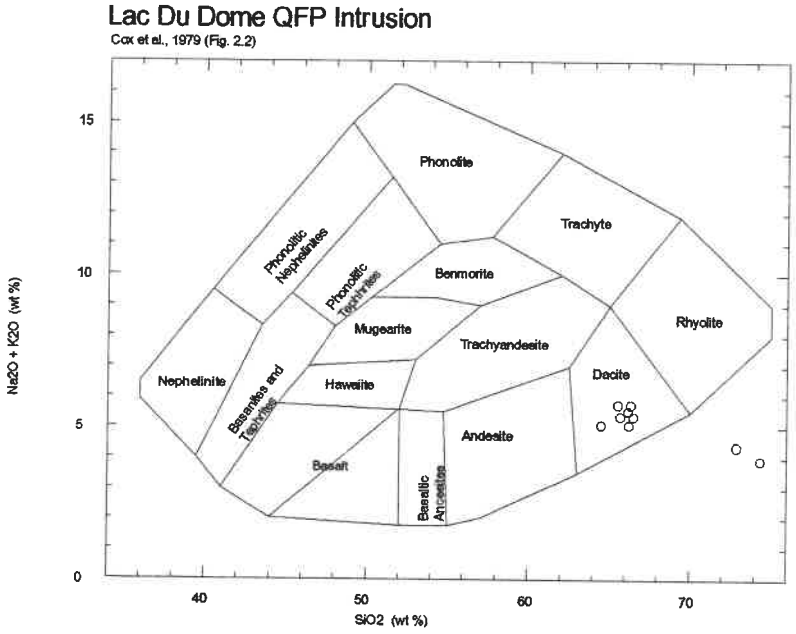

Appendix 4-3
AFM plot (LDD intrusion).

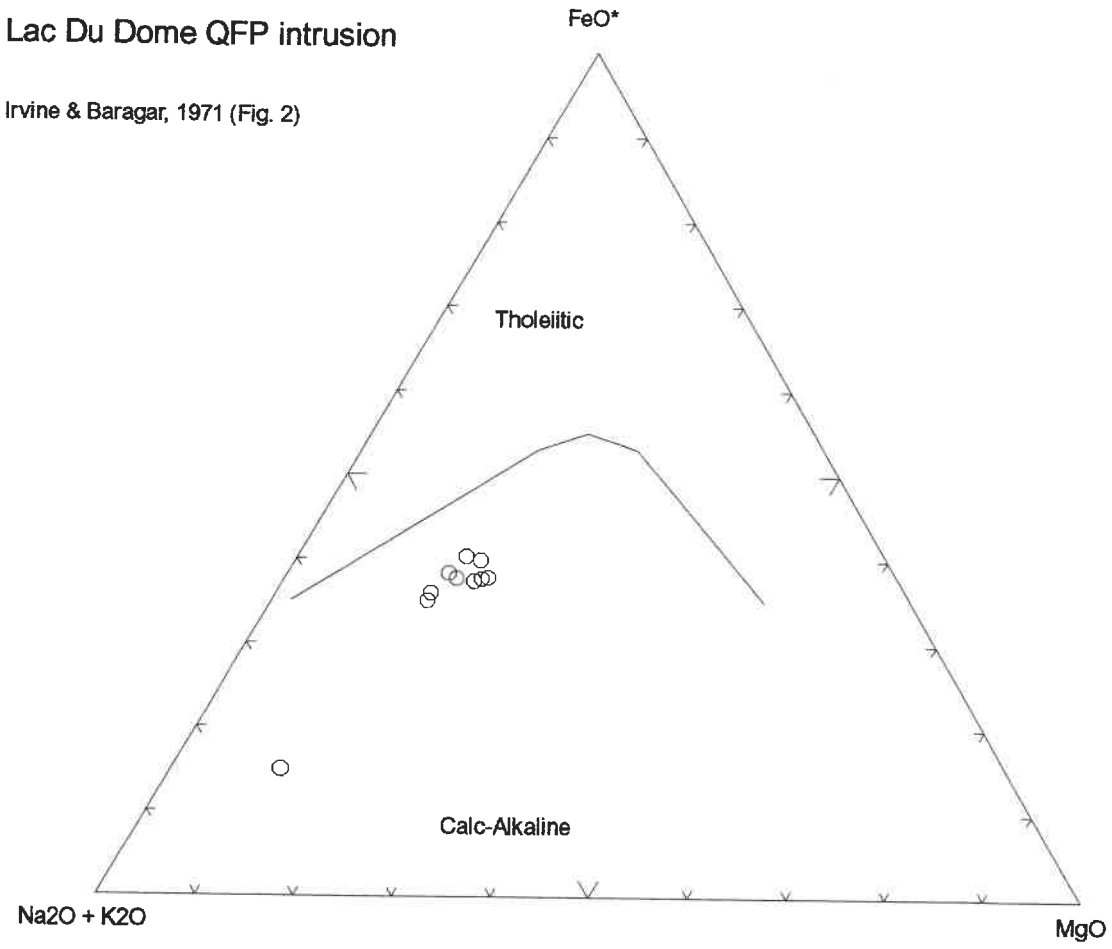

FeO recalculated by Newpet (Clarke, 1990).

Appendix 4-4
Plots of major elements vs. east-west coordinates (LDD intrusion).

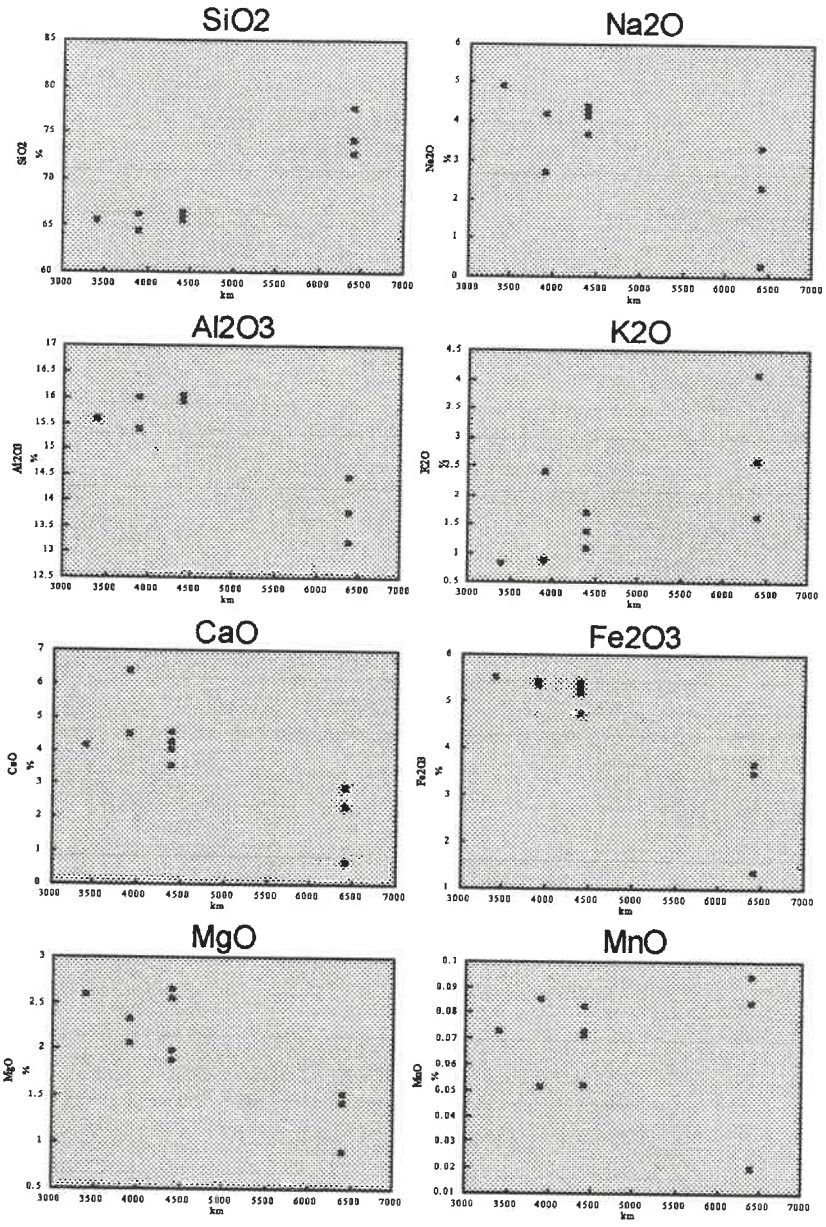

X-axis represent east-west coordinates relative to the Normetal deposit at 0 km.

Appendix 5

Sericite chemical data and plots.

Appendix 5-1
Chemical data for sericites.

Mine Horizon Sericite Data

Sample	DDH	SiO2	TiO2	Al2O3	FeO	MgO	CaO	Na2O	K2O	H2O	Total
TS-52	15	46.9	0.0	38.3	0.9	0.3	0.0	4.4	4.6	4.6	100.0
TS-32	5	47.3	0.2	34.7	0.9	0.7	0.0	0.9	9.6	4.6	99.0
TS-43	6	46.9	0.0	39.4	0.7	0.0	1.3	3.2	5.2	4.6	101.3
TS-8	28	45.6	0.0	35.9	1.6	0.0	0.0	1.3	9.2	4.5	98.1
TS-18	1	46.8	0.0	37.4	0.8	0.0	0.2	3.6	5.6	4.6	99.0
TS-18	1	46.7	0.0	36.0	1.1	0.3	0.0	2.2	7.4	4.6	98.3
TS-18	1	46.5	0.0	36.2	1.2	0.4	0.0	2.5	7.0	4.6	98.5
TS-28	4	47.2	0.2	38.7	0.9	0.5	0.3	3.9	4.9	4.6	101.1
TS-28	4	44.7	1.9	35.6	1.0	0.0	0.2	2.5	6.4	4.6	96.8
TS-28	4	46.0	0.0	37.1	0.8	0.0	0.3	3.4	5.4	4.6	97.7
TS-44	6	45.1	0.0	36.6	1.1	0.2	0.2	3.2	6.0	4.6	97.0
TS-45	11	43.4	0.0	35.0	3.7	1.5	0.2	2.1	6.0	4.5	96.6
TS-45	11	46.7	0.0	36.6	1.1	0.2	0.0	1.9	7.7	4.6	98.8
TS-46	12	47.4	0.0	38.6	0.7	0.3	0.0	3.6	5.3	4.6	100.5
TS-65	20	45.8	1.4	37.1	0.7	0.0	0.2	4.4	3.6	4.6	97.8
TS-65	20	46.2	1.2	37.4	0.9	0.0	0.3	4.6	3.4	4.6	98.6
TS-50	14	46.9	0.2	37.2	1.1	0.0	0.0	3.1	6.3	4.6	99.5
TS-50	14	45.4	0.3	37.5	3.2	0.9	0.0	4.9	2.9	4.6	99.7
TS-53	16	40.9	0.2	30.8	11.1	1.6	0.0	0.7	7.7	4.3	97.3
TS-53	16	38.3	0.2	30.2	14.3	3.0	0.0	0.6	6.4	4.2	97.3
TS-54	16	48.0	0.0	37.4	0.5	0.0	0.4	3.9	4.2	4.7	98.9
TS-67	23	47.2	0.0	34.0	1.3	0.3	0.0	0.8	9.8	4.5	97.9
TS-67	23	46.2	0.2	34.9	1.3	0.5	0.0	0.7	9.9	4.5	98.2
Averages		45.75	0.26	36.205	2.218	0.458	0.144	2.71	6.281	4.57	98.6

RBS Sericite Data

Sample	D.D.H.	SiO2	TiO2	Al2O3	FeO	MgO	CaO	Na2O	K2O	H2O	Total
TS-56	17	45.4	0.2	34.0	2.2	0.5	0.0	0.5	10.6	4.5	97.9
TS-57	17	48.4	0.2	38.2	0.7	0.0	0.0	4.2	4.0	4.7	100.5
TS-42	6	46.9	0.3	34.8	1.1	1.0	0.0	0.8	10.3	4.5	99.7
TS-37	1	48.8	0.3	32.6	1.4	1.6	0.0	0.2	11.4	4.5	100.7
TS-37	1	47.9	0.6	31.0	1.8	1.6	0.0	0.3	11.3	4.5	99.0
TS-39	2	47.3	0.3	32.8	1.1	0.9	0.0	0.3	10.8	4.5	98.1
TS-39	2	47.7	0.3	32.8	1.3	1.3	0.0	0.4	11.0	4.5	99.4
TS-41	4	48.2	0.2	34.2	1.1	1.2	0.0	0.5	10.9	4.5	100.8
TS-41	4	47.3	0.3	33.8	1.1	0.9	0.0	0.4	10.8	4.5	98.9
TS-41	4	47.0	0.2	33.6	1.0	1.0	0.0	0.5	10.9	4.5	98.7
TS-47	12	51.8	0.0	35.2	0.5	0.2	0.0	2.7	6.4	4.7	101.5
TS-47	12	46.5	0.0	36.6	0.7	0.2	0.0	1.6	8.9	4.6	99.1
TS-47	12	47.8	0.0	37.3	0.6	0.4	0.0	2.3	8.1	4.6	101.1
TS-66	20	46.9	0.3	30.5	3.0	1.9	0.0	0.3	10.4	4.5	97.8
TS-66	20	47.8	0.2	31.2	2.5	1.6	0.0	0.5	10.7	4.5	98.8
TS-48	14	47.1	0.2	35.6	1.9	0.7	0.0	0.7	10.4	4.5	101.0
TS-48	14	43.1	0.2	34.7	6.9	1.5	0.0	0.6	8.7	4.4	100.2
M-90-94	s	45.6	0.0	36.9	0.6	0.3	0.0	1.7	7.9	4.6	97.5
M-90-94	s	51.5	0.0	36.9	0.2	0.0	0.6	2.8	3.2	4.7	100.0
Averages		47.525	0.2	34.348	1.556	0.886	0.033	1.118	9.305	4.54	99.5

Appendix 5-2
Plots of sericite compositions from the Mine Horizon vs. east-west coordinates.

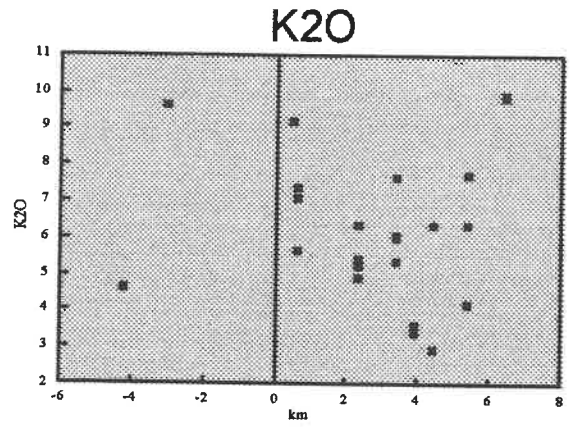

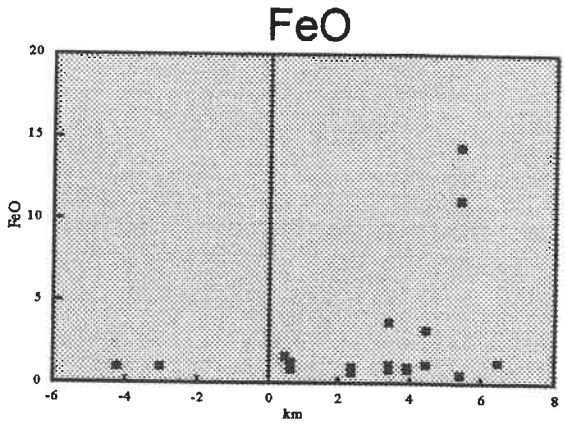

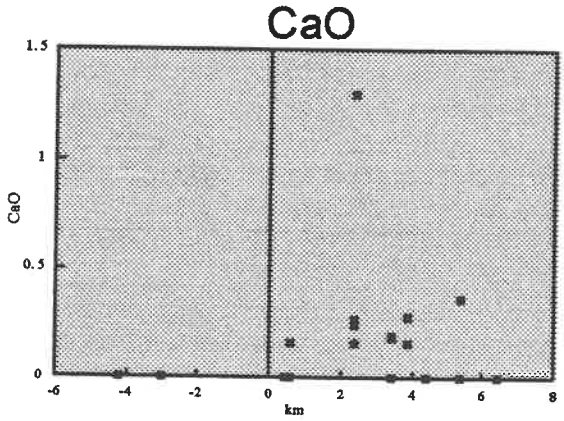

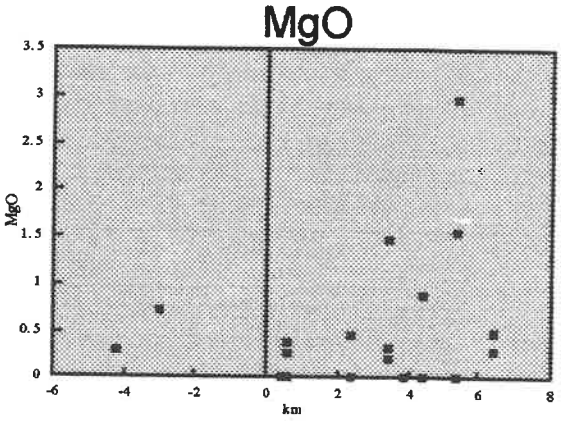

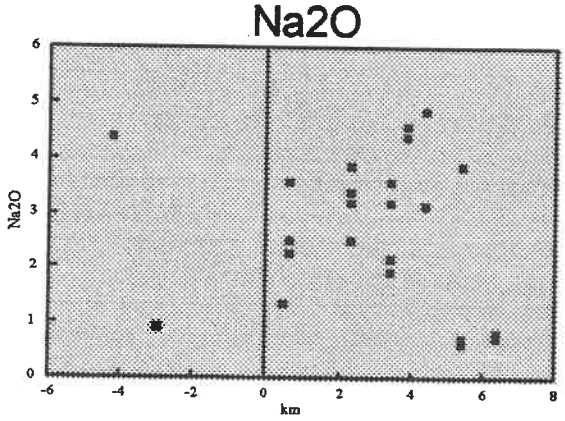

Appendix 5-3
Plots of K2O-Na2O and FeO-MgO substitution for sericites from the Mine Horizon.

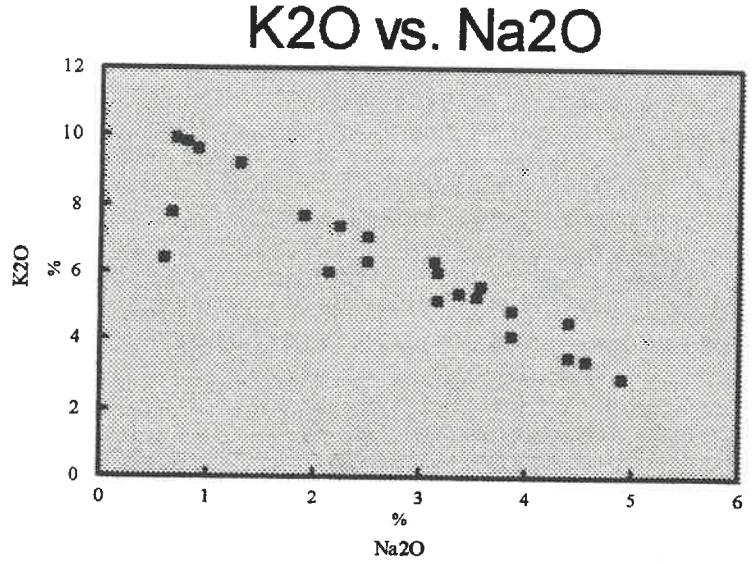

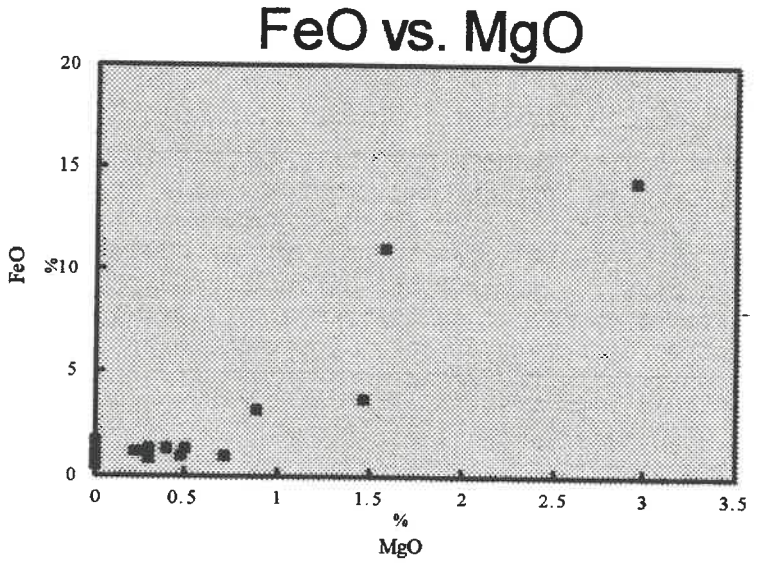

Appendix 5-4
Plots of sericite compositions from the RBS vs. east-west coordinates.

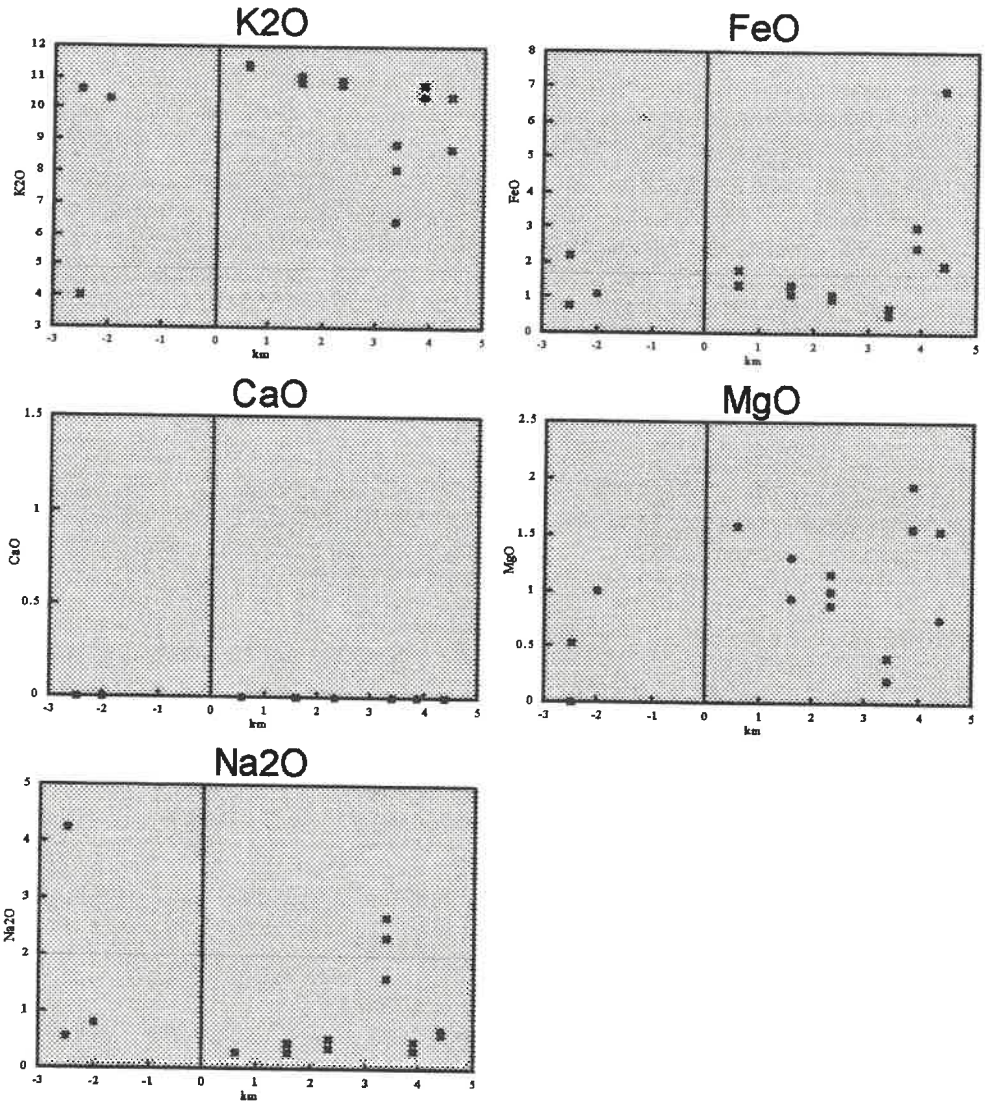

Appendix 6

Chlorite chemical data and plots from the Mine Horizon.

Appendix 6-1 Chemical data for chlorites (Mine Horizon).

SAMPLE	D.D.H.	SiO2	Al2O3	FeO	MnO	MgO	Na2O	H2O	Total
TS-52	NC-91-15	25.9	25.3	27.6	0.0	9.5	0.4	11.5	100.2
TS-52		27.9	26.7	25.6	0.0	9.2	0.9	11.7	102.0
TS-52		28.0	26.5	24.6	0.0	8.7	1.2	11.7	100.7
TS-52		24.8	24.9	28.5	0.0	9.6	0.6	11.4	99.8
TS-52		24.7	24.8	29.0	0.0	11.1	0.4	11.3	101.3
TS-59	NC-91-17	23.1	23.0	31.3	0.0	8.2	0.4	11.1	97.1
TS-59		23.9	22.9	30.7	0.6	8.8	0.6	11.1	98.6
TS-59		23.9	23.7	31.2	0.2	9.6	0.4	11.2	100.2
TS-59		25.0	22.8	29.8	0.5	9.5	0.0	11.3	98.9
TS-59		24.7	22.2	31.4	0.6	9.6	0.4	11.1	100.0
TS-59		23.7	22.9	30.6	0.0	9.4	0.0	11.1	97.7
TS-59		23.7	23.2	31.3	0.6	8.6	0.0	11.1	98.5
TS-59		24.4	22.8	31.2	0.6	9.6	0.3	11.2	100.1
TS-59		24.5	22.1	30.1	0.5	9.9	0.0	11.2	98.3
TS-43	NC-91-06	25.4	23.4	21.9	0.0	15.2	0.4	11.7	98.0
TS-43		25.7	23.6	21.6	0.2	15.8	0.0	11.7	98.6
TS-43		25.4	23.6	21.2	0.0	15.3	0.4	11.7	97.6
TS-43		25.7	24.2	21.4	0.0	14.9	0.4	11.8	98.4
TS-43		25.5	23.0	21.5	0.0	15.5	0.3	11.7	97.5
TS-44	NC-91-06	37.3	31.8	9.0	0.0	5.1	1.8	12.9	97.8
TR-90-49A	SURF	27.7	21.9	23.8	0.3	13.6	0.8	11.5	99.6
T-90-31C	SURF	24.3	23.0	28.4	0.0	11.4	0.3	11.3	98.7
T-90-31C		25.6	22.8	27.7	0.0	10.4	0.3	11.2	98.0
T-90-31C		23.8	22.8	28.8	0.0	10.9	0.2	11.2	97.7
TS-90	NMAR	23.6	22.6	30.2	0.4	9.2	0.3	11.1	97.4
TS-90		23.8	24.3	30.9	0.4	9.3	0.4	11.2	100.3
TS-90		24.1	22.9	30.4	0.4	9.4	0.7	11.2	99.1
TS-12	N-89-99	24.0	23.3	28.7	0.0	11.0	0.4	11.3	98.7
TS-12		24.9	22.7	28.2	0.0	11.0	0.3	11.3	98.4
TS-3	N-87-54	23.2	23.1	30.4	0.4	8.2	0.4	11.2	96.9
TS-3		23.2	23.3	31.0	0.5	8.0	0.6	11.1	97.8
TS-83		23.4	23.4	32.2	0.4	8.9	0.3	11.1	99.7
TS-7	N-87-28	23.5	23.4	33.6	0.0	7.4	0.3	11.0	99.1
TS-7		22.9	22.3	33.9	0.0	7.3	0.2	11.0	97.7
TS-7		23.1	23.1	34.3	0.1	7.6	0.5	11.0	99.6
TS-7		23.1	23.2	34.3	0.2	7.2	0.4	11.0	99.5
TS-8	N-87-28	23.8	22.8	31.3	0.2	9.3	0.4	11.1	98.9
TS-8		23.0	22.9	31.4	0.3	9.0	0.3	11.1	98.1
TS-8		23.6	22.9	31.6	0.0	9.0	0.0	11.1	98.3
TS-8		23.7	23.7	30.9	0.0	9.4	0.4	11.2	99.3
TS-8		22.6	22.4	31.9	0.2	8.2	0.0	11.1	96.5
TS-8		23.1	23.3	31.6	0.0	8.8	0.3	11.1	98.1
TS-19	NC-90-01C	24.2	23.9	26.3	0.0	12.0	0.3	11.4	98.0
TS-19		25.1	24.5	29.9	0.0	9.6	0.3	11.3	100.7
TS-40	NC-90-03	28.4	26.9	14.5	0.0	16.3	0.5	12.3	98.9
TS-40		28.4	25.4	13.2	0.0	15.9	0.3	12.3	95.5
TS-40		26.3	25.3	16.2	0.0	16.8	0.0	12.1	96.7
TS-65	NC-91-20	26.7	26.5	27.2	0.0	9.0	0.6	11.5	101.6
TS-65		25.6	25.5	30.6	0.0	10.2	0.4	11.3	103.5
TS-50	NC-91-14	29.4	27.2	22.3	0.0	7.4	0.9	11.8	99.0
TS-50		23.6	24.2	28.5	0.0	10.4	0.6	11.3	98.7
TS-50		24.6	24.8	29.1	0.0	10.5	0.5	11.3	100.9
TS-50		24.5	23.9	29.6	0.0	11.0	0.5	11.3	100.8
TS-50		24.0	24.0	29.3	0.0	10.4	0.3	11.3	99.2
TS-50		27.5	26.1	25.6	0.2	8.9	1.0	11.6	100.8
TS-50		25.9	25.3	27.5	0.0	9.8	0.7	11.4	100.6
TS-50		25.3	24.9	29.1	0.0	10.6	0.5	11.4	101.7
TS-53	NC-91-16	24.7	23.1	29.5	0.3	11.3	0.3	11.3	100.6
TS-53		24.1	23.0	28.1	0.2	11.7	0.0	11.3	98.5
TS-53		24.5	24.4	27.7	0.3	12.4	0.3	11.4	101.0
TS-53		24.8	23.5	27.4	0.2	12.8	0.0	11.4	100.2
TS-53		24.3	23.4	27.4	0.3	11.7	0.5	11.4	99.0
TS-54	NC-91-16	27.5	25.5	20.2	0.0	10.9	0.7	11.9	96.7
TS-54		24.8	22.7	23.7	0.0	13.2	0.4	11.6	96.4
TS-54		25.2	24.4	22.5	0.0	12.1	0.5	11.7	96.4
TS-67	NC-91-23	24.1	22.8	30.8	0.0	9.6	0.5	11.2	99.0
TS-68		25.4	24.4	26.4	0.0	13.3	0.5	11.5	101.5

Appendix 6-2
Plots of chlorite compositions vs. east-west coordinates (Mine Horizon).

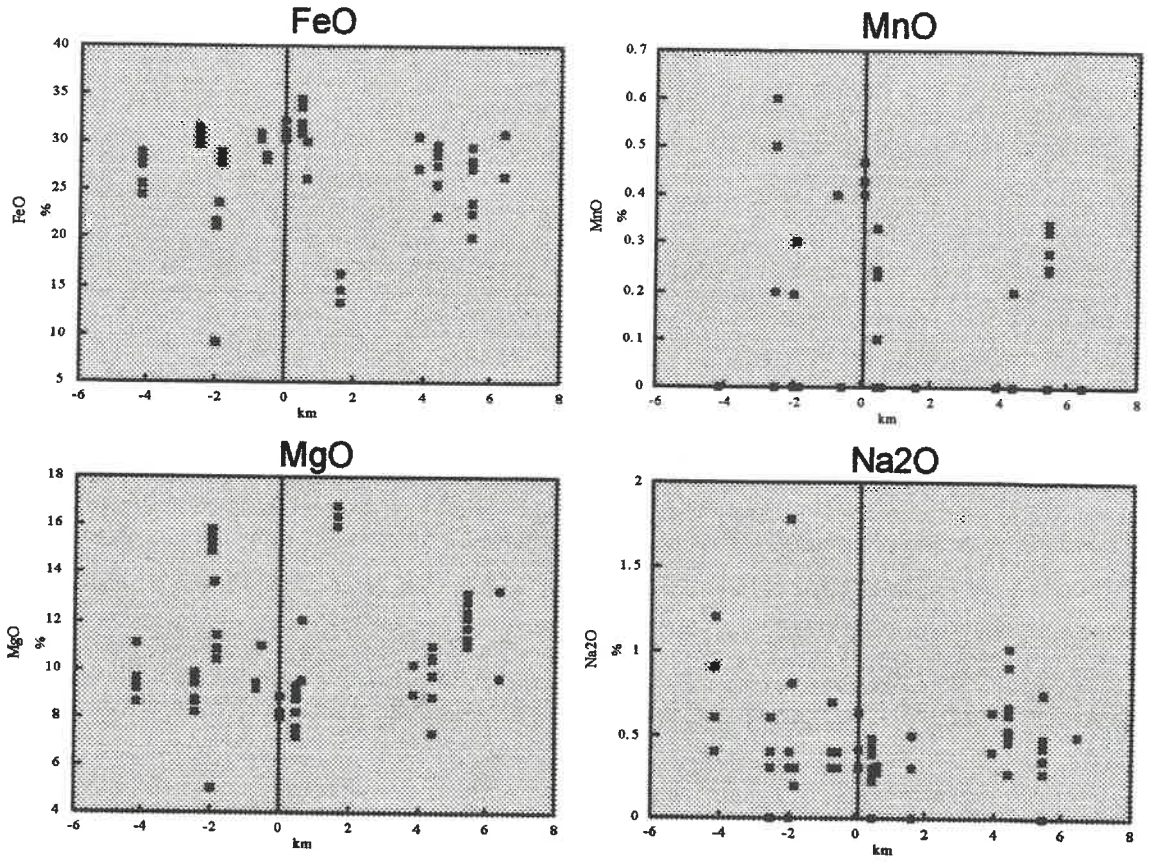

Appendix 6-3
Plots of chlorite compositional ratios vs. east-west coordinates (Mine Horizon).

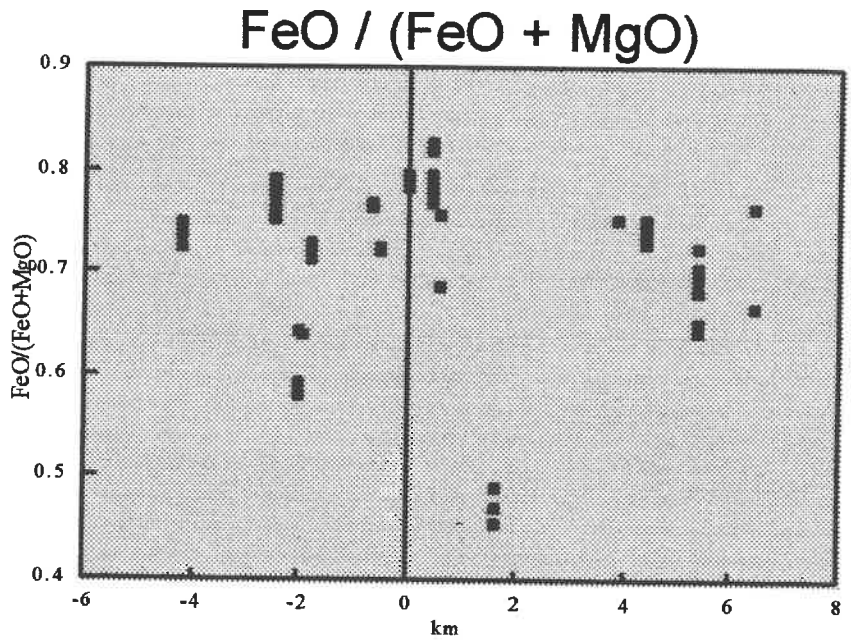

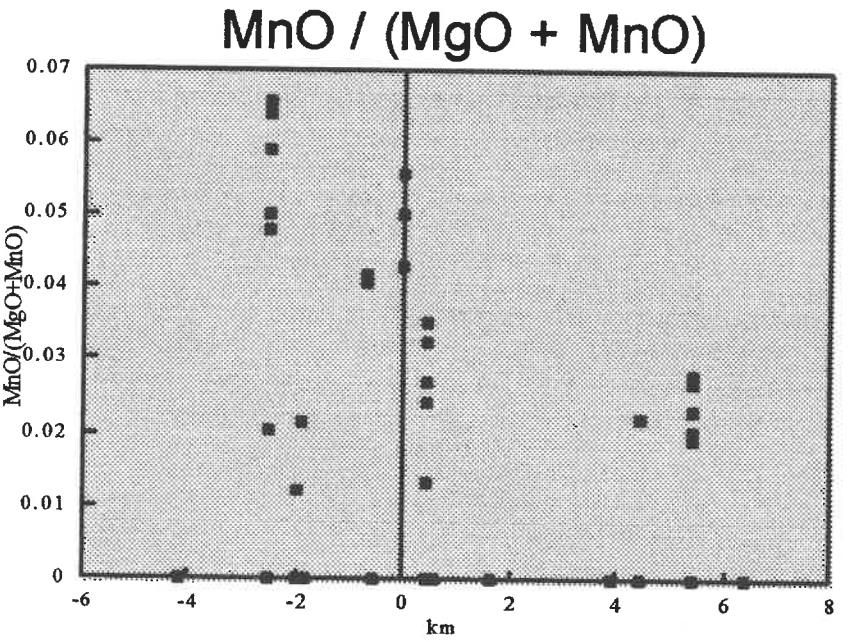

Appendix 6-3 (continued).

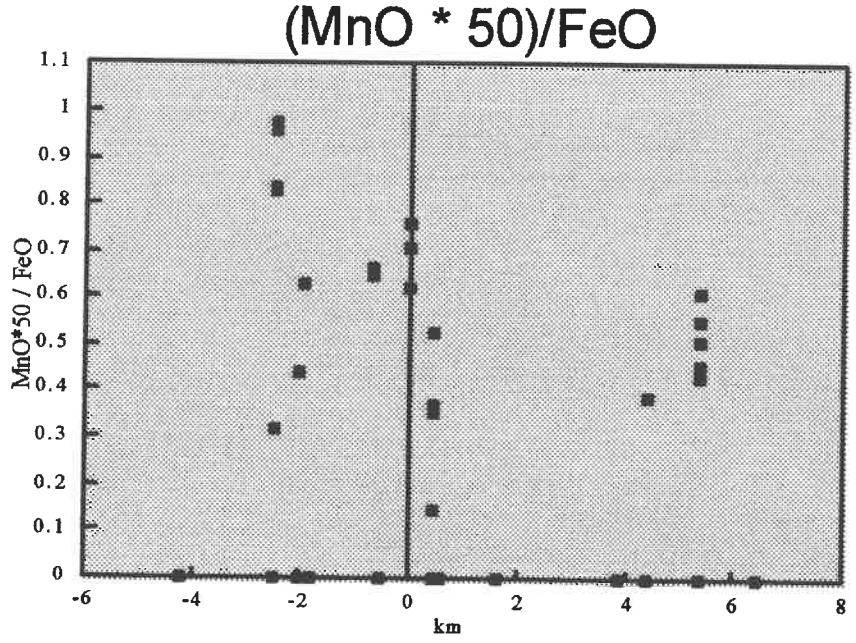

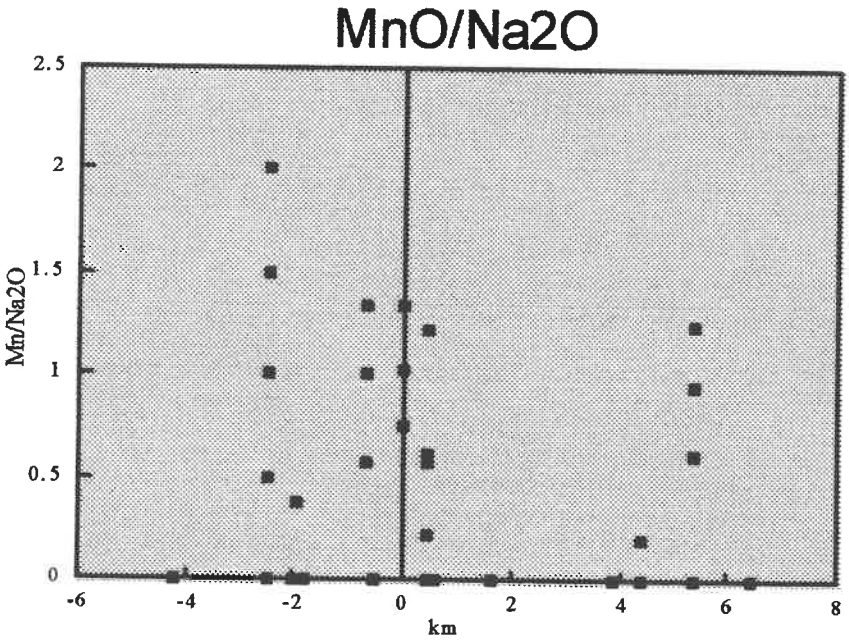

Appendix 7

Chlorite data and plots from the RBS.

Appendix 7-1
Chemical data for chlorites (RBS).

SAMPLE	D.D.H.	SiO2	Al2O3	FeO	MnO	MgO	Na2O	H2O	Total
TS-31	NC-90-05	25.4	22.9	22.4	0.4	14.8	0.4	11.6	98.0
TS-31		24.1	22.8	21.9	0.5	13.6	0.3	11.6	94.8
TS-31		24.1	22.1	22.5	0.5	13.5	0.0	11.6	94.3
TS-31		25.1	23.6	23.1	0.5	14.0	0.3	11.6	98.0
TS-72	NC-90-05	23.6	24.1	33.5	0.4	7.9	0.6	11.0	101.1
TS-72		23.8	24.1	33.3	0.4	7.7	0.3	11.0	100.6
TS-72		23.8	23.8	33.3	0.5	8.3	0.0	11.0	100.7
TS-84	NC-91-25	24.5	23.2	27.0	0.2	12.7	0.5	11.4	99.4
TS-84		25.0	22.6	26.6	0.0	13.3	0.5	11.4	99.4
TS-86	NC-91-25	24.4	23.5	28.5	0.2	11.4	0.0	11.3	99.3
TS-86		26.0	22.0	27.1	0.0	13.1	0.0	11.3	99.5
TS-42	NC-91-06	24.6	23.8	26.6	0.0	12.2	0.4	11.4	99.0
TS-42		25.1	24.1	25.6	0.0	13.6	0.5	11.5	100.4

Appendix 7-2
Plots of chlorite compositions vs. east-west coordinates (RBS).

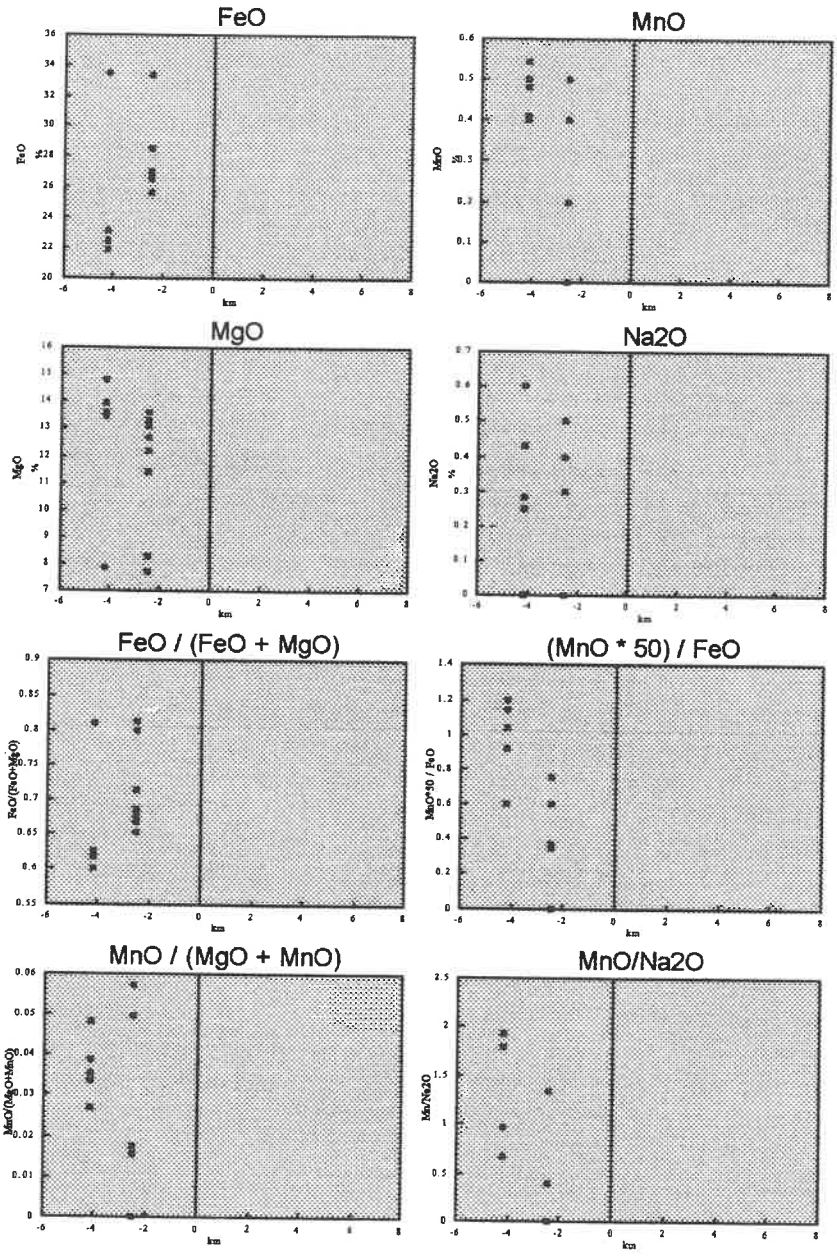

Appendix 8

Chloritoid chemical data and plots from the Mine Horizon.

Appendix 8-1
Chemical data for chloritoides (Mine Horizon).

Sample	D.D.H.	Na2O	MgO	Al2O3	SiO2	MnO	FeO	Total
TS-52	NC-91-15	0.0	2.6	40.0	24.4	0.3	23.8	91.1
TS-52		0.3	2.8	40.6	25.1	0.0	24.0	92.8
TS-52		0.0	2.4	40.9	24.6	0.2	25.8	93.9
TS-52		0.0	2.1	40.2	24.5	0.0	25.7	92.5
TS-59	NC-91-17	0.4	2.8	41.0	24.5	0.9	22.4	92.0
TS-59		0.0	2.0	40.5	24.9	0.6	24.9	92.9
TS-59		0.0	3.1	41.3	25.1	0.8	22.6	92.9
TS-59		0.0	3.2	41.3	25.0	0.7	22.1	92.3
TS-59		0.3	3.2	41.7	25.3	0.4	23.0	93.9
TS-59		0.4	3.1	41.4	24.9	0.5	22.7	93.0
TS-59		0.3	2.9	41.7	25.1	0.3	24.2	94.5
TS-60	NC-91-17	0.0	1.1	40.2	24.5	0.2	26.8	92.8
TS-60		0.0	1.3	39.9	24.1	0.2	26.3	91.8
TS-60		0.3	1.1	40.3	24.7	0.3	26.9	93.6
TS-60		0.2	1.6	40.9	24.9	0.4	26.2	94.2
TS-60		0.2	1.4	40.5	24.6	0.3	26.7	93.7
TS-60		0.3	1.7	41.3	25.9	0.3	26.2	95.7
TS-44	NC-91-06	0.3	2.5	42.0	25.7	0.2	26.1	96.8
TS-44		0.0	2.7	42.6	25.6	0.2	25.8	96.9
TS-44		0.3	2.7	42.8	25.6	0.3	25.3	97.0
TS-44		0.0	2.1	40.2	24.2	0.3	24.8	91.7
TS-44		0.2	2.7	40.1	24.7	0.0	24.6	92.3
GR-90-42	SURF	0	3.4	41.2	25.6	0.3	24.5	95.0
GR-90-42		0	3.5	41.2	24.9	0.4	23.7	93.7
GR-90-42		0	3.2	41.5	24.9	0.5	23.1	93.2
TS-90	NMAR	0.2	2	41.2	25.1	1.1	24.7	94.3
TS-90		0.3	2	41.2	25	1.1	24.6	94.2
TS-90		0.2	2	41.6	25.5	1.2	25.2	95.7
TS-15	N-89-99	0.0	3.2	41.1	25.1	0.0	25.1	94.5
TS-15		0.3	2.7	41.4	25.2	0.2	26.3	96.1
TS-15		0.3	3.1	40.6	25.1	0.2	25.6	94.9
TS-3	N-87-54	0.0	1.6	40.2	24.4	2.0	23.5	91.7
TS-3		0.0	1.6	40.5	24.4	1.9	24.1	92.5
TS-7	N-87-28	0.0	1.2	39.7	24.6	0.3	25.9	91.7
TS-7		0.0	1.2	39.7	24.1	0.8	25.4	91.1
TS-7		0.2	1.3	40.2	24.8	0.7	26.0	93.2
TS-7		0.0	1.5	39.8	24.9	0.6	24.1	90.9
TS-7		0.0	1.5	39.4	24.3	0.6	25.9	91.8
TS-7		0.0	1.4	40.1	24.3	0.6	25.9	92.3
TS-7		0.0	1.4	39.6	24.1	0.4	25.8	91.3
TS-7		0.0	1.5	39.8	24.4	0.7	25.6	91.9

Appendix 8-1, (continued).

Sample	D.D.H.	Na2O	MgO	Al2O3	SiO2	MnO	FeO	Total
TS-19	NC-90-01C	0.0	2.8	40.7	24.6	0.3	23.2	91.5
TS-19		0.0	3.1	41.0	24.7	0.2	22.6	91.6
TS-19		0.3	2.7	39.7	25.2	0.4	23.7	92.0
TS-18		0.0	1.3	40.5	24.8	0.0	26.6	93.3
TS-18		0.2	1.9	41.2	24.9	0.4	25.4	94.0
TS-18		0.0	0.8	39.7	24.1	0.2	27.4	92.2
TS-18		0.0	1.1	40.0	24.1	0.0	27.2	92.5
TS-18		0.3	1.3	40.1	24.5	0.4	26.7	93.2
TS-18		0.3	1.6	40.3	24.7	0.3	25.9	93.1
TS-18		0.0	1.3	40.6	24.9	0.2	27.0	94.1
TS-40	NC-90-03	0.3	3.3	41.2	24.8	0.2	22.6	92.4
TS-40		0.0	3.3	41.2	24.9	0.6	22.3	92.3
TS-40		0.3	3.8	41.6	25.3	0.4	21.2	92.6
TS-40		0.0	3.0	41.0	25.0	0.2	22.7	91.9
TS-40		0.3	3.5	40.4	24.6	0.7	19.7	89.2
TS-40		0.2	3.8	40.7	24.5	0.6	20.1	89.9
TS-40		0.3	3.7	41.4	25.2	0.4	21.6	92.6
TS-28	NC-90-04	0.0	2.3	40.8	25.2	0.4	25.6	94.2
TS-28		0.0	2.0	40.7	24.6	0.4	25.3	93.0
TS-28		0.0	2.3	41.4	25.0	0.3	24.5	93.4
TS-28		0.3	2.3	41.4	25.6	0.4	24.5	94.4
TS-28		0.0	2.5	40.4	24.9	0.5	25.5	93.8
TS-28		0.0	2.6	41.0	25.0	0.2	25.0	93.9
TS-45	NC-91-11	0.2	2.2	41.1	25.1	0.2	24.7	93.6
TS-45		0.0	2.3	40.8	24.5	0.2	24.5	92.3
TS-45		0.0	2.2	40.8	24.9	0.1	24.0	92.0
TS-45		0.4	1.8	40.9	25.4	0.0	25.1	93.6
TS-74	NC-91-11	0.3	2.0	40.4	25.0	0.0	26.9	94.6
TS-74		0.0	2.1	40.4	24.9	0.0	25.8	93.2
TS-74		0.0	2.2	40.4	24.9	0.2	26.2	93.9
TS-46	NC-91-12	0.3	1.7	40.8	24.8	0.2	26.4	94.2
TS-46		0.0	1.5	40.5	25.6	0.2	25.8	93.6
TS-46		0.0	1.4	40.2	24.7	0.3	26.2	92.8
TS-46		0.0	1.7	40.6	24.7	0.0	25.9	93.0
TS-46		0.3	1.2	40.5	24.7	0.2	27.4	94.3
TS-46		0.2	1.1	40.5	24.8	0.0	26.9	93.6
TS-75		0.2	3.7	40.7	25.1	0.4	23.9	94.0
TS-75		0.0	3.3	40.0	24.6	0.4	24.1	92.4
TS-75		0.3	3.3	40.8	24.7	0.4	24.0	93.5
TS-76		0.3	1.6	40.7	24.7	0.3	27.0	94.6
TS-76		0.2	1.5	39.8	24.4		27.8	93.7
TS-76		0.2	1.4	39.1	24.2		27.6	92.5

Appendix 8-1, (continued).

Sample	D.D.H.	Na2O	MgO	Al2O3	SiO2	MnO	FeO	Total
TS-65	NC-91-20	0.0	1.7	40.5	25.6	0.3	26.7	94.8
TS-65		0.0	1.7	40.1	24.7	0.2	26.2	92.9
TS-65		0.0	1.6	40.3	24.8	0.2	26.6	93.5
TS-65		0.0	1.5	40.0	24.6	0.0	27.0	93.1
TS-50	NC-91-14	0.2	2.1	40.8	24.7	0.0	26.1	94.0
TS-50		0.0	2.4	40.6	25.1	0.0	24.9	93.1
TS-50		0.0	2.5	41.2	25.3	0.0	25.2	94.2
TS-50		0.0	2.2	40.3	25.0	0.2	25.0	92.7
TS-50		0.0	2.0	40.0	24.1	0.2	25.0	91.3
TS-77		0.0	0.7	40.3	24.4		28.1	93.5
TS-77		0.0	0.8	40.0	24.4		27.2	92.4
TS-77		0.0	0.8	39.5	24.4		28.9	93.6
TS-54	NC-91-16	0.0	2.7	40.8	25.2	0.4	25.2	94.2
TS-54		0.0	3.2	41.2	24.9	0.3	23.1	92.7
TS-54		0.3	3.2	42.2	25.4	0.4	23.6	95.2
TS-78		0.3	1.5	41.2	24.6	0.3	26.4	94.3
TS-67	NC-91-23	0.3	1.5	40.2	24.4	0.3	26.6	93.3
TS-67		0.1	2.1	40.5	24.6	0.3	25.5	93.1
TS-67		0.4	2.0	40.8	24.9	0.0	24.8	92.9
TS-67		0.3	1.9	40.5	24.7	0.0	25.9	93.3
TS-67		0.0	1.6	41.0	25.2	0.0	26.1	93.9
TS-67		0.0	1.5	40.2	24.5	0.0	25.8	92.0
TS-67		0.3	1.7	39.7	24.6	0.0	26.8	93.1
TS-68		0.2	2.6	41.4	25.0	0.4	23.9	93.5
TS-68		0.0	2.0	40.6	24.7	0.3	24.8	92.4
TS-68		0.3	3.2	41.0	24.6	0.4	22.9	92.4
TS-68		0.0	3.1	41.6	25.3	0.4	22.9	93.3
TS-68		0.3	1.9	41.3	24.8	0.3	25.5	94.1
TS-68		0.4	2.0	41.1	24.8	0.3	25.1	93.7
TS-68		0.2	2.8	41.1	25.2	0.3	23.9	93.5
TS-80	NC-91-23	0.0	2.8	40.2	24.6	0.5	24.1	92.2
TS-80		0.0	3.3	41.0	25.7	0.2	23.6	93.8
TS-81		0.2	3.2	40.2	24.4	0.3	23.7	92.0
TS-81		0.0	2.6	40.0	24.7		25.0	92.3
TS-81		0.4	3	40.8	24.7	0.2	25.3	94.4

Appendix 8-2
Plots of chloritoid compositions vs. east-west coordinates (Mine Horizon).

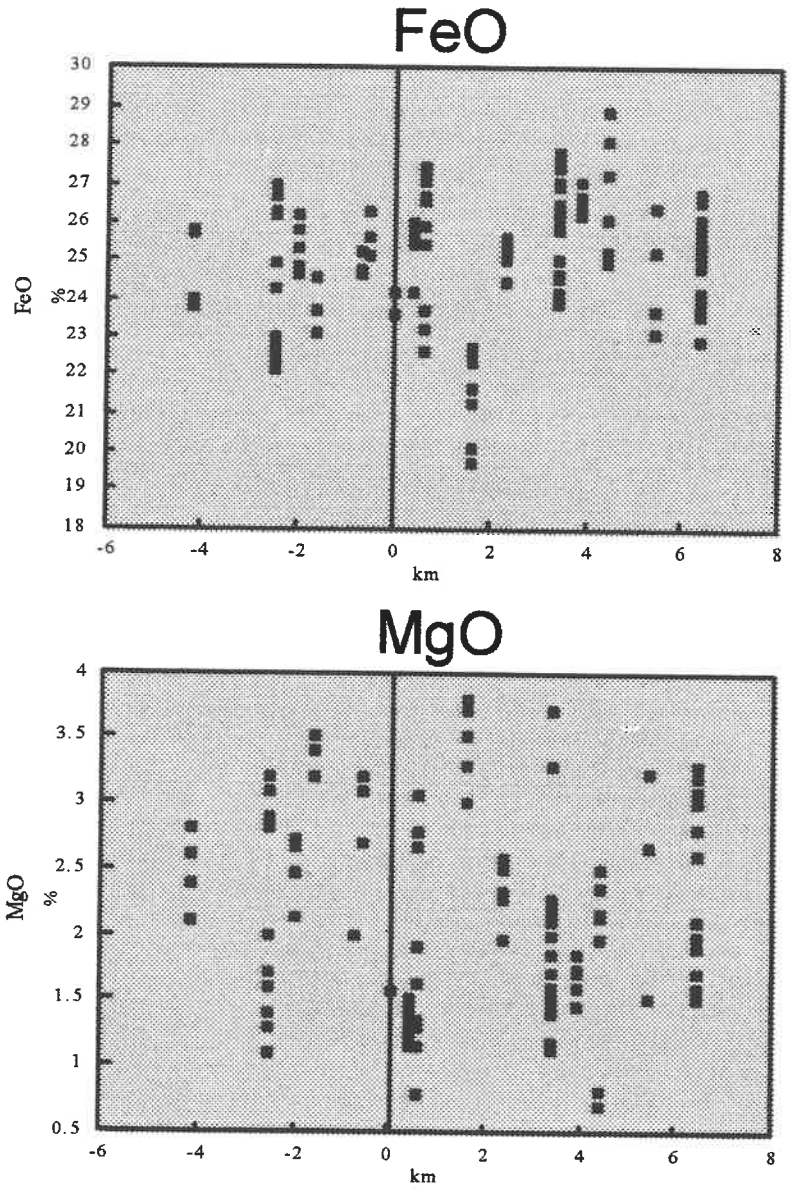

Appendix 9

Choritoid chemical data and plots from the RBS.

Appendix 9-1

Sample	D.D.H.	Na2O	MgO	Al2O3	SiO2	MnO	FeO	Total
TS-31	NC-90-05	0.0	2.7	41.3	24.8	1.9	22.0	92.6
TS-32		0.3	2.8	41.0	24.9	0.7	22.9	92.6
TS-32		0.0	2.6	41.0	25.2	0.9	22.3	92.0
TS-32		0.3	3.0	41.0	24.7	0.7	22.1	91.8
TS-32		0.0	2.9	41.0	24.6	1.0	22.7	92.1
TS-72		0.3	1.6	40.9	24.6	1	25.9	94.3
TS-72		0	1.5	40.8	24.5	1.3	25.6	93.7
TS-72		0.2	1.9	41	24.8	0.9	25.8	94.6
TS-84	NC-91-25	0.3	3.8	41.9	25.2	0.4	22.8	94.4
TS-85		0.2	3.4	41.5	24.9	1.4	22.4	93.8
TS-85		0.3	3.5	42.4	25.6	1.4	22.1	95.3
M-90-94	Surface	0.0	3.7	40.7	24.5	0.5	21.4	90.8
M-90-94		0.0	4.4	41.6	25.2	0.5	20.4	92.0
M-90-94		0.0	2.6	40.3	24.3	0.4	22.8	90.4
M-90-94		0.0	3.3	40.9	25.1	0.3	22.1	91.6
M-90-94		0.0	3.9	41.2	24.8	0.6	21.2	91.6

Chemical data for chloritoids (RBS).

Appendix 9-2
Plots of chloritoid compositions vs. east-west coordinates (RBS).

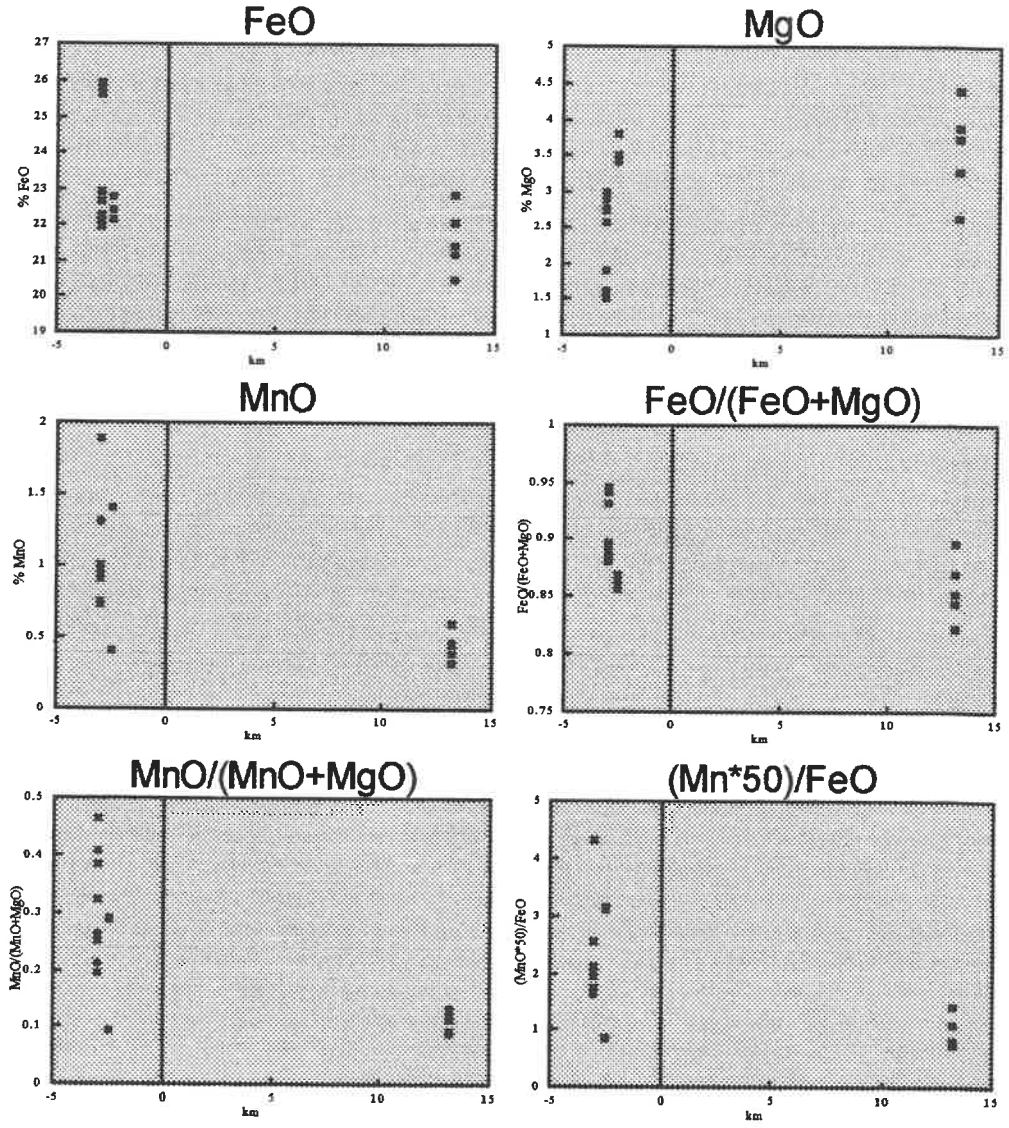

Appendix 10

Ankerite chemical data and plots from the Mine Horizon.

Appendix 10-1
Chemical data for ankerites (Mine Horizon).

T.S.	D.D.H.	CaO	MgO	FeO	MnO	CO2	TOTAL
TS-52	NC-91-15	28.6	12.5	17.2	0.5	46.9	105.7
TS-52		28.3	12.9	15.8	0.8	46.5	104.3
TS-52		28.5	13.3	15.8	0.7	47.0	105.3
TS-52	NC-91-15	28.6	14.4	14.7	0.7	47.6	106.0
TS-59	NC-91-17	28.0	8.1	23.7	0.7	45.8	106.3
TS-59		28.5	9.2	21.8	1.2	46.5	107.2
TS-60	NC-91-17	29.5	14.9	12.7	0.6	47.6	105.3
TS-43	NC-91-06	29.2	16.7	10.5	0.3	47.8	104.5
TS-43		29.8	19.0	6.4	0.3	48.2	103.7
TS-43		28.9	12.2	17.9	0.6	47.3	106.9
TS-43		29.0	13.1	16.8	0.4	47.6	106.9
TS-43		29.1	13.8	16.1	0.4	48.0	107.4
TS-44	NC-91-06	28.6	14.0	14.7	0.5	47.0	104.8
TS-44		29.4	14.5	14.0	0.4	47.8	106.1
TS-44		29.1	12.8	16.7	0.5	47.4	106.6
T-90-31C	SURF	29.9	13.2	14.6	0.7	47.26	105.7
T-90-31C		29.7	13.8	15	0.6	47.94	107
T-90-31C		29.7	13.2	15.3	0.7	47.53	106.4
TS-12	N-89-99	29.3	12.3	15.9	1.1	46.8	105.4
TS-12		28.9	14.2	13.6	1.6	47.5	105.8
TS-12	N-89-99	28.7	10.9	18.4	0.7	46.1	104.8
TS-15	N-89-99	28.6	14.3	14.3	0.4	47.1	104.7
TS-15		30.3	13.6	14.5	0.0	47.5	105.9
TS-15		29.1	14.5	14.5	0.7	48.0	106.8
TS-83	N-87-54	27.6	9.5	18.9	2.0	44.9	102.9
TS-83		26.6	10.0	15.5	4.3	44.0	100.4
TS-83		26.9	8.8	19.6	1.7	43.8	100.8
TS-7	N-87-28	28.8	8.7	21.0	0.9	45.5	104.9
TS-7		28.5	13.8	13.8	0.6	46.3	103.0
TS-8	N-87-28	28.6	13.5	15.3	1.0	47.2	105.6
TS-8		28.2	12.6	15.1	2.0	46.4	104.3
TS-18	NC-90-01C	28.3	7.8	23.3	0.6	45.3	105.3
TS-19	NC-90-01C	29.3	15.1	12.8	1.0	47.9	106.1
TS-19		29.5	15.1	12.7	0.6	47.8	105.7
TS-19		28.8	16.1	10.4	2.2	47.9	105.4
TS-19		29.5	18.2	7.6	0.8	48.2	104.3
TS-40	NC-90-03	28.3	17.7	7.3	0.8	46.5	100.6
TS-40		29.5	18.2	6.9	0.9	47.8	103.3
TS-40		28.3	18.0	7.9	0.7	47.1	102.0
TS-28	NC-90-04	29.5	14.6	12.7	0.9	47.4	105.1

Appendix 10-1 (continued).

T.S.	D.D.H.	CaO	MgO	FeO	MnO	CO2	TOTAL
TS-45	NC-91-11	29.3	16.6	10.8	0.5	48.1	105.3
TS-45		28.8	15.4	12.6	0.3	47.4	104.5
TS-74	NC-91-11	30.0	14.0	15.0	0.5	48.3	107.8
TS-74		28.6	10.6	20.2	0.6	46.8	106.8
TS-74		29.0	9.5	19.8	0.6	45.6	104.5
TS-74		28.8	10.9	20.0	0.6	47.1	107.4
TS-46	NC-91-12	28.8	12.1	17.5	0.6	46.8	105.8
TS-46		29.1	12.9	16.6	0.4	47.4	106.4
TS-75	NC-91-12	29.0	13.0	16.5	0.4	47.3	106.2
TS-75		29.0	12.4	17.4	0.4	47.2	106.4
TS-75		29.9	17.7	9.5	0.6	49.0	106.7
TS-75		30.2	18.4	8.5	0.7	49.4	107.2
TS-76	NC-91-12	28.6	10.8	20.4	1.0	47.4	108.2
TS-76		30.4	15.0	12.5	0.5	48.2	106.6
TS-76		30.7	15.0	12.4	0.4	48.3	106.8
TS-65	NC-91-20	29.5	14.5	10.4	2.5	46.9	103.8
TS-65		29.3	12.9	15.9	0.6	47.2	105.9
TS-65		29.0	13.4	15.2	0.6	47.1	105.3
TS-65		29.6	12.6	15.9	0.2	46.9	105.2
TS-65		28.9	13.1	15.9	0.6	47.1	105.6
TS-65		29.9	14.2	13.3	0.7	47.6	105.7
TS-50	NC-91-14	28.8	11.3	18.4	0.4	46.4	105.2
TS-50		29.9	13.4	14.1	0.7	47.1	105.2
TS-77	NC-91-14	28.3	5.8	25.1	0.8	44.4	104.4
TS-77		29.1	6.9	23.6	0.5	45.1	105.2
TS-77		28.5	5.4	25.6	0.5	44.3	104.3
TS-77		28.5	5.3	25.7	0.7	44.3	104.5
TS-54	NC-91-16	29.4	16.7	10.5	0.3	48.0	104.9
TS-78	NC-91-16	29.1	12.7	16.1	1.1	47.2	106.2
TS-78		29.4	15.4	12.9	1.7	48.8	108.2
TS-78		29.5	16.7	10.7	1.1	48.6	106.6
TS-67	NC-91-23	29.1	12.7	16.4	0.9	47.3	106.4
TS-68	NC-91-23	28.5	13.7	14.1	1.9	47.1	105.3
TS-68		29.3	16.7	9.6	1.4	48.0	105.0
TS-68		29.0	14.1	14.8	1.2	48.0	107.1
TS-68		30.2	18.2	8.6	0.7	49.3	107.0
TS-68		28.7	15.5	12.3	1.5	47.9	105.9
TS-68		29.2	15.9	10.7	0.9	47.4	104.1
TS-81	NC-91-23	29.8	17.5	9.0	0.5	48.3	105.1
TS-81		29.4	15.7	11.8	0.8	47.9	105.6
TS-81		30.3	15.6	11.3	0.3	47.9	105.4

Appendix 10-2
Plots of ankerite compositions vs. east-west coordinates (Mine Horizon).

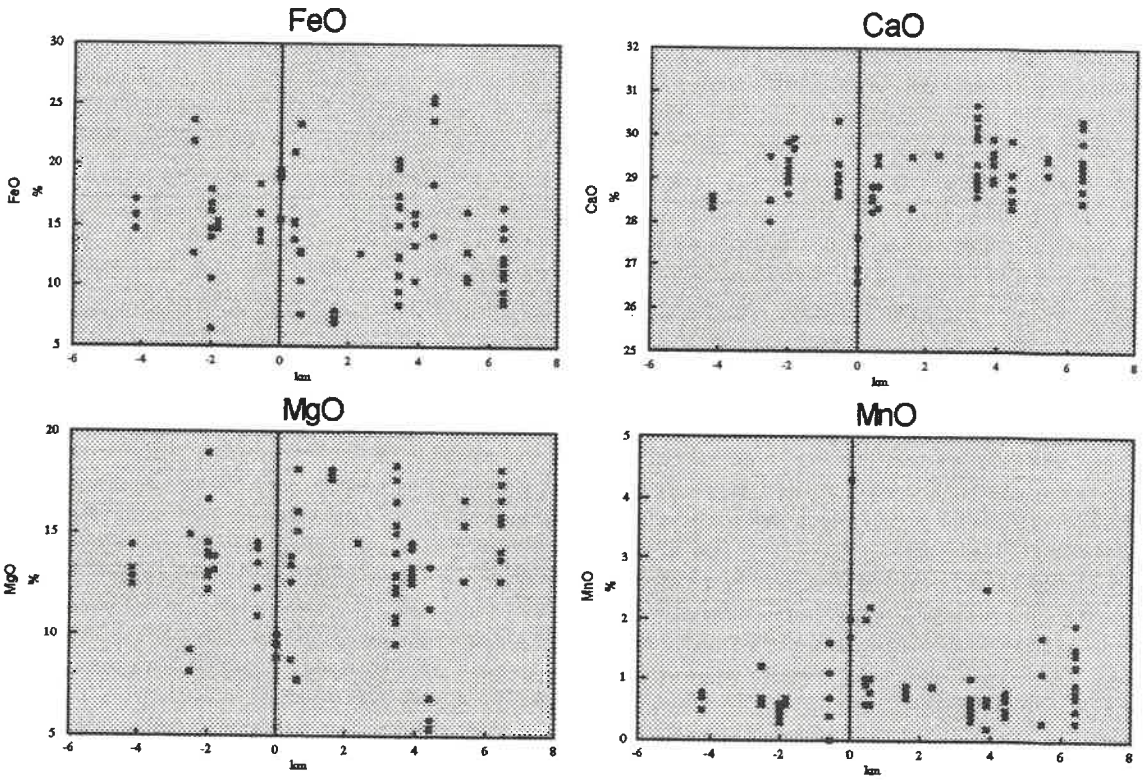

Appendix 10-3
Plot of FeO/(FeO+MgO) vs. east-west coordinates for ankerite (Mine Horizon).

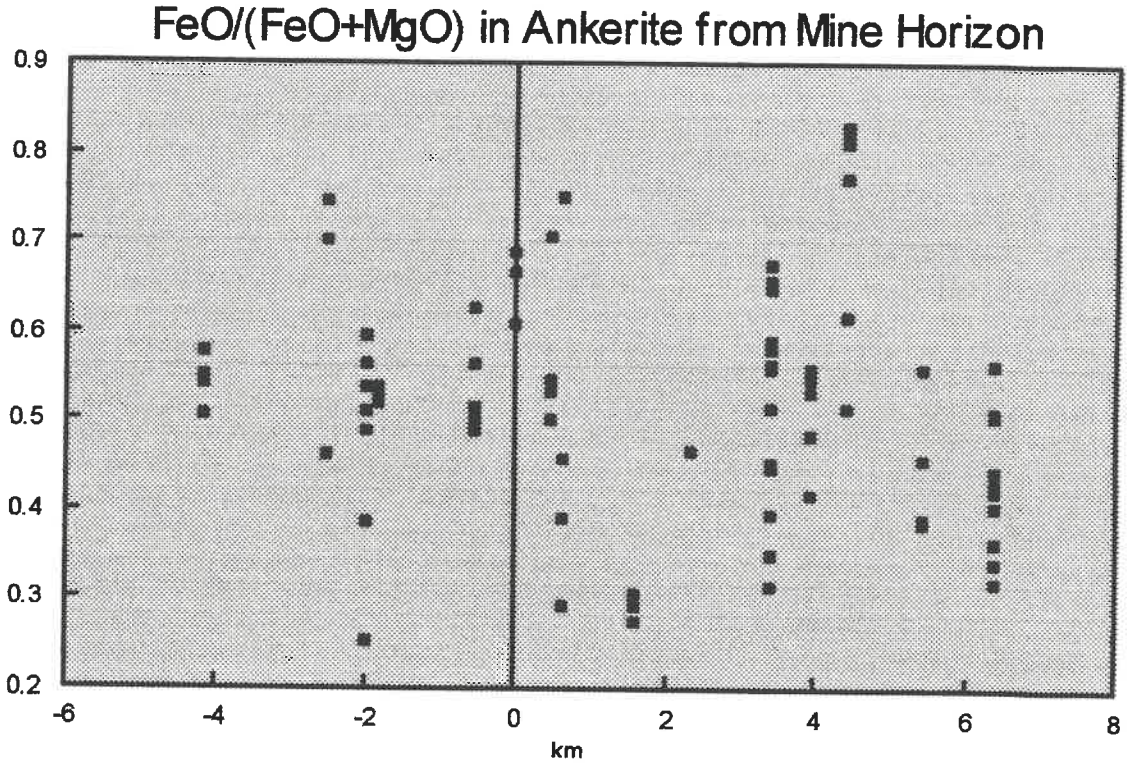

Appendix 11

Ankerite chemical data and plots from the RBS.

Appendix 11-1
Chemical data for ankerites (Mine Horizon).

Sample	D.D.H.	CaO	MgO	FeO	MnO	CO2	TOTAL
TS-51	NC-91-15	31.6	19.2	2.4	1.2	48.0	102.4
TS-86	NC-91-25	29.9	14.8	12.8	0.6	47.8	105.9
TS-86		30.2	15.3	11.7	1.1	48.3	106.6
TS-86		30.1	15.2	11.3	0.9	47.7	105.2
TS-42	NC-91-06	28.5	14.7	13.7	1.5	47.7	106.1
TS-37	NC-90-01C	30.1	18.6	4.7	2.5	48.3	104.2
TS-37		29.2	16.0	9.9	0.6	46.8	102.5
TS-39	NC-90-02	31.2	17.2	7.9	0.6	48.4	105.3
TS-41	NC-90-04	29.4	15.2	11.8	0.7	47.3	104.4
TS-47	NC-91-12	28.5	11.1	18.0	0.6	45.9	104.1
TS-47		28.3	13.9	13.9	1.1	46.6	103.8
TS-47		28.7	10.5	19.0	0.6	46.0	104.8
TS-47		28.1	11.0	19.4	0.7	46.4	105.6
TS-63	NC-91-18	32.6	16.7	5.7	0.7	47.7	103.4
TS-63		32.7	18.8	3.6	0.7	48.8	104.6
TS-63		31.4	14.1	10.5	1.5	47.4	104.9

Appendix 11-2
Plots of ankerite compositions vs. east-west coordinates (Mine Horizon).

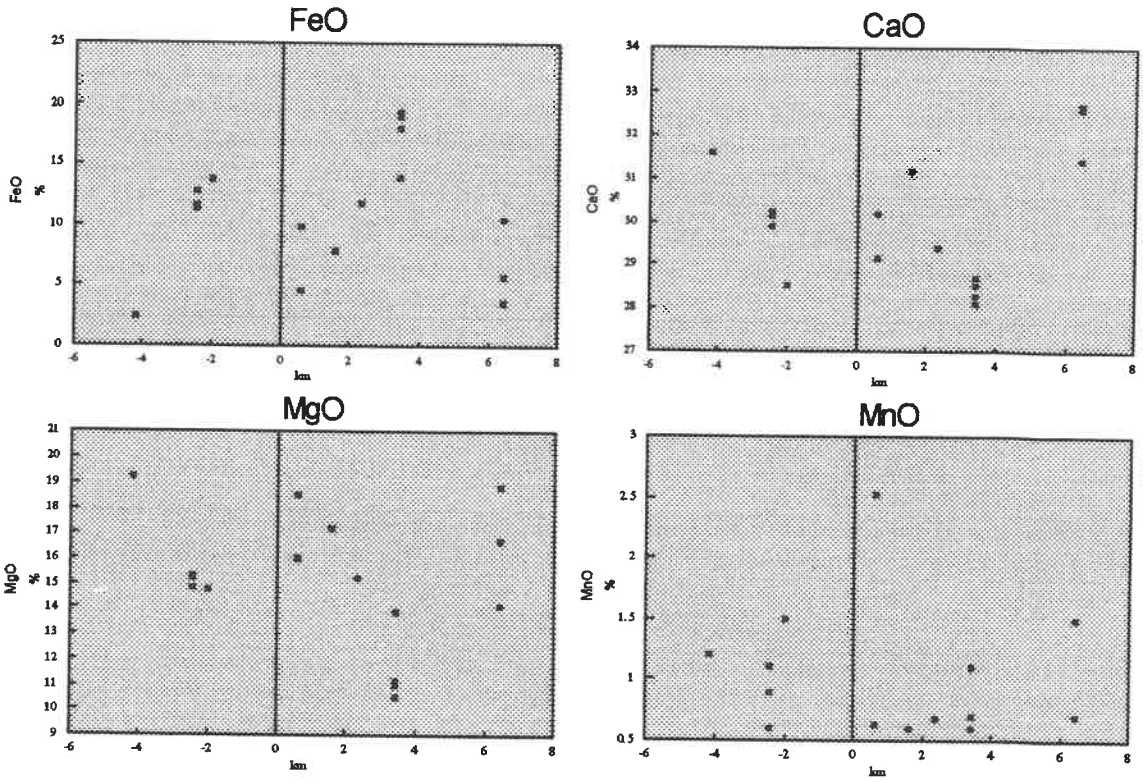

Appendix 11-3
Plots of compositional ratios of ankerites vs. east-west coordinates (Mine Horizon).

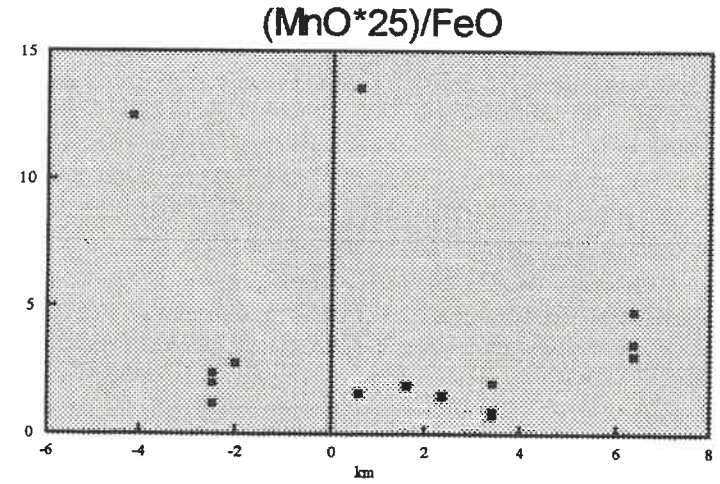

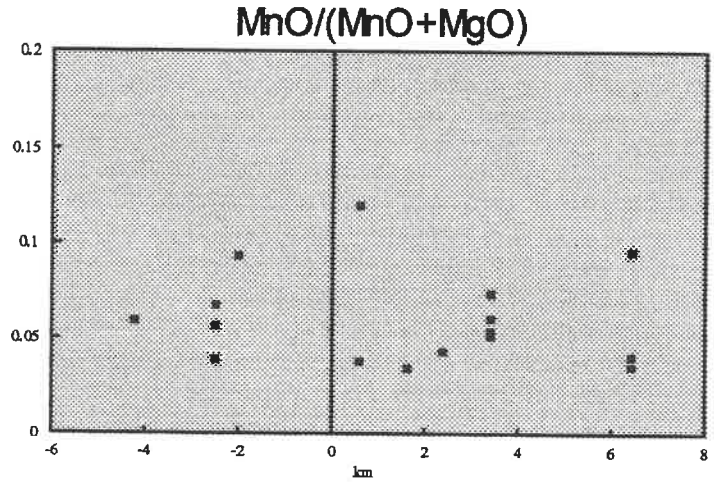

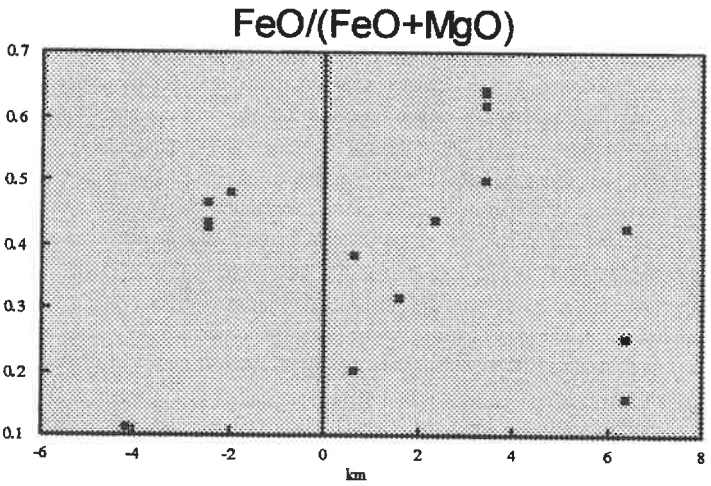

Appendix 12

Siderite, calcite and tourmaline compositions.

Siderite Compositions

Sample	D.D.H.	CaO	MgO	FeO	MnO	CO2	TOTAL
TS-3	N-87-54	1.3	9.9	45.4	5.6	43.1	105.3
TS-3		0.9	12.1	46.7	1.5	43.5	104.6
TS-3		0.8	12.2	47.0	1.7	43.8	105.5
TS-3		0.8	8.2	51.0	0.7	41.3	102.0
TS-3		1.1	9.8	38.9	12.8	43.3	105.9
TS-3		0.5	10.6	45.1	5.1	42.8	104.1
TS-3		1.2	8.1	49.9	2.5	41.9	103.6
TS-8	N-87-28	0.5	16.5	43.3	2.2	46.2	108.7
TS-69	NC-91-23	0.2	13.3	47.0	1.4	44.3	106.2
TS-69		0.2	12.7	49.5	1.2	45.1	108.7
TS-31	NC-90-05	0.0	4.0	52.0	2.5	37.8	96.3
TS-84	NC-91-25	0.5	20.9	38.6	0.9	47.4	108.3
TS-84		0.5	23.0	37.2	0.4	48.5	109.6
TS70A	SURF	0.3	11.7	49.3	1.8	44.3	107.4
		0.3	10.7	50.3	2.1	44.0	107.4
		0.4	11.3	49.7	2.2	44.5	108.1

Calcite Compositions

T.S.	D.D.H.	CaO	MgO	FeO	MnO	CO2	TOTAL
TS-34	NC-90-05	52.8	1.2	1.8	0.7	44.4	100.9
TS-48	NC-91-14	54.1	0.0	0.3	0.3	42.8	97.5
TS-53	NC-91-16	51.1	0.3	3.1	1.1	43.0	98.7
TS-66	NC-90-20	53.8	0.4	0.4	0.5	43.2	98.2
TS-51	NC-91-15	54.7	0	0	0.6	43.3	98.6
D-90-42	SURF	53.1	0.3	0.7	0.8	42.9	97.8
T-90-42	SURF	53.0	0.4	1.0	0.2	42.8	97.4
TR-90-49A	SURF	53.3	0.5	1.2	0.6	43.5	99.1

Tourmaline Compositions from Sample TS-19, Hole NC-90-01

Sample	Na2O	MgO	Al2O3	SiO2	CaO	MnO	Fe2O3	TiO2	Total
TRM001	1.2	5.7	33.9	37.3	0.4	0.2	8.3	0.0	87.0
TRM002	1.4	6.2	33.9	37.2	0.4	0.0	6.9	0.4	86.3
TRM003	2.1	5.6	31.1	36.3	0.3	0.0	10.8	0.4	86.6
TRM004	1.6	5.8	31.5	36.3	1.0	0.0	10.4	0.5	87.0
TRM005	2.0	5.7	31.1	36.4	0.4	0.0	10.9	0.4	86.8
TRM006	2.0	5.8	31.5	36.3	0.6	0.0	11.0	0.7	87.9

Appendix 13

Mineralogical abundances (petrographic).

Appendix 13-1
Average mineralogical abundances in the RBS.

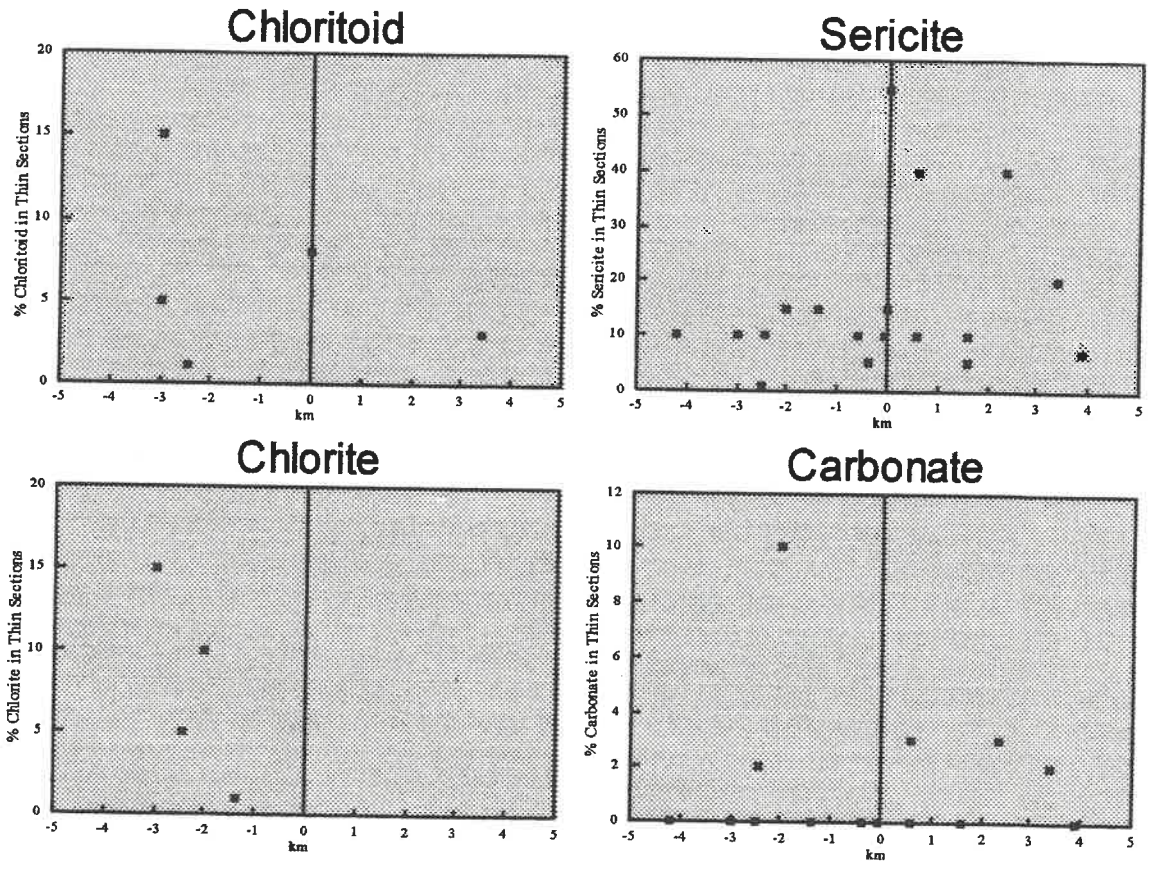

Appendix 13-2
Carbonate distribution by species in the RBS.

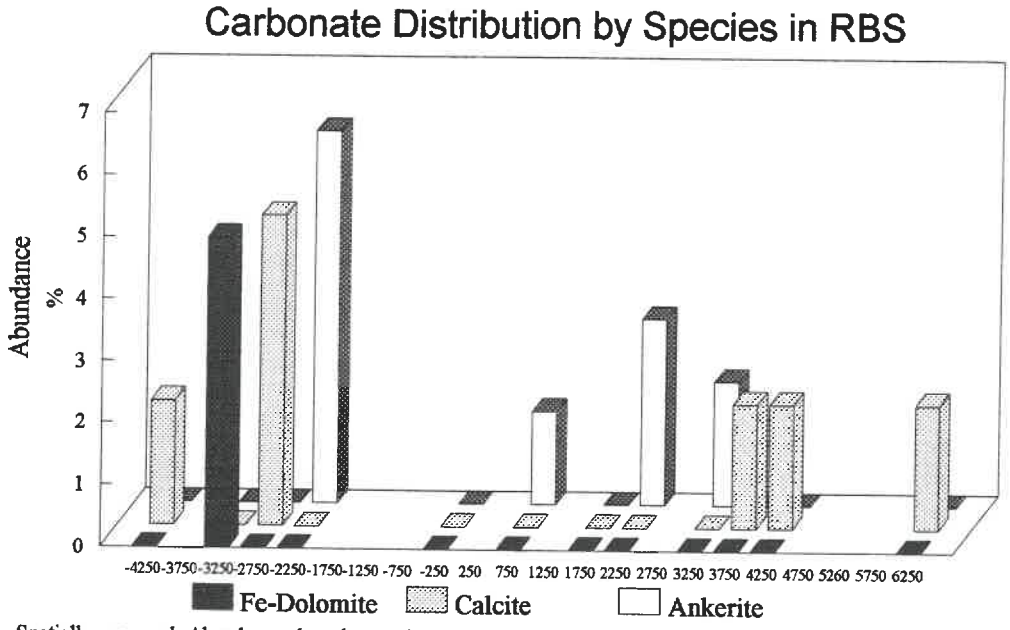

Spatially averaged, Abundances based on carbonate staining.

X-axis represents East-West coordinates (Normetal deposit at 0).

Appendix 13-3
Average mineralogical abundances in the Mine Horizon.

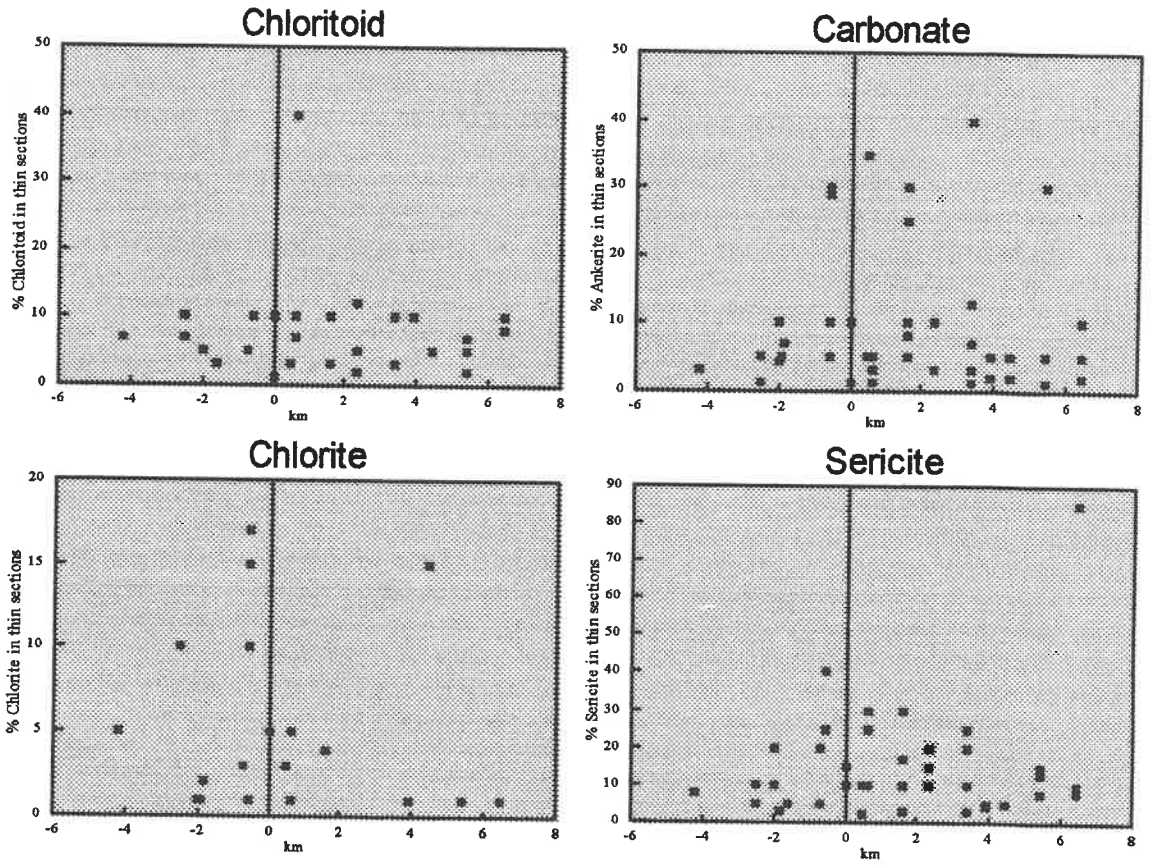

Appendix 13-4
Carbonate distribution by species in the Mine Horizon.

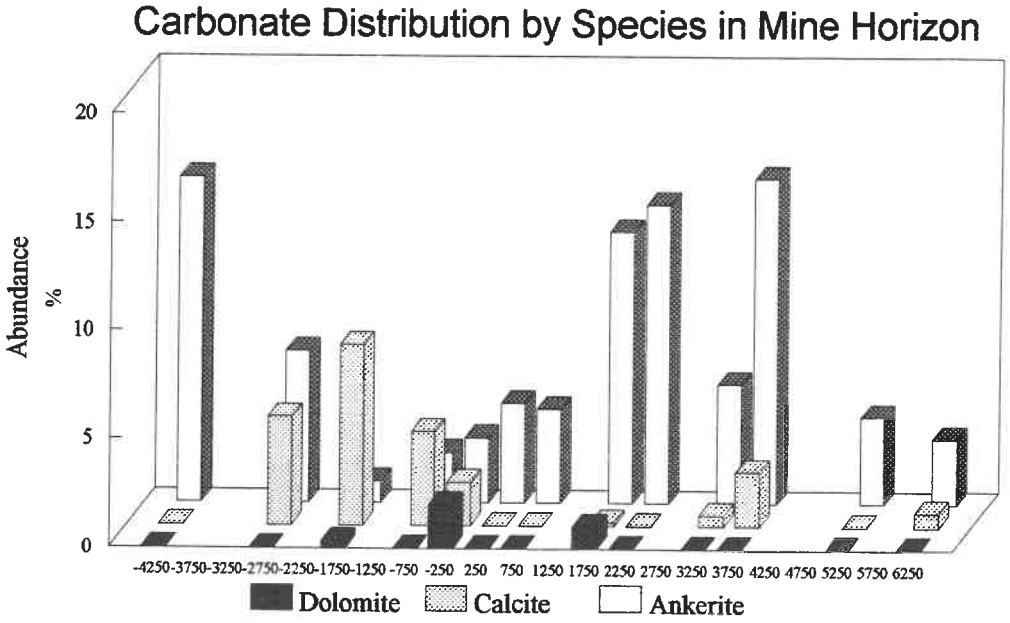

Spatially averaged, abundances based on carbonate stainging.

X-axis represents East-West coordinates (Normetal deposit at 0)

Appendix 14

Oxygen isotope data.

Mine Horizon

Sample	DDH	D18O
TS-08	N-87-28	11.2
TS-83	N-87-54	11.3
TS-15	N-89-99	12.1
TS-18	NC-90-01C	11.9
TS-40	NC-90-03	12.5
TS-28	NC-90-04	10.8
TS-44	NC-91-06	10.6
TS-43	NC-91-06	11.1
TS-74	NC-91-11	10.7
TS-45	NC-91-11	8.8
TS-76	NC-91-12	11.4
TS-46	NC-91-12	10.1
TS-77	NC-91-14	11
TS-50	NC-91-14	9.6
TS-52	NC-91-15	12.7
TS-78	NC-91-16	13.5
TS-54	NC-91-16	11.8
TS-59	NC-91-17	11.1
TS-65	NC-91-20	8.4
TS-64	NC-91-20	9.6
TS-80, 81	NC-91-23	13.1
TS-68	NC-91-23	12.8
TS-67	NC-91-23	13.1
TR-90-49A	SURF	11.0
T-90-31C	SURF	11.7
NMAR-90-5	SURF	12.1
GR-90-42	SURF	13.8

RBS

Sample	DDH	D18O
TS-82	N-89-99	14.8
TS-37	NC-90-01C	12.3
TS-39	NC-90-02	15.2
TS-41	NC-90-04	14.7
TS-33	NC-90-05	10.3
TS-32	NC-90-05	12.1
TS-31	NC-90-05	12.1
TS-42	NC-91-06	10.8
TS-51	NC-91-15	14.5
TS-58	NC-91-17	12.3
TS-63	NC-91-18	13.6
TS-85	NC-91-25	11.6
T-90-19A	SURF	15.4
D-90-12	SURF	16.1
D-90-42	SURF	14.2
T-91-141	SURF	15.1
10108	SURF	13.4
VH-90-01	SURF	13.9
VH-90-05	SURF	15.2

Other

Sample	DDH	D18O
10027	SURF	16.3
MR-90-94	SURF	14.4

Appendix 15

Plots of oxygen isotope data vs. mineralogical abundances.

Appendix 15-1
For the RBS.

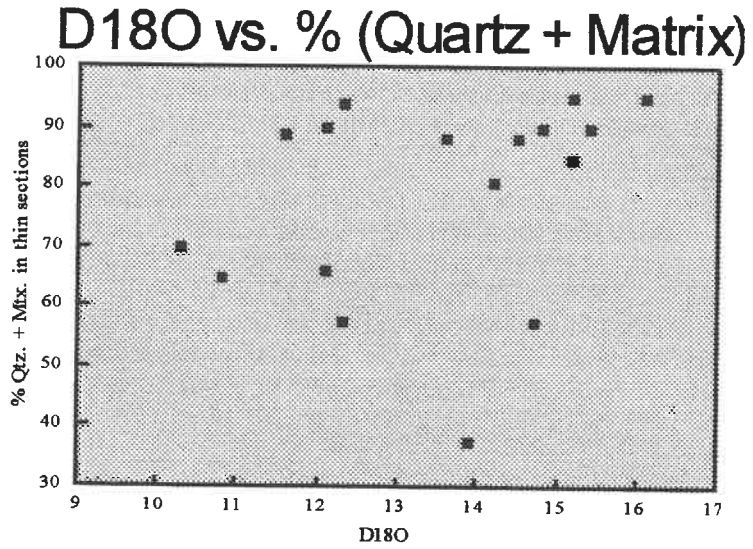

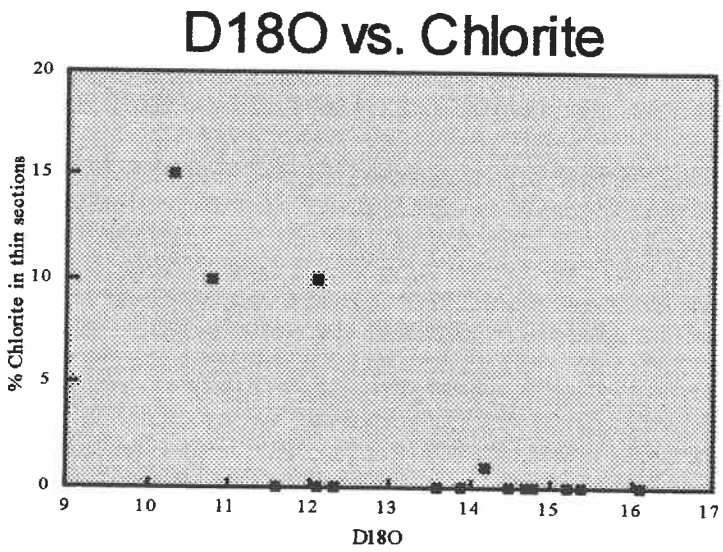

Appendix 15-2
For the Mine Horizon.

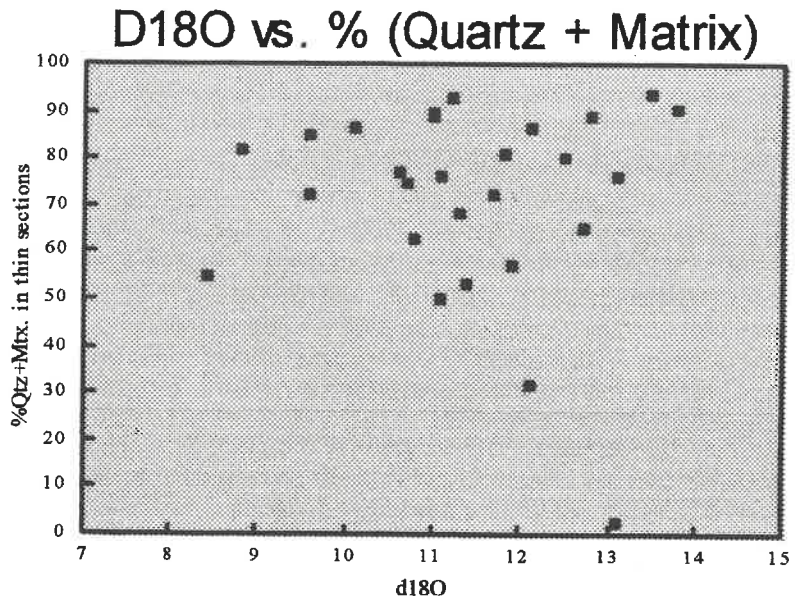

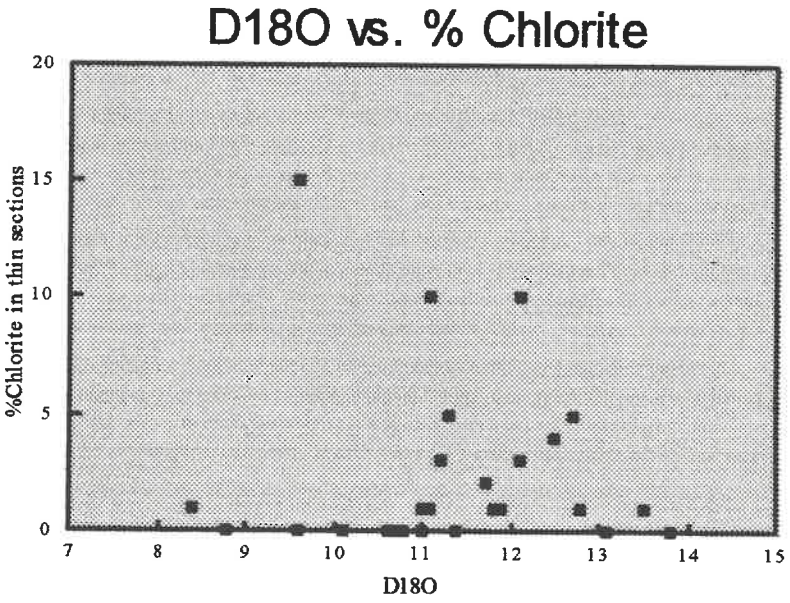

Appendix 16

Normative mineralogy for the RBS.

Appendix 16-1
Normative mineral abundance data.

Sample	Δ18O	sericite	ankerite	chlorite	albite	Quartz
D-90-12	16.1	11.7	0.0	0.5	0.0	70.2
D-90-42	14.2	12.3	1.9	0.0	0.0	62.4
T-90-141	15.1	8.6	6.7	0.7	13.9	47.4
T-90-19A	15.4	6.7	0.3	3.9	19.0	44.0
VH-90-01	13.9	16.5	0.2	13.2	12.9	50.2
VH-90-05	15.2	12.4	0.0	0.0	0.0	65.6
TS-37	12.3	17.9	9.5	0.0	0.0	47.0
TS-39	15.2	10.5	0.8	6.4	8.1	52.6
TS-41	14.7	26.5	3.4	3.8	0.0	27.2
TS-42	10.8	17.2	3.2	23.1	0.0	43.5
TS-51	14.5	15.4	2.5	0.0	0.0	58.7
TS-58	12.3	2.2	0.3	2.2	34.6	31.3
TS-63	13.6	7.5	10.6	8.1	19.5	33.9
TS-85	11.6	8.2	0.2	13.2	12.9	50.2
TS-82	14.8	12.0	0.0	1.8	3.2	62.1

Appendix 16-2
Plots of petrographic vs. normative mineral abundances.

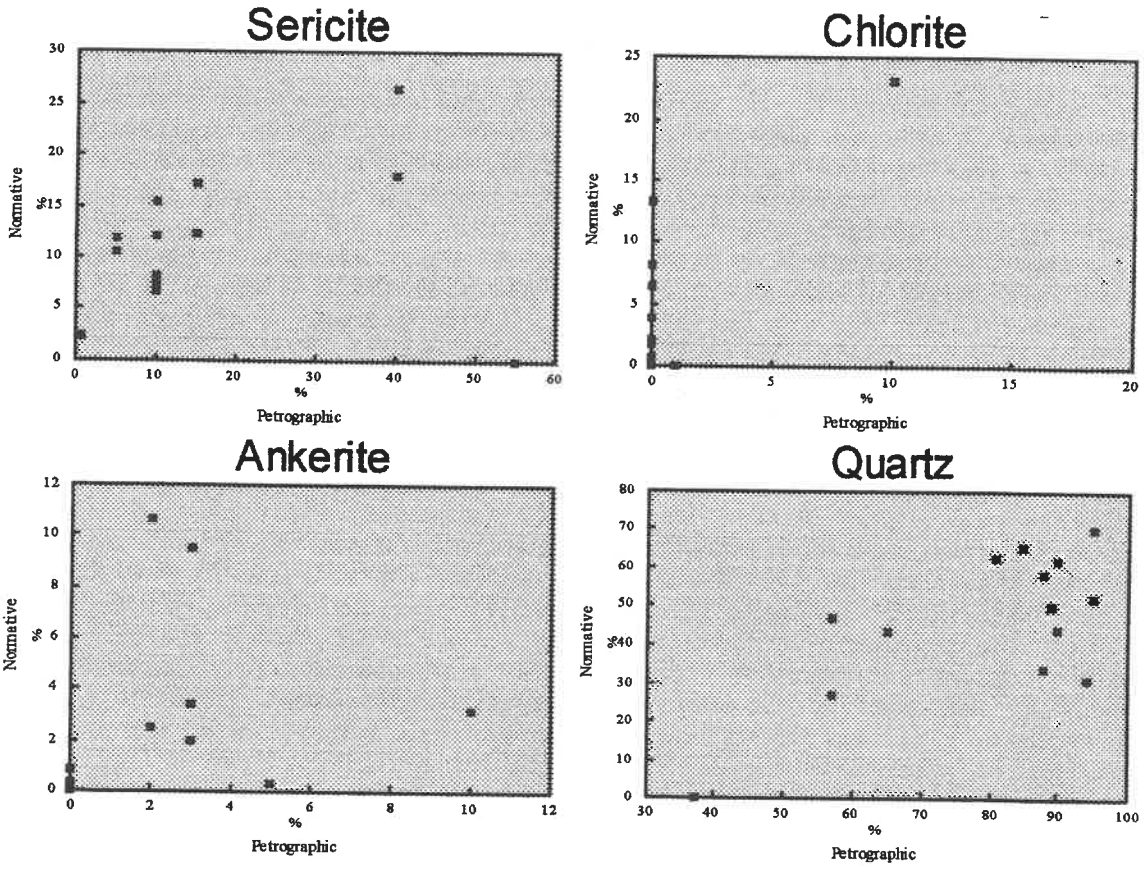

Appendix 16-3
Plots of oxygen isotope data vs. normative mineral abundances.

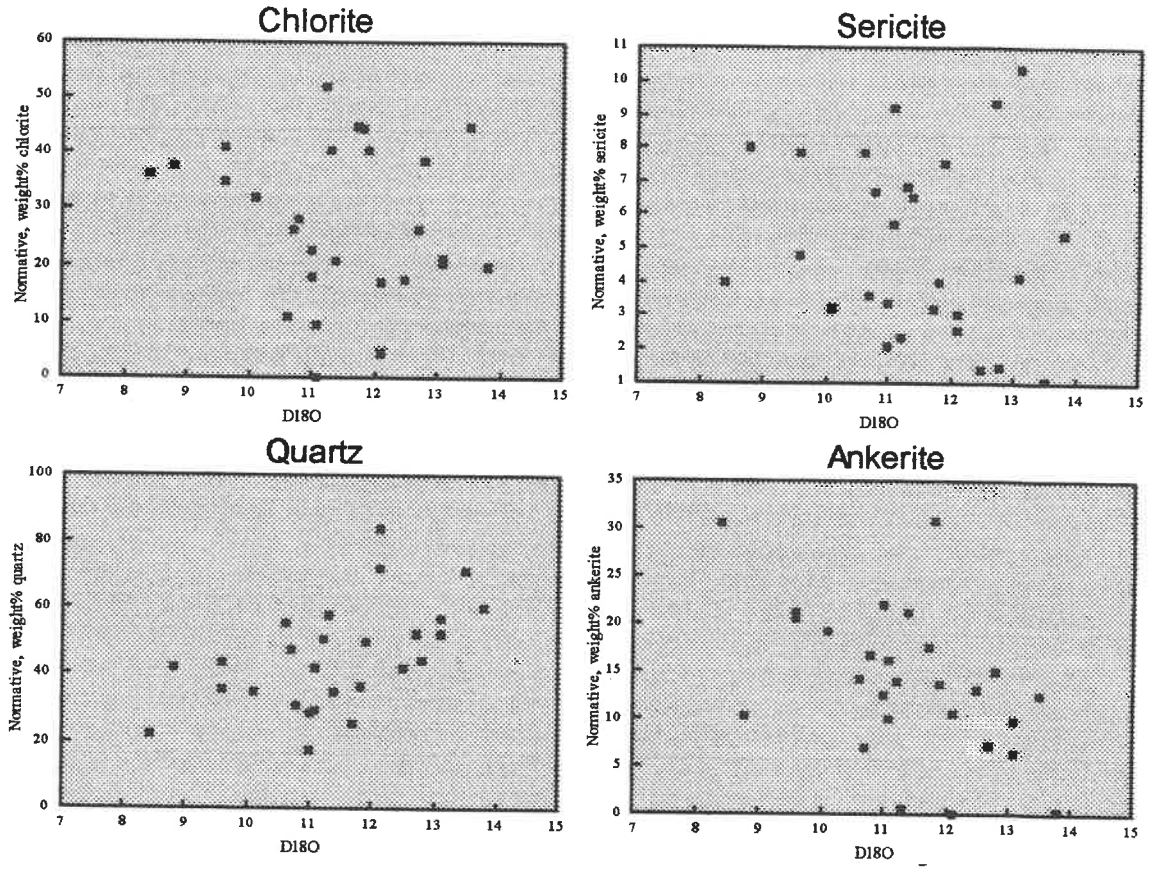

Appendix 17

Normative mineralogy for the Mine Horizon.

Appendix 17-1
Normative mineral abundance data.

Sample	Δ18O	Sericite	Ankerite	Chlorite	Albite	Quartz
GR-90-42	13.8	5.4	0.3	20.0	5.7	60.5
NMAR-90-05	12.1	2.6	0.0	16.9	0.0	83.9
T-90-31C	11.7	3.2	17.5	45.0	17.7	24.9
TR-90-49A	11	2.1	12.5	17.7	29.7	17.7
TS-08	11.2	2.3	13.7	52.0	5.2	50.5
TS-15	12.1	3.0	10.4	4.1	5.0	71.7
TS-18	11.9	7.5	13.5	40.5	0.0	49.5
TS-28	10.8	6.7	16.6	28.2	12.5	30.8
TS-40	12.5	1.4	13.2	17.3	20.4	42.2
TS-43	11.1	9.2	10.0	0.0	10.2	42.0
TS-44	10.6	7.8	14.1	10.6	1.7	55.3
TS-45	8.8	8.0	10.4	37.7	2.9	41.8
TS-46	10.1	3.2	19.1	32.4	15.7	34.6
TS-50	9.6	4.8	20.4	41.2	8.5	35.8
TS-52	12.7	9.4	7.1	26.4	0.0	52.4
TS-54	11.8	4.0	30.7	44.7	7.7	36.6
TS-59	11.1	5.7	16.0	9.3	20.1	28.9
TS-64	9.6	7.8	21.0	34.9	0.9	43.2
TS-65	8.4	4.0	30.5	36.5	16.1	22.0
TS-67	13.1	10.4	6.4	20.4	0.0	52.4
TS-68	12.8	1.5	15.1	38.9	13.5	44.4
TS-74	10.7	3.6	6.8	26.2	13.1	47.2
TS-76	11.4	6.5	21.1	20.8	11.5	34.6
TS-77	11	3.3	21.8	22.8	20.3	28.8
TS-78	13.5	1.1	12.4	45.1	0.0	71.3
TS-80	13.1	4.1	9.8	21.1	7.1	57.0
TS-83	11.3	6.9	0.6	40.7	0.0	57.6

Appendix 17-2
Plots of petrographic vs. normative mineral abundances

Sericite

Regression Output:

Constant		4.005995
R Squared		0.287882
No. of Observations		27
X Coefficient(s)	0.082946	
Std Err of Coef.	0.026091	

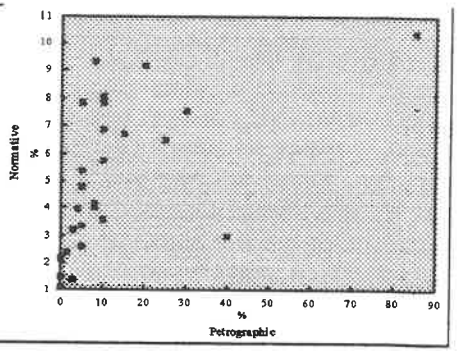

Chlorite

Regression Output:

Constant		28.499
R Squared		0.006
No. of Observations		27
X Coefficient(s)	-0.284	
Std Err of Coef.	0.726	

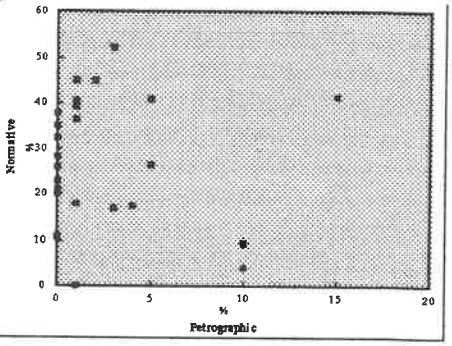

Quartz

Regression Output:

Constant		45.703
R Squared		0.000
No. of Observations		27
X Coefficient(s)	-0.008	
Std Err of Coef.	0.153	

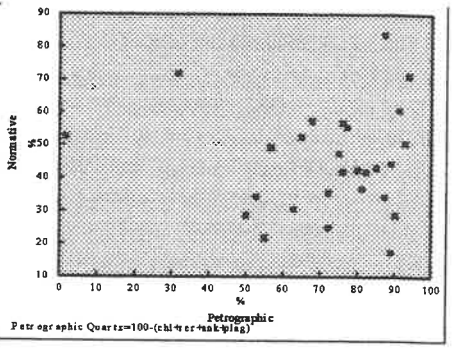

Ankerite

No regression due to incomplete data

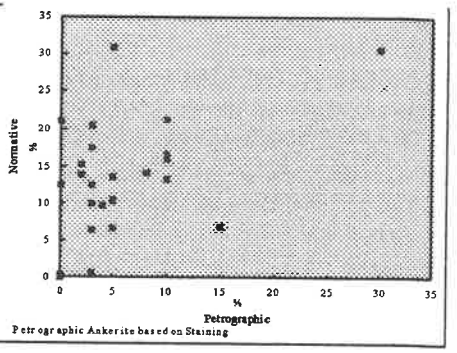

Appendix 17-3
Plots of oxygen isotope data vs. normative mineral abundances.

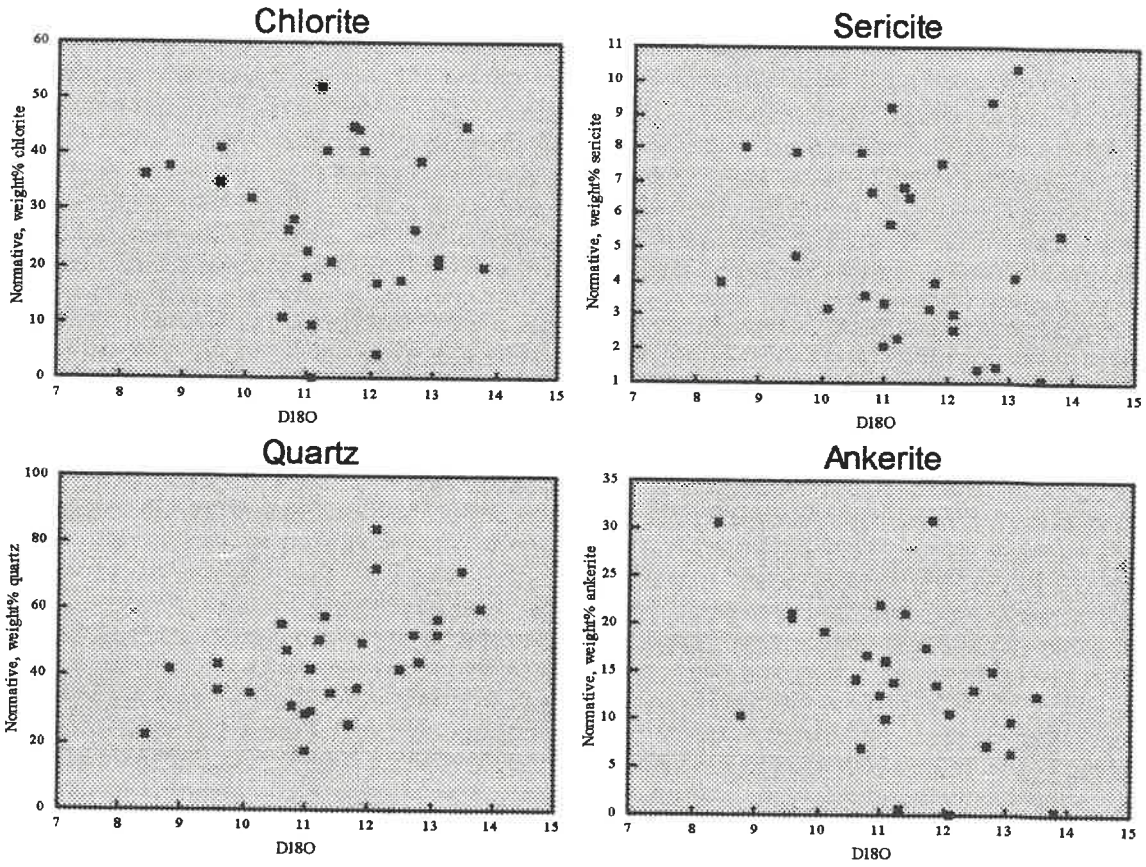

Appendix 18
List of samples, summary descriptions and stratigraphic position.
In order by diamond drill hole no.

Hole NC-90-1C 6+00E

Sediments 84.72 - 111.46[1], Mine Horizon 328.23 - 353.43 (370.82)

TS-36	RBS. Massive rhyolite, aphyric yellow coloured, sericite alteration.	
WRA 10702	55.44 to 55.89	Thin section
TS-37	RBS. Massive and autoclastic aphyric rhyolite breccia, sericite-ankerite alteration.	
WRA 10703	79.20 to 80.03	Polished section and $\delta^{18}O$
TS-16	Pink and green dacitic lapilli/agglomerate tuff, sericite-chloritoid-ankerite alteration.	
WRA 10737	215.10 - 215.20	Thin section
TS-17	Dacitic lapilli Tuff? Carbonate-chlorite alteration.	
WRA 10739	266.72 - 266.73	Thin section
TS-18	Mine Horizon. Felsic lapilli tuff, sericite-chloritoid-silica alteration.	
WRA 10708	329.89 to 331.31	Polished and thin section, and $\delta^{18}O$
TS-19	Chloritoid sericite shist, chlorite-Tourmaline alteration and minor Py and Cpy.	
WRA 10724	360.06 - 360.11	Thin section
TS-20	Sericite-ankerite-chloritoid shist.	
WRA 10724	364.18 - 364.22	Thin section
TS-21	Felsic lapilli tuff.	
	377.62 - 377.72	Thin section

Hole NC-90-2 16+00E

Sediments 231.33-261.72, Cont. in DDH 3

TS-38	RBS. Massive aphyric rhyolite, yellow coloured sericite-ankerite alteration.	
WRA 10751	216.39 to 217.18	Thin section
TS-39	RBS. Plagioclase phyric rhyolite lapilli tuff, sericite and ankerite alteration.	
WRA 10752	225.94 to 227.20	Polished section and $\delta^{18}O$

[1] Down-hole distance in meters for intersection of specified horizon. Distances in brackets indicate intersections of Mine Horizon like alteration.

Appendix 18 (continued).

Hole NC-90-3 16+00E

Continuation of DDH 2, Sediments 0 - 41.4, Fe Formation 164 - 165, Mine Horizon (262.36) 278.71- 326.83

TS-22	Felsic lapilli tuff, sericite-ankerite alteration.		
WRA 10773		275.07 - 275.12	Thin section
TS-23	Felsic tuff/sericite-chloritoid-ankerite shist		
		279.20 - 279.27	Thin section
TS-40	Mine Horizon. Quartz phyric rhyolite tuff/sericite-chloritoid-ankerite shist.		
WRA 21563		292.26 to 292.36	Polished section and $\delta^{18}O$
TS-24	Mine Horizon. Felsic tuff/sericite-ankerite-chloritoid shist.		
WRA 10776		295.26 - 295.36	Thin section
TS-25	Mine Horizon. Felsic tuff/sericite-ankerite-chloritoid shist.		
WRA 10776		296.87 - 296.91	Thin section
TS-26	Felsic tuff/sericite-ankerite-chloritoid shist.		
		320.24 - 320.29	Thin section
TS-27	Quartz, feldspar phyric rhyolite .		
WRA 10788		329.15 - 329.22	Polished section

Hole NC-90-4 23+50E

Sediments 29.95 - 96.47, Mine Horizon (423.66 - 435.75) 458.85 - 476.16 (490.22), Sulfidic chert 545.46 - 546.20

TS-41	RBS. Massive rhyolite, sericite-ankerite-silica alteration.		
WRA 21564		27.37 to 27.64	Polished section and $\delta^{18}O$
TS-28	Mine Horizon. Lapilli tuff, chloritoid-sericite alteration.		
WRA 2605		436.18 to 463.27	Polished and thin section, $\delta^{18}O$
TS-49	Mine Horizon. Felsic tuff/sericite-ankerite-chloritoid shist.		
		461.81 to 461.88	Thin section
TS-29	Felsic tuff/sericite-ankerite-chloritoid shist.		
WRA 2609		469.05 to 469.10	Thin section

Appendix 18 (continued).

TS-30 Felsic tuff/sericite-ankerite-chloritoid shist.
WRA 2626 525.70 - 525.74 **Thin section**

Hole **NC-90-5** 30+00W

Sediments 239.65 - 303.00, Mine Horizon abscent

TS-31 RBS. Massive rhyolite, autoclastic bx., chlorite-sericite alteration and minor Py.
WRA 10857 106.39 - 106.47 **Polished section and $\delta^{18}O$**

TS-32 RBS. Massive rhyolite, chlorite-sericite alteration and minor Py and Sph.
WRA 10331 182.74 - 182.79 **Polished section and $\delta^{18}O$**

TS-72 & 73 RBS. Massive greenish-grey aphyric rhyolite.
WRA 10330 224.40 - 238.55 **Polished section**

TS-33 RBS. Strongly chloritized aphyric massive rhyolite.
WRA 10330 237.28 - 237.36 **Thin section and $\delta^{18}O$**

TS-34 Massive dacite, chlorite-calcite alteration.
WRA 10352 417.60 - 417.71 **Thin section**

TS-35 Massive dacite with minor relict (coroded) feldspar, chlorite-sericite alteration.
WRA 10352 420.46 - 420.56 **Thin section**

Hole **NC-91-06** 20+00W

Sediments 288.24 - 298.36, Mine Horizon (372.88) 380.66 - 404.28 (435.00)

TS-42 RBS. Massive rhyolite, sericite-ankerite-chlorite alteration as well minor pyrite.
WRA 21565 287.82 to 288.85 **Polished section and $\delta^{18}O$**

TS-44 Mine Horizon. Intermediate lapilli tuff, chloritoid-sericite-ankerite alteration.
WRA 21566 383.32 to 383.61 **Polished section and $\delta^{18}O$**

TS-43 Mine Horizon. Intermediate lapilli tuff, chloritoid-sericite-ankerite alteration.
WRA 10390 399.42 to 399.59 **Polished section and $\delta^{18}O$**

Hole **NC-91-11** 34+00E

Continuation of DDH 12. Mine Horizon? 109.90 - 117.80

Appendix 18 (continued).

TS-45 Mine Horizon. Dacitic lapilli tuff overlying Lac du Dome QFP. Chloritoid alteration.
WRA 19401 28.80 to 29.20 Polished section and $\delta^{18}O$

TS-74 Mine Horizon type alteration. Dacitic lappilli tuff.
WRA 19406 109.90 - 114.15 Polished section

Hole NC-91-12 34+00E

LDD QFP 0 - 12.80, Sediments? 122 - 131, Mine Horizon 336 - 356.6, MHT 475.92 - 503.88, Cont. in DDH 11

TS-47 Stratigraphicly equal to RBS. Overlying Lac du Dome QFP. Rhyolitic tuff, chloritoid alteration.
WRA 19167 79.7 to 80.0 Polished section

TS-46 Mine Horizon, overlying LDD intrusion. Dacitic lappilli tuff, chloritoid-sericite-ankerite alteration.
WRA 21567 354.83 to 355.24 Polished section and $\delta^{18}O$

TS-75 Mine Horizon type alteration. Chloritoid-sericite-ankerite alteration.
489.99 - 490.12 Polished section

TS-76 Mine Horizon. Chloritoid-sericite-ankerite alteration.
WRA 10462 501.79 - 502.00 Polished section and $\delta^{18}O$

Hole NC-91-14 44+00E

LDD QFP 0 - 193.24, No sediments @ 225.05, Mine Horizon 330.23 -341.02 (341.83), MHT 544.20 - 583.55

TS-48 Stratigraphicly equal to RBS. Overlying Lac du Dome QFP. Sericite alteration.
WRA 21568 222.34 to 223.77 Polished section

TS-50 Mine Horizon. Felsic lapilli tuff/chloritoid-ankerite-sericite shist.
WRA 19283 332.36 to 332.78 Polished section and $\delta^{18}O$

TS-77 Mine Horizon type alteration. Felsic lapilli tuff/chloritoid-ankerite-sericite shist.
WRA 3941 582.51 - 582.68 Polished section and $\delta^{18}O$

Hole NC-91-15 42+00W

Appendix 18 (continued).

Thin Seds. 95 - 102, Sediments 186 - 267.60, Mine Horizon 410.36 - 419.22

TS-51	RBS. *Silicious, aphanitic massive rhyolite, sericite alteration.*	
WRA 21569	184.19 to 184.47	Polished section and $\delta^{18}O$
TS-52	*Mine Horizon type alteration. Rhyolite/dacite tuff, sericite-chlorite alteration.*	
WRA 21570	415.73 to 416.24	$\delta^{18}O$
	417.72 to 417.80	Polished section

Hole **NC-91-16** 54+00E

Seds. 27.43 -31.95, Main Flow Rhy? 32 - 42, Sediments 42 - 56, Mine Horizon 426 - 552, Chert & Oxide Fe Form. 574 -576

TS-53	Mine Horizon. *Sericite-chloritoid-ankerite shist, silica alteration.*	
WRA 21571	429.80 to 430.07	Polished section
TS-78	Mine Horizon. *Chert.*	
WRA 19543	442.82 - 442.95	Polished section and $\delta^{18}O$
TS-54	Mine Horizon. *Sericite-chloritoid-ankerite shist, silica alteration.*	
WRA 19553	456.28 to 456.42	Polished section and $\delta^{18}O$
TS-55	*Diorite, chloritoid-ankerite-silica alteration.*	
WRA 19560	496.33 to 498.32	Thin section

Hole **NC-91-17** 25+00W

Continuation of DDH 25, Thin seds. 157 -158.5, Sediments 296 - 319, Mine Horizon 450.49 -464.30

TS-56 & TS-57	Massive rhyolite underlying thin graphitic, sulfidic argilite below sediments. TS-56 *Chlorite alteration,* TS-57 *Chloritoid alteration.*	
WRA 19382	143.80 to 143.91	Polished sections
TS-58	RBS. *Massive rhyolite/autoclastic bx. with abundant sulfide veinlets.*	
WRA 21572	293.34 to 294.48	Polished section and $\delta^{18}O$
TS-60	Mine Horizon. *Quartz phyric felsic lapilli tuff, chloritoid-chlorite alteration.*	
	456.59	Polished section

Appendix 18 (continued).

TS-59 Mine Horizon. Quartz phyric felsic lapilli tuff, chloritoid-chlorite alteration.
WRA 19468 462.80 to 462.90 Polished section and $\delta^{18}O$

Hole **NC-91-18** 64+00E

LDD QFP 0 - 152, Sediments 171 - 210, Cont. DDH in 23

TS-61 LDD quartz-feldspar porphyry.
WRA 21573 67.00 to 67.30 Thin section

TS-62 Rhyolite underlying thin sedimentary unit below sediments.
WRA 21574 151.06 to 151.35 Polished section

TS-63 RBS. Massive rhyolite underlying main sediments, relatively "fresh".
WRA 21575 169.90 to 170.08 Thin section and $\delta^{18}O$

Hole **NC-91-20** 39+00E

LDD QFP 578 - 514, No Sediments @ 496, Mine Horizon 383.54 - 339, MHT 86.08 - 0

TS-66 Stratigraphicly equal to RBS. Overlying Lac du Dome QFP. Massive feldspar phyric rhyolite.
WRA 21576 505.08 to 505.33 Polished section

TS-65 Mine Horizon. Felsic lapilli tuff/sericite-ankerite-chloritoid shist, silica alteration.
WRA 19785 381.88 to 388.98 Polished section and $\delta^{18}O$

TS-64 Mine Horizon. .Quartz phyric lapilli tuff/sericite-ankerite shist.

WRA 19774 367.28 to 367.42 Polished section and $\delta^{18}O$

Hole **NC-91-23** 64+00E

Continuation of DDH 18, Mine Horizon type 369.70 374, Mine Horizon 403 - 446, Carb. Fe. Form. 446 - 461, Mine Horizon type 461 - 467

TS-80 & 81 Mine Horizon type alteration. Dacitic lapilli tuff, sericite-ankerite-chloritoid alteration.
WRA 21332 381 - 381.15 Polished section and $\delta^{18}O$

Appendix 18 (continued).

TS-67 Mine Horizon. Dacitic lapilli tuff/sericite-chloritoid shist.
WRA 21577 412.96 to 413.27 **Polished section and $\delta^{18}O$**

TS-68 Mine Horizon. Sericite-chloritoid altertion, tourmaline?
WRA 24578 434.73 to 434.98 **Polished section and $\delta^{18}O$**

TS-91-92 Carbonate facies iron Formation. Spherical texture.
456

TS-69 Carbonate facies iron Formation.
458.50 to 460.00 **Polished section.**

TS-91-91 Carbonate facies iron Formation. Pull apart textures.
481.88 **Thin section**

Hole **NC-91-25** 24+65W

Thin Seds. 431- 433, Sediments 537 - 594, Mine Horizon not intersected, Cont. in DDH 17

TS-86 **Mine Sequence rhyolite.** Chlorite-chloritoid alteration.
WRA 21463 79.22 - 79.40

TS-84 **Mine Sequence rhyolite.** In-situ(?) brecciated lapilli tuff.
384 **Polished section**

TS-85 RBS. Massive rhyolite showing little visible alteration.
WRA 3068 515.16 - 515.33 **Polished section and $\delta^{18}O$**

Hole **N-87-28** 4+50E

Mine Horizon (221) 260 - 269 (289)

TS-05 Pink and green agglomerate, silica-carbonate clasts, chloritoid-sericite mtx, (hematized?).
WRA 10539 65.58 - 65.64 **Thin section**

TS-06 Andesitic lapilli tuff, ankerite-chloritoid alteration.
WRA 10541 121.10 - 121.19 **Thin section**

TS-07 Mine Horizon type alteration. Felsic tuff bx., ankerite-chloritoid alteration.
222.35 - 222.41 **Polished section**

Appendix 18 (continued).

TS-08 Mine Horizon. Felsic lapilli tuff, ankerite-chlorite alteration.
WRA 10586 263.46 - 263.52 **Polished section and $\delta^{18}O$**

TS-09 Felsic tuffaceous lapillistone, sericite-chloritoid-ankerite alteration.
274.37 - 274.48 **Thin section**

Hole N-87-54 0+00

Hole N-87-54, Mine Horizon 62 - 67

TS-01 Sample from below Mine Horizon. Felsic lapilli tuff/chloritoid-ankerite shist.
WRA 10548 31.00 - 31.10 **Thin section**

TS-02 Felsic sericite-ankerite-chloritoid shist.
56.2 - 56.3 **Polished section**

TS-83 Mine Horizon. Felsic lapilli tuff/sericite-ankerite-chloritoid shist.
WRA 10549 62 - 67 **Polished section and $\delta^{18}O$**

TS-03 Mine Horizon. Quartz phyric felsic lapilli tuff, sericite-chlorite-ankerite alteration.
65.3 - 65.4 **Polished section**

TS-04 Quartz eyed dacitic tuff, minor chloritoid.
75.58 - 78.71 **Thin section**

Hole N-89-99 5+69W

Sediments 27 - 95, Mine Horizon 427 - 470, MHT 490 - 503

TS-82 RBS. Felsic fragmental.
WRA 10552 10 - 21.6 **Polished section and $\delta^{18}O$**

TS-10 Diabase dyke. Chloritoid, carbonate alteration.
WRA 10559 237.55 - 237.67 **Thin section**

TS-11 Dacitic tuff, sericite-chloritoid-magnetite alteration.
WRA 10562 371.96 - 372.04 **Thin section**

TS-12 Mine Horizon. Felsic tuff, chloritoid-sericite-chlorite-garnet-silica alteration.
WRA 10591 429.90 - 429.96 **Thin section**

Appendix 18 (continued).

TS-13 Green and pink hematized and/or ankeritized andesite. Sericite-chlorite alteration.
441.72 - 441.84 Polished section

TS-14 Dacite/andesite, sericite-chlorite-chloritoid alteration.
450.30 - 450.35 Thin section

TS-15 Dacite/andesite, sericite-chloritoid-ankerite alteration.
WRA 10563 457.66 - 457.71 Thin section and $\delta^{18}O$

Surface Samples

T-90-19A RBS.
WRA 10143 L0+50W, 1+00S Polished section and $\delta^{18}O$

D-90-12 RBS.
WRA 10205 L4+00W, 1+50S Polished section and $\delta^{18}O$

D-90-42 RBS.
WRA 10213 L14+00W, 2+25S Polished section and $\delta^{18}O$

T-90-31C Mine Horizon.
WRA 10155 L18+20W, 3+75S Polished section and $\delta^{18}O$

TR-90-49A Mine Horizon.
WRA 10176 L19+45W, 5+75S Polished section and $\delta^{18}O$

GR-90-42 Mine Horizon.
WRA 10029 L16+00W, 4+40S Polished section and $\delta^{18}O$

T-90-141 RBS.
WRA 12935 L2-14+00W,8+75S

TS-87 Normetmar outcrop, underlying andesite.
WRA 7+00W Polished section

TS-90 Normetmar outcrop, Mine Horizon.
WRA 7+00W Polished section

TS-88 Normetmar outcrop, Mine Horizon.
WRA 7+00W Polished section

TS-89 Normetmar outcrop, Overlying andesite.
WRA 7+00W Polished section

Appendix 18 (continued).

NMAR-90-05	Normetmar outcrop, directly underlying Mine Horizon. Cherty heterolithic lapilli tuff.	
WRA 10119	7+00W	$\delta^{18}O$
M-90-94		
	L3-12+00E (13.2 km East)	$\delta^{18}O$
WRA 12936	Main Flow rhyolite.	
	L21+4W	$\delta^{18}O$
WRA 10027		
	L1+09W	$\delta^{18}O$
VH-90-01	RBS.	
	L0+28W	$\delta^{18}O$
VH-90-05	RBS.	
	L0+32W	$\delta^{18}O$